Title
PHOTOFRAGMENTATION DYNAMICS OF IODOHALOETHANES

Author
Minton, T.K.

Publication Date
1986-08-01

Lawrence Berkeley Laboratory
UNIVERSITY OF CALIFORNIA

Materials & Molecular Research Division

PHOTOFRAGMENTATION DYNAMICS OF IODOHALOETHANES

T.K. Minton
(Ph.D. Thesis)

August 1986

Prepared for the U.S. Department of Energy under Contract DE-AC03-76SF00098

DISCLAIMER

Photofragmentation Dynamics of Iodohaloethanes

Timothy K. Minton
Ph.D. Thesis

Department of Chemistry
University of California
Berkeley, California 94720

and

Materials and Molecular Research Division
Lawrence Berkeley Laboratory

August 1986

Photofragmentation Dynamics of Iodohaloethanes

Timothy Karl Minton

Abstract

The technique of photofragmentation translational spectroscopy has been utilized to study the photodissociation of many iodohaloethanes at excitation wavelengths of 248, 266, and 308 nm. These wavelengths fall within the range of the n(I)$\longrightarrow\sigma^*$(C–I) absorption continuum of the alkyl iodides, while the two shorter wavelengths, 248 and 266 nm, also lie in the range of the low energy tail of the n(Br)$\longrightarrow\sigma^*$(C–Br) continuum. Nervertheless, C–I bond fission predominates at all three wavelengths and is the focus of these studies. Primary C–I dissociation can yield two states of atomic iodine: ground state I($^2P_{3/2}$) and spin-orbit excited state I($^2P_{1/2}$). Secondary dissociation of a portion of the haloethyl radical product usually occurs, either because the radicals are formed with enough internal excitation to break the weak C–X bond or because they can absorb additional photons and dissociate.

Chapter 1 (in conjunction with Chapter 2) and Chapter 3 provide detailed investigations into the photofragmentation dynamics of two iodohaloethanes, CH_2ClCH_2I and CF_2BrCH_2I, thus illustrating the methodology of these studies, and Chapter 4 summarizes the results for these molecules along with five other similar systems and discusses some trends that have become manifest. The center-of-mass trans-

lational energy distributions of the photofragments have been derived for both the $I(^2P_{1/2})$ and $I(^2P_{3/2})$ dissociation channels, yielding the relative probability for each channel (which varies widely as a function of the excitation wavelength and the substituents on the iodoethane). The translational energy distributions also reveal the general trend that, on the average, about 50% of the excess energy appears in translation. Angular distributions of the photofragments with respect to the laser polarization indicate that primary (C–I) photodissociation proceeds via a parallel transition (i.e., the transition moment must be nearly parallel to the C–I bond) for every system studied. Finally, the energy threshold for spontaneous secondary dissociation was observed for a number of systems, enabling the determination of the reaction enthalpy for RXI $\longrightarrow$ R + X + I, from which the heat of formation $\Delta H_f^\circ(0)$ of the iodohaloethane parent can be calculated and the stability of the haloethyl radical can be inferred.

to Janet, who makes everything worthwhile

Contents

ACKNOWLEDGEMENTS

My six years as a graduate student have ranged from miserable to ecstatic, but overall, they have been exciting and gratifying. To be sure, the Lee group has been an eye-opening experience—from the blow guns, fireworks, and drafting room parties (in the pre-collimation era) to the impressive hardware, intense dedication, and scientific excellence, all of which are abundant in the the group.

At the pinnacle of scientific excellence is Yuan Lee, who has never ceased to amaze me with his vast knowledge and problem solving capabilities. It has truly been a pleasure to have been able to benefit from his guidance as a research director. In addition, his ability to secure plenty of funding has enabled his students (including me) to spend more time worrying about scientific problems and less time concerned with equipment problems. Yuan's scientific merit has also attracted many foreign scientists to the group, which I have found very enriching.

While Yuan was the general guiding light during my graduate tenure, much of my day-to-day education (and amusement) came from the many coworkers and friends that I have had the pleasure to meet. The work on chloroiodoethane in Chapter 1 was done with Peter Felder and Rick "Brud" Brudzynski (two long-time "B-team" members). Peter was very helpful in teaching me to operate the machine and in seeing me through my first complete experiment—from data taking to paper writing. I really appreciated his willingness to answer all my questions. I must give him credit also for founding, along with me, the art of oscilloscope licking (our data was so good we had to find a way to vent our excitment), which has been a continuing theme in the sometimes base group humor. Brud also helped me out a great deal on the B-machine, and he played a significant role in the development of the MPI machine. I am sorry that our research paths did not coincide more, because he was a good coworker and I always thought I would enjoy tackling more

experiments with him. Nevertheless, I have been fortunate enough to have worked with him and to have had him as an office mate and friend.

I have benefitted greatly from the work I did with Gil Nathanson (Chapters 2-4). I am extremely lucky to have had the opportunity to work with and learn from Gil. He was always enthusiastic, hardworking, and overflowing with good ideas. Furthermore, he was patient enough to field a myriad of questions from me. The innumerable marathon sessions at the blackboard have really helped me to grasp the more subtle scientific points of our experiments.

The experiments described in this thesis actually represent a relatively small fraction of the time that I have spent at Berkeley. I worked on many projects that, for various reasons, did not reach fruition. Dan Neumark was my first coworker (mentor) in the group, and I thank him for helping me learn the ropes and for putting up with me when I was just a "boy." Jeremy Frey was my next coworker, and I am grateful to him for the many discussions we had. He was a patient and willing teacher. On a later project, I collaborated with Howard Nathel, which was without doubt a unique alliance, but one I enjoyed. Howard taught me how to "have needs," how to "invent," and how not to be shocked by anything. He was also a good singing partner. Thanks are also in order for Marion Helfand, who worked with me after Howard left. I wish her success on the MPI machine. Finally, Stacey Shane deserves recognition for helping in the analysis of CF_2BrCF_2I.

In addition to coworkers, numerous other group members have augmented my graduate study with instructive discussions. Doug Krajnovich was a very valuable source of information. Rick Buss also gave me a great deal of assistance. Ralph Page (my other office mate) often aided me when I had a laser problem or just a general question. I was happy to be able to discuss photodissociation of alkyl iodides with Laurie Butler, with whom I shared some common scientific interests.

I received many a clear explanation on some general point of science from Mitchio Okumura, and I would like to thank Mitchio also for forging the way with LaTeX, the typesetting program used to print this thesis. I would like to extend my appreciation to some others who have taken time to lend me their expertise: Carl Hayden, Sandy Bustamente, Alec Wodtke, Sheng-Yu Huang, and Charlie Bahr. Finally, I must say thanks to all my friends in the Lee group for making my six years fun, instructive, and exciting.

Several persons not directly a part of research in the group deserve special thanks. Ann Weightman, our "administrative assistant," was capable and tough. She always knew how to circumvent standard channels in order to make things happen to benefit our group. She was also of inestimable value as a counselor for those of us who had automobile problems or questions. Fred Wolff, of the campus machine shop, gave many helpful suggestions when I was designing and building. Tony Moscarelli in the 70A shop was fast and precise when I needed a part in a hurry, or, if I wanted to do the work myself, he would willingly lend me a hand. He, too, contributed greatly to my automobile repair education. Lastly, Fred Vogelsberg and Ed Arnold were always pleasant and helpful when I had an electronics breakdown or just a question.

These thesis acknowledgements would be grossly incomplete if I failed to mention some of my family. My mother and father have encouraged me to persevere to the end. Thoughout my life, their love and support has often given me the extra boost that I needed in order to overcome a hurdle. Another family member, who played *the* key role in my graduate career, is my wife, Janet. Not only has she stayed up all hours of the day and night to type my thesis during the final weeks, but she has been understanding and encouraging no matter how much I have complained about lab. In short, she has constantly believed in me and loved me, and I could

not ask for a better relationship than ours. The completion of my degree would seem deficient without her. Thanks Janet, for everything!

This work was supported by the Director, Office of Energy Research, Office of Basic Energy Sciences, Chemical Sciences Division of the U.S. Department of Energy under Contract No. DE-AC-0376SF00098.

Chapter 1

Photodissociation of 1,2-Chloroiodoethane at 248 and 266 nm; the Enthalpy of Formation of CH_2ClCH_2I

I. INTRODUCTION

Excitation of the alkyl iodides in the 200-300 nm region of the spectrum leads to transitions of a non-bonding 5pπ iodine electron to a σ^* molecular orbital,[1(c),1(d)] which is seen as the familiar $n \longrightarrow \sigma^*$ continuum.[2] It has long been known[3-6] that the photodissociation of alkyl halides in this region yields two states of atomic iodine:

$$\mathrm{RI} + h\nu \begin{cases} \nearrow \mathrm{R} + \mathrm{I}^*(^2P_{1/2}) \\ \searrow \mathrm{R} + \mathrm{I}(^2P_{3/2}) \end{cases} \qquad (1)$$

For small RI, the major pathway is toward formation of the spin-orbit excited state ($^2P_{1/2}$) of iodine (which we will denote I*). This phenomenon has led to the development of the iodine laser.[4]

Photofragmentation translational spectroscopy studies [7-13] have shown that the following $n \longrightarrow \sigma^*$absorption, dissociation proceeds directly along the repulsive surface, with a large fraction of the excess energy released in translation. For example,

in CH_3I, the fraction of excess energy appearing in translation is approximately 0.85, and in C_2H_5I, this fraction is ~0.60. Even in fluorinated alkyl iodides, [10,11] such as C_2F_5I and C_2F_4BrI, in which lower frequency vibrations and larger exit impact parameters could result in excitation of more fragment vibrational and rotational degrees of freedom, about 50% of the excess energy appears in translation. From the anisotropy in the product angular distributions, it is seen that the lifetime of the excited state must be less than one rotational period. Dzvonik, Yang, and Bersohn[7] made a careful study of the anisotropy in the broadband photodissociation of CH_3I and concluded that the lifetime after absorption of a photon was 0.07 psec.

The anisotropy of the product angular distributions with respect to the polarization of the laser also provides information regarding the orientation of the transition moment of the $n \longrightarrow \sigma^*$ transition. According to the molecular orbital theory of Mulliken,[1] the $n \longrightarrow \sigma^*$ continuum is composed of three overlapping bands, which arise from transitions from the ground N state to the ^1Q, $^3Q_1$, and $^3Q_0$ states. The $N \longrightarrow {}^3Q_0$ transition should be polarized parallel to the C–I bond and should correlate to formation of I^*, while the $N \longrightarrow {}^1Q$ and $N \longrightarrow {}^3Q_1$ transitions should be polarized perpendicular to the C–I bond and should correlate to formation of ground state I. For the diatomics, I_2 and HI, Mulliken's predictions have been borne out by experiment.[12,14] However, in the case of the alkyl iodides, both I and I^* are observed to occur via parallel transitions at 266 nm,[8] suggesting that curve crossing is important. The underlying structure of the $n \longrightarrow \sigma^*$continuum for CH_3I has been probed with magnetic circular dichroism (MCD),[15] but even with this information, the relative yields of I^* and I at a particular wavelength cannot be predicted because of the complication of curve crossing.

Due to interest in the iodine laser, the quantum yields of I^* from photodissociation of alkyl iodides have received considerable attention, but despite all the effort

spent, disagreement abounds even in the ubiquitous methyl iodide studies. Table I shows various I^* quantum yields reported for CH_3I at 266 and 248 nm. The most reliable values in the table should be the results obtained by photofragmentation translational spectroscopy at 266 nm. This method, based on the pioneering work of Wilson and co-workers,[8,16-18] utilizes the fact that the products from the I^* channel recoil slower than the products from the I channel, and it is ideal because it yields an absolute ratio of I^* and I atoms. Consistent with the photofragmentation spectroscopy results at 266 nm is the value of Hunter, Lunt, and Kristjansson[19] who used an optoacoustic technique. But at 248 nm, none of the experiments agree. In a recent study using laser induced VUV fluorescence,[20] I^* quantum yields at 248 nm for many alkyl iodides were reported. The drawback of this study is that the average of the values from Refs. 13 and 21 for CH_3I was used as a calibration standard. Clearly, the wide range of reported I^* quantum yields for CH_3I make it a rather tenuous standard. I^* quantum yields from UV photolysis of alkyl iodides certainly require further investigation.

The energetics of the dissociation of CH_2ClCH_2I resulting from an $n \longrightarrow \sigma^*$ transition present many interesting features for a photofragment translational spectroscopy study. For example, the photon energy at an excitation wavelength of 266 nm is 107.5 kcal/mole, but only about 55 kcal/mole of energy is needed to break the C–I bond, leaving ~52 kcal/mole excess energy. If electronically excited I^* is formed, this excess energy is reduced by 21.7 kcal/mole to ~30 kcal/mole. The C–Cl bond energy in the C_2H_4Cl fragment has been estimated to be only about 20 kcal/mole, so unless a substantial fraction of the excess energy is carried away in translation, the internal energy in the chloroethyl fragment will exceed the C–Cl dissociation limit. If about 50% of the excess energy appears in translation, as has been seen in other iodoethanes,[10,11] then the photodissociation channel leading to

formation of ground state I is likely to result in complete secondary dissociation of the C_2H_4Cl fragment into C_2H_4 and Cl, while the channel leading to I* might leave only a fraction of the chloroethyl radicals with enough internal energy to dissociate.

In the primary photodissociation process of 1,2-chloroiodoethane, the momentum of the system must be conserved. Accordingly, the C_2H_4Cl and I fragments will move with opposite directions in the center of mass coordinate system as shown schematically in Fig. 1. As the total energy of the system is also conserved, the smaller the recoil velocity, or kinetic energy, the larger the internal energy of the alkyl fragment. If the internal excitation of the C_2H_4Cl radical exceeds the C–Cl bond dissociation energy, then the radical will dissociate and will be depleted from the C_2H_4Cl velocity (or time-of-flight) distribution. The minimum translational energy of stable C_2H_4Cl corresponds to production of C_2H_4 + Cl with zero kinetic energy and no internal excitation. Consequently, by determining the minimum in the total translational energy distribution for all fragments that leads to stable chloroethyl radicals, the energy required to break both the C–I and C–Cl bonds in 1,2-chloroiodoethane can be determined, from which the heat of formation ΔH_f° of CH_2ClCH_2I can be estimated.

As Fig. 1 illustrates, if we measure the velocity (or time-of-flight) distribution of one fragment, we can derive the energetics for the whole system by using conservation of energy and momentum. Detection of iodine will yield the total translational energy distribution, $P(E_T)$, of the primary photodissociation products for both I* and I channels, but if we observe the stable C_2H_4Cl fragment, the range of the $P(E_T)$ distribution which we derive and the knowledge of the C–Cl bond dissociation energy in the C_2H_4Cl radical will allow the identification of the iodine electronic state that is associated with the production of stable chloroethyl radicals. As will be seen, stable C_2H_4Cl product correlates only with I* formation because ground

state I does not carry away enough energy to stabilize the chloroethyl product. Thus, the measurement of both the C_2H_4Cl and I fragments makes it possible to discriminate between the $P(E_T)$ distributions for the I^* and I channels, allowing the I^*/I branching ratio to be deduced.

From angular and time-of-flight distributions at both 248 and 266 nm, the polarization dependence of the photodissociation processes can be derived, permitting a comparison of the excitation of two different parts of the $n \longrightarrow \sigma^*$ continuum and revealing the relation between the initial excitation and the extent of subsequent curve crossing.

In addition to our interest in the detailed dynamics of the photofragmentation of CH_2ClCH_2I, we wished to test the possibility of producing a molecular beam of cold C_2H_4Cl radicals by photodissociation. If stable C_2H_4Cl radicals can be prepared by crossing a pulsed supersonic molecular beam with a UV laser just outside the nozzle, the radicals produced in the high density region will be confined in the beam, and after being cooled in the expansion, they will survive unperturbed.

This beam of 2-chloroethyl radicals could then be used for a time resolved experiment which would directly probe the time scale of the intramolecular energy transfer from a locally excited C–H overtone stretching mode to other vibrational degrees of freedom by the measurement of the dissociation lifetime. The C_2H_4Cl radical would be an ideal system to study for the following reasons. First, as the C–Cl bond is fairly weak, only four quanta of C–H stretch (i.e., excitation of the third overtone) are needed to reach well above the dissociation limit. Second, the predicted RRKM lifetime of C_2H_4Cl when excited to the third overtone is on the order of a few picoseconds. Thus, if the intramolecular relaxation from the local excitation of the C–H stretching modes to other modes is slower than a few picoseconds, then the experimental dissociation lifetime would provide a good mea-

sure of the rate of intramolecular energy transfer. Finally, there is more than one C–H stretching mode accessible, allowing the rates of two different intramolecular relaxation processes to be compared.

II. EXPERIMENT

The apparatus used was a universal crossed molecular beam machine[22] in which an ultraviolet laser was substituted for one of the molecular beams (see Fig. 2). The resulting configuration was a supersonic molecular beam of CH_2ClCH_2I (custom synthesized by Fairfield Chemical, Blythewood, SC) which was crossed at right angles by the UV laser. Photodissociation products were detected in the plane of the laser and molecular beams by a rotatable mass spectometer. The flight path length from the interaction region to the ionizer was 20.8 cm. Two different lasers were used in order to study the photodissociation of 1,2-chloroiodoethane at both 248 and 266 nm.

In both experiments, the molecular beam was formed by bubbling a carrier gas through liquid CH_2ClCH_2I which was held at 20°C (vapor press. = 7 Torr) and then expanding the mixture through a 0.005 in. (0.12 mm) dia. nickel nozzle. The nozzle was heated at the tip to prevent cluster formation. The molecular beam passed through three stages of differential pumping before it reached the main chamber where it intersected the laser. A skimmer was used to define the beam to an angular divergence of 2°. The distance from the nozzle to the interaction region was about 9.5 cm.

For the 248 nm experiment, an unpolarized Lambda Physik EMG 101 laser was used on the KrF transition at a repetition rate of 40 Hz. The average pulse energy was ~125 mJ. Two optics were used to focus the laser. A 50 cm fl MgF_2 cylindrical lens oriented to focus the beam horizontally was followed immediately

by a 35 cm fl UV-grade fused silica spherical lens, giving a final spot size of 2.2 mm wide and 4.5 mm high in the interaction region. The CH_2ClCH_2I was seeded in He at a total stagnation pressure of 700 Torr (1% CH_2ClCH_2I/99% He) and the nozzle temperature was 130°C, yielding a peak velocity of 1590 m/sec with a velocity spread (FWHM) of 9%.

For the 266 nm experiment, the fourth harmonic of a Quanta Ray DCR-1 Nd:YAG laser was used. The output was polarized horizontally—i.e., in the plane of the molecular beam and detector. A Quanta Ray Harmonic Generator, Model HG-2, was used to generate the fourth harmonic. The output from the harmonic generator passed through a Pellin-Broca prism after which the unwanted first and second harmonics were directed into a beam dump. The fourth harmonic went directly from the prism into the machine through a 50 cm fl UV-grade fused silica spherical lens. The final spot diameter at the interaction region was 2.8 mm. Average pulse energies were ~30 mJ. The molecular beam conditions for the experiment at this wavelength differed from those at 248 nm in that Ar was used as the carrier gas and the stagnation pressure was 400 Torr (1.8% CH_2ClCH_2I/98.2% Ar). Also, the nozzle was heated to 228°C. The resulting beam had a peak velocity of 707.8 m/sec with an average velocity spread of 8.4%.

The molecular beam velocity distributions were determined by fitting time-of-flight (TOF) measurements on the beam to an assumed form for the $N(v) \propto v^2 \exp[-(v/\alpha - S)^2]$, (see refs. 10 and 23). The TOF measurements were obtained differently for the two experiments. At 266 nm, the usual method of a "single-shot" slotted disk was employed to chop the beam. However, at 248 nm, a holeburning method was used. In holeburning, the detector is positioned along the molecular beam axis and tuned to the parent mass. Molecules photodissociated by a laser pulse scatter off axis and give rise to a hole in the TOF. The shape of the

hole registered at the ionizer contains the information about the velocity distribution. In this way, the velocity distribution can be measured at any point during the experiment without insertion of the slotted disk. The disadvantage of holeburning is that the signal-to-noise ratio is much worse than in the conventional slotted disk method.

At 248 nm, TOF measurements were made at detector angles from 5° to 30°. Signal was detected at m/e = 127, 63, 35, and 26, corresponding to I^+, $C_2H_4Cl^+$, Cl^+, and $C_2H_2^+$, respectively. The respective integrated counts/laser pulse at 10° were 1.95, 0.02, 0.72, and 0.67. Due to the fragmentation of C_2H_4Cl in the ionizer and the high mass 28 background in the detector, masses 63 and 28 were not suitable for monitoring the chloroethyl product, but mass 26 proved to be an acceptable mass for this purpose. Mass 35 (Cl^+) was not used for monitoring C_2H_4Cl because most of the mass 35 signal was found to arise from Cl atoms. Typical counting durations were 20,000 laser pulses for I^* and 500,000 pulses for $C_2H_2^+$.

At 266 nm, TOF measurements were made at detector angles from 7° to 35°. Signal was detected at m/e = 127(I^+) and 26($C_2H_2^+$). The mass 26 TOF was only taken at 7°, where we observed ~0.04 counts/pulse of signal. Mass 127 at 10° gave ~0.98 counts/pulse. Mass 26 was counted for 176,000 pulses, while the mass 127 TOF's were counted for 40,000 pulses.

It should be noted that the two experiments reported here were performed six months apart. The change to different experimental conditions was suggested from the analysis of the first experiment (at 248 nm).

III. RESULTS AND ANALYSIS

The experimental data with which we derive the center of mass product translational energy distribution $P(E_T)$ and the c.m. angular distribution $w(\theta)$ for the

photodissociation products are the TOF distributions $N(t)$ and the laboratory angular distributions $N(\Theta)$. For a single photon dipole transition, the c.m. angular distribution of the fragments must have the form,[18(b)]

$$w(\theta) = \frac{1}{4}\pi[1 + \beta P_2(\cos\theta)], \tag{2}$$

where θ is the angle between the electric vector of the laser light and the c.m. recoil direction of the products. β is the anisotropy parameter and must lie in the range $-1 \leq \beta \leq 2$. The $P(E_T)$ and β are determined by comparing calculated TOF and angular distributions with the experimental data. The calculated distributions are obtained by assuming a $P(E_T)$ distribution and a value for β and then convoluting them with the beam velocity distribution, ionizer length, and other apparatus effects. By varying the $P(E_T)$ and β, the best simultaneous fits to all the data are obtained.

It should be noted that the TOF distributions show the total time for a fragment to go from the interaction region to the ionizer, and after ionization, through the quadrupole mass spectrometer to the Daly-type ion counter. The true TOF from the interaction region to the ionizer is given by subtracting the relatively short ion flight time (typically <5% of the total flight time) from the measured TOF. The ion flight time for a singly charged ion of mass m has been estimated experimentally, and it can be expressed in μsec by the formula $\alpha\sqrt{m}$ where the parameter α is a function of ion energy and other spectrometer parameters and is equal to 1.80 for the 248 nm experiment and 1.94 for the 266 nm experiment.

A. TOF and angular distributions

Figure 3 shows the TOF data along with the best fits at various laboratory angles for the iodine fragment at 266 nm. Two components in the TOF are definitely apparent. Similar effects have been observed in other alkyl iodides[8,9] where the

fast component is attributed to formation of ground state $I(^2P_{3/2})$ while the slow component is ascribed to the formation of the spin-orbit excited state $I^*(^2P_{1/2})$.

In the case of the TOF data at 248 nm (Fig. 4), the fast shoulder is not so obvious partly because the translational energy distributions for products leading to ground and excited state iodine are not as separated as they are at 266 nm (see Sec. III B) and also because the molecular beam velocity in the 248 nm experiment was more than twice that in the 266 nm experiment, yielding poorer time resolution.

The effect of the molecular beam velocity as well as the reason for the observation of two different peaks in the 248 nm TOF can be seen by considering the experiment in terms of the kinematic diagram shown in Fig. 5. The vertical arrow is the molecular beam velocity vector. The center of mass is at the tip of this vector. An arrow from the c.m. to one of the circles represents the velocity that a particular recoiling fragment has in the c.m. coordinate system after photodissociation. The angle between this c.m. fragment velocity vector and the line on which the molecular beam velocity vector lies is the c.m. angle θ of the product. The angle between the molecular beam velocity vector and the laboratory velocity vector of the product is the laboratory angle Θ. We detect products at a particular Θ, and we can see a peak in the TOF spectrum at an arrival time corresponding to the velocity vector $\mathbf{V}_{lab}$ which intersects the most probable c.m. product velocity as shown by the Newton circle. The TOF spectrum is weighted by the transformation Jacobian from velocity to time. As can be seen, a slower beam velocity would mean better angular and temporal resolution for a given recoil velocity distribution. In addition, slight offsets in the timing of the experiment are less important with the slower beam.

There are advantages to the fast beam velocity, however. First, the signal is higher because the products are concentrated in a smaller laboratory angular range. Second, in the case where we see the "forward" and "backward" peaks in the TOF,

as in the 248 nm data, we are sampling two different c.m. angles for each laboratory angle, making the fit to the TOF distribution very sensitive to the anisotropy parameter β.

The angular distributions $N(\Theta)$ for the I fragment are shown in Figs. 6 and 7 for 266 and 248 nm, respectively. The 266 nm distribution is fit quite nicely by $\beta = 1.8$. However, $\beta = 1.8$ did not fit the 248 nm angular distribution well. In fact, $\beta = 2.0$ gives a better fit, but the TOF distributions at 248 nm gave the most consistent fits for $\beta = 1.8$. The poor fit in the angular distribution is attributed to a possible systematic error in the determination of the laboratory angle. An error of 0.5° in Θ, which could arise from a combination of a slight misalignment of the laser and molecular beams as well as the uncertainty in the detector position, would account for the observed effect. Nevertheless, this error will not materially affect the conclusions of the experiment.

As mentioned in Section II, we observed the chloroethyl fragment at $m/e = 26$. The total TOF distribution for mass 26 at 248 nm (Fig. 8) exhibits an interesting feature. There is a large "spike" superimposed on a broad background. This background arises from secondary dissociation of the C_2H_4Cl into C_2H_4 and Cl, while the spike is the TOF distribution of the chloroethyl radical which survives. Fig. 9 shows a blow-up of the spike with the best fit. The mass 26 TOF at 266 nm (Fig. 10) did not show a broad background partly because of the relatively poor signal-to-noise ratio, but mainly because of the fact that a large fraction of the C_2H_4Cl product survives. In both mass 26 TOF distributions, shaded areas are shown with the best fit, illustrating the range of uncertainty in the fits to the slow side.

Another mass which was considered for observing the chloroethyl fragment was mass 35(Cl^+), whose TOF is shown in Fig. 11. While the TOF does show evidence of a peak at ~82 μsec corresponding to the stable C_2H_4Cl fragment, it certainly

does not exhibit the definite spike seen in the mass 26 TOF. Thus, most of the Cl^+ ions arise from Cl atoms rather than C_2H_4Cl.

B. Product translational energy distributions

The fits to the TOF and angular distributions were calculated using the $P(E_T)$ distributions shown in Fig. 12. Because photodissociation can lead either to $I^*(^2P_{1/2})$ or $I(^2P_{3/2})$ product, the total $P(E_T)$ is the sum of two distributions. The energetics of the photodissociation process enable us to determine the ground and excited state components of the total $P(E_T)$.

A representation of the energetics is shown in Fig. 13. The energy available for translation and internal excitation of the products (E_{avl} for production of I or E^*_{avl} for production of I^*) is given by the energy conservation expressions,

$$\begin{aligned} E_{avl} = h\nu + E^P_{avl} \quad - \quad & D^\circ_0(C-I) = E_T + E^R_{int}, \\ E^*_{avl} \quad = \quad & E_{avl} - E_{so}, \end{aligned} \tag{3}$$

where E^P_{int} is the internal energy of the CH_2ClCH_2I parent, which is almost negligible, and E^R_{int} is the internal energy of the C_2H_4Cl fragment after photodissociation. D°_0(C–I) for CH_2ClCH_2I is estimated to be 55.3 ± 1 kcal/mole (see Discussion). The photon energy $h\nu$ is 115 kcal/mole at 248 nm and 107.5 kcal/mole at 266 nm. E_{so} is the 21.7 kcal/mole spin-orbit splitting between I and I^*.

The minimum internal energy of the chloroethyl fragment (E^R_{int}) when ground state I is formed is given by subtracting the observed maximum E_T from the available energy (E_{avl}). At 248 nm, this minimum E^R_{int} is 21.8 kcal/mole, and at 266 nm, it is 19.0 kcal/mole. These energies are expected to be near or above the C–Cl dissociation limit for the C_2H_4Cl radical.[24] Hence, all ground state I formation should lead to secondary dissociation of the C_2H_4Cl fragment. The $P(E_T)$ derived from

the fit to the mass 26 TOF should then reflect only the formation of I*. Thus, subtracting this $P(E_T)$ for I* formation from the total $P(E_T)$ will give the $P(E_T)$ for ground state I formation.

A complication in the reasoning above (but an important feature in this experiment) occurs because the effect of secondary dissociation is also seen in the $P(E_T)$ for I* formation. At both wavelengths, particularly at 248 nm, even when I* is formed, some of the C_2H_4Cl radicals have more than enough internal energy to break the C–Cl bond. Consequently, the low translational energy (high E_{int}^R) side of the $P(E_T)$ derived from the mass 26 TOF is "chopped off" relative to the total $P(E_T)$, such that the minimum energy is observed to be ~15 kcal/mole at 248 nm and ~9.3 kcal/mole at 266 nm. From Eq. (3), the total energy required for the dissociation of both the iodine and the chlorine from CH_2ClCH_2I can be determined [assuming E_{int}^P is equal to zero (see Discussion)] as follows:

$$D_0^\circ(CH_2ClCH_2 - I) + D_0^\circ(C_2H_4 - Cl) = h\nu - E_{so} - E_T\text{min}, \quad (4)$$

where $D_0^\circ(C_2H_4\text{–}Cl)$ has been replaced for $E_{int}^R(\text{max})$. This sum of dissociation energies is just the change in enthalpy ΔH at 0 K for the reaction,

$$CH_2ClCH_2I \longrightarrow C_2H_4 + I + Cl \quad (5)$$

We observe $\Delta H = 78.3 \pm 1$ kcal/mole in the 248 nm experiment and $\Delta H = 76.5 \pm 1$ kcal/mole in the 266 nm experiment. The disagreement between these two values will be considered in the following section.

From the areas under the $P(E_T)$ distributions, we can estimate a branching ratio for the formation of I* to I. At 248 nm, $I^*/I = 1.5$, while at 266 nm, $I^*/I = 3$. These results can be compared with observations for C_2H_5I. Ref. 20 obtains $I^*/I = 2.1$ at 248 nm, while ref. 8 estimates $I^*/I \cong 3$ at 266 nm. Our results do contain some

uncertainty. Because the ionization cross section in the ionizer might vary with fragment internal excitation, the true shape of the mass 26 derived $P(E_T)$ which is used to separate the contribution of I* and I in the total $P(E_T)$ distribution could be slightly different from the one which we found. The effect of internal excitation on ionization cross section has been observed in the multiphoton dissociation of ethyl vinyl ether,[25] but its magnitude is not easily obtainable.

Finally, we can compare the fraction of the available energy that went into translation for the two wavelengths. The results are summarized in the following table:

Wavelength	$\langle E_T^* \rangle / E_{avl}^*$	$\langle E_T \rangle / E_{avl}$
248 nm	0.58	0.46
266 nm	0.57	0.46

IV. DISCUSSION

A. Anisotropy and polarization

In the two experiments presented here, the anisotropy parameter β is approximately equal to 1.8 regardless of whether I or I* is formed. Assuming dissociation is fast compared to a rotational period and neglecting vibrations,[18(b)] $\beta = 2$ when the transition moment lies along the bond dissociation coordinate (parallel transition) and $\beta = -1$ when the transition moment and the bond dissociation coordinate are at 90° (perpendicular transition). Evidently, the processes which we observed are indicative of nearly parallel transitions along the C–I bond.

The question of why β is 1.8 and not 2.0 merits further attention. Considering a truly parallel transition, if the lifetime of the excited state were long enough to

allow slight rotation during the dissociation, β would be less than 2. Rotational as well as vibrational motion of the parent could impart a velocity component which is perpendicular to the axial velocity of recoil, thus lowering β. In addition, a transition moment which is not quite parallel to the C–I bond could account for the lower value of β. Finally, β would be lowered if the repulsive force were not operating exactly along the original C–I bond direction during dissociation. In order to assess whether molecular rotation is the cause of an anisotropy parameter of less than 2, we performed an experiment at 266 nm, similar to the ones described here, on the photodissociation of CH_3I. The anisotropy parameter was found to be exactly 2.0 (for both I and I^* channels). Because of the symmetry of this system, the transitions should be either purely parallel or purely perpendicular, and β could only be slightly different from 2 or −1 if the dissociation were affected by rotation or vibration. Since $\beta = 2.0$, these effects must not be important. In view of the fact that the beam of CH_2ClCH_2I (and of CH_3I) is produced by a supersonic expansion using a rare gas carrier, the rotational temperature is expected to be very low (see part B). Therefore, as in the case of CH_3I, the rotational motion of CH_2ClCH_2I is not expected to be important.

The significance of parallel and perpendicular transitions with respect to low electronic states of the hydrogen and alkyl halides has been discussed extensively by Mulliken[1] and others.[10,12,15,19,26,27] As mentioned in the Introduction, ground state iodine should be formed by a transition from the ground N state to the $^3Q_1$ or ^1Q states, which would be polarized perpendicular to the C–I bond, while the excited state iodine channel should be correlated to a transition to the $^3Q_0$ state, which would be polarized parallel to the C–I bond. The three of these overlapping Q states together are responsible for the characteristic $n \longrightarrow \sigma^*$ absorption continuum of alkyl halides seen in the UV. The fact that we see only a parallel polarization

dependence for both I and I* formation can be explained by assuming the exclusive absorption to $^3Q_0$ and the significant probability of subsequent curve crossing to the $^3Q_1$ or the ^1Q state. The observation of different I*/I branching ratios at 248 and 266 nm is not surprising because the extent of curve crossing is no doubt a function of excitation energy. In fact, based on the MCD results of Gedanken and Rowe[15] for CH_3I, it is reasonable to assume that excitation at a much higher energy part of the continuum would result in absorption to the ^1Q state in addition to the $^3Q_0$ state, yielding not only a different branching ratio, but a complicated combination of polarization dependences due to curve crossing from $^3Q_0$ to ^1Q and vice versa. We were limited in our experiment by current lasers, so we could only study the photodissociation process at two wavelengths, but when a tunable UV laser of sufficient power becomes available, it would be instructive to study the photodissociation of an alkyl iodide as a function of excitation energy. Such a study in combination with an MCD investigation should reveal underlying structure of the $n \longrightarrow \sigma^*$ continuum and the probability of curve crossing at various excitation energies.

B. Thermochemistry

Our data provide a direct measurement of the energy necessary to break both the C–I and C–Cl bonds in 1,2-chloroiodoethane (assuming no exit channel barrier for C_2H_4Cl decomposition.[24,28] The major error in our reported ΔH for reaction (5) is the uncertainty in the fits to the TOF distributions at mass 26, where a long counting time is required and we only have data at one angle. In order to obtain an accurate value, the fits to the slow side of the mass 26 TOF's must be reliable. The fact that the 248 nm experiment and the 266 nm experiment yield slightly different numbers (see Section III, part B) warrants a detailed comparison of the

two experiments. The uncertainty in the low translational energy side of the $P(E_T)$ distribution for each experiment can be seen in the shaded areas in Fig. 12, which correspond to the shaded regions of Figs. 9 and 10. Of course the uncertainties in the entire fits to the mass 26 TOF's will be comparable to that shown in the slow tails, but only the low translational energy threshold is of consequence in determining the total C–I plus C–Cl bond energy. In both experiments, the uncertainty in the fit represents about a 2 kcal/mole uncertainty in the threshold. Thus, the ranges of the two uncertainties overlap slightly. Nevertheless, we will not average the results of the two experiments, but rather, we will take the lower value, 76.5 ± 1 kcal/mole. The reason for our choice is as follows: because of the decreased temporal resolution due to the high velocity of the molecular beam in the 248 nm experiment and the relatively poor method in which we measured the beam velocity (holeburning), the molecular beam velocity used in the fits could easily be in error by 2%, which could shift the $P(E_T)$ distribution up to 1.5 kcal/mole. (The shaded area in Fig. 12 illustrates the error assuming a well known molecular beam velocity distribution.) In addition to the uncertainty in the beam velocity, the fact that the angular distribution could not be fit exactly makes suspect the use of the 248 nm experimental conditions to derive an energy accurate to ± 1 kcal/mole. In contrast, the 266 nm experiment was performed with a slow, carefully calibrated molecular beam, allowing good temporal resolution in the TOF data. The total error in the $P(E_T)$ due to the uncertainty in the beam velocity for this experiment should be no more than 0.5 kcal/mole. Therefore, the major uncertainty in the $P(E_T)$ is simply the statistical counting error.

Another possibility for error in the determination of the low energy threshold for the mass 26 derived $P(E_T)$ must be considered: the effect of the initial internal energy in the CH_2ClCH_2I parent. Since there are very few low frequency modes

(<700 cm^{-1}) in the parent, and since these modes will be partially relaxed in the expansion, the vibrational energy distribution will be roughly exponential with the maximum probability in the ground vibrational state.

If all the modes in the molecule were relaxed to their ground vibrational energy levels, the energy available (E^*_{avl}) would be well defined, and the $P(E_T)$ distribution obtained from the chloroethyl fragment would rise almost vertically from the minimum translational (maximum internal) energy allowed to the C_2H_4Cl radical. On the other hand, if the CH_2ClCH_2I parent were vibrationally excited, then E^*_{avl} would be raised by that amount of excitation. As the difference between E^*_{avl} and the point at which stable C_2H_4Cl radicals are observed is constant (i.e., the C–Cl bond energy of the radical), an increase in E^*_{avl} due to vibrational excitation of the parent must result in a shift toward higher energy in the position of the low translational energy threshold for the $P(E_T)$ obtained from the chloroethyl fragment. Because there is a maximum probability of all the parent molecules in the ground vibrational state, the observed threshold in the $P(E_T)$ will not be affected by E^P_{int}.

The distribution of vibrational energies will, however, change the shape of the $P(E_T)$ in the region of the threshold. The non-vertical rise which we observe can be explained by assuming that the shape of the $P(E_T)$ distribution is unchanged when E^*_{avl} is increased (in other words, assuming the net effect of the Franck-Condon factors is not altered when starting from higher vibrational levels). The entire $P(E_T)$ curve will then be shifted up in energy. The net result is a $P(E_T)$ distribution which is a convolution of $P(E_T)$ curves which arise from and are weighted by the vibrational energy distribution in the CH_2ClCH_2I parent. Hence, the low energy side of the mass 26 derived $P(E_T)$ will rise more gently than would be expected if all the parent modes were relaxed.

Rotational excitation will not be very important because of the efficient rota-

tional cooling in the molecular beam. The rotational temperature can be estimated by assuming it is equal to the terminal longitudinal translational temperature in the beam, which is related to the α parameter in the form for the velocity distribution (see Section II) by[23]

$$\alpha = \left(\frac{2kT}{m}\right)^{1/2}. \tag{6}$$

For the experiment at 266 nm, T $\cong$ 4 K, and at 248 nm, T$\cong$ 3 K. These temperatures correspond to negligible rotational energies.

One final consideration in the calculation of the C–I plus C–Cl bond energy is whether or not secondary dissociation occurs on a time scale short compared to the flight time from the interaction region to the ionizer. Using chloroethyl frequencies from Schlegel,[24] moments of inertia and activated complex frequencies estimated by Skinner and Rabinovitch,[28] and a C–Cl bond energy of 20 kcal/mole, we performed an RRKM calculation. The calculated lifetime of the chloroethyl radical with only 0.1 kcal/mole above the dissociation limit is $<10^{-8}$ sec, while the flight time to the ionizer is $\sim 10^{-4}$ to 10^{-5} sec. Consequently, there will be no possibility that any radical with more internal energy than $D_0^\circ(C_2H_4\text{–}Cl)$ could survive to be counted.

Given our result of 76.5 $\pm$ 1 kcal/mole for the ΔH at 0 K of reaction (5), the heat of formation $\Delta H_f^\circ(0)$of 1,2-chloroiodoethane follows directly (refer to Table II): $\Delta H_{f,0}^\circ(CH_2ClCH_2I)$ = –7.8 $\pm$ 1 kcal/mole. Using the method of group contributions,[29,30] the heat of formation of CH_2ClCH_2I can be estimated by adding $1/2[\Delta H_{f,0}^\circ(CH_2ClCH_2I)]$ and $1/2[\Delta H_{f,0}^\circ(CH_2ICH_2I)]$ to give –3.7 kcal/mole. Even in the limits of accuracy in the reported heats of formation, the two results disagree by about 2 kcal/mole. Because of the sparsity of thermochemical data on the 1,2-dihaloethanes containing two different halogens, the group contribution method of calculating ΔH_f°'s has not been tested very thoroughly. A 2-4 kcal/mole discrepancy between theory and experiment could be quite reasonable.

If the C–I bond energy of 1,2-chloroiodoethane were known, it would be a simple matter to obtain the C–Cl bond energy of the chloroethyl radical from our experimental results. $D_0^\circ(CH_2ClCH_2–I)$ can be estimated roughly by studying the changes in the heats of formation in the following scheme:

$$\begin{array}{ccc} CH_3CH_3 & \xrightarrow{-7.0} & CH_2ClCH_3 \\ \Big\downarrow{\scriptstyle 18.2} & & \Big\downarrow{\scriptstyle 15.5} \\ CH_3CH_2I & \xrightarrow[-9.7]{} & CH_2ClCH_2I \end{array} \qquad (7)$$

The numbers shown are the changes in $\Delta H_f^\circ(0)$ for each step in units of kcal/mole. It is seen that CH_2ClCH_2I is 2.7 kcal/mole more stable than we would predict assuming simple bond additivity in the heats of formation. This added stability of the molecule probably manifests itself in the inceased bond energy of the C–Cl, C–C, and C–I bonds, though the distribution of the energy is not clear. Weissman and Benson[31] estimate an increase of 2.5 kcal/mole in the C–C bond energy on going from CH_3CH_3 to CH_3CH_2Cl, and from CH_3CH_3 to CH_2ClCH_2Cl, they report an increase of 2.8 kcal/mole in the C–C bond energy. These numbers, while illustrating the chlorine substitution effect, are subject to errors of at least ± 1 kcal/mole. For our purpose, we will assume an increase of 1 kcal/mole in $D_0^\circ(CH_2ClCH_2–I)$ over $D_0^\circ(CH_3CH_2–I)$. The result is a C–I bond energy for 1,2-chloroiodoethane of 55.3 ± 1 kcal/mole (at 0 K), leading to: $D_0^\circ(C_2H_4–Cl) = 76.5 - 55.3 = 21.2 \pm 2$ kcal/mole and $\Delta H_{f,0}^\circ(C_2H_4Cl) = 21.9 \pm 2$ kcal/mole.

A comparison can be made with the chloroethyl radical heat of formation which we estimate and the $\Delta H_{f,0}^\circ(C_2H_4Cl)$ derived by different methods. Assuming $D_0^\circ(CH_3CH_2–H) = D_0^\circ(CH_2ClCH_2–H)$, then $\Delta H_{f,0}^\circ(C_2H_4Cl)$ is calculated from data in Table II to be 23.6 ± 1 kcal/mole. Schlegel and Sosa[24] have performed *ab initio* calculation for the reaction of Cl with C_2H_4, where they report a theoretical value

of 19.5 ± 2 kcal/mole for the C–Cl bond energy of the chloroethyl radical at 0 K, corresponding to a $\Delta H^{\circ}_{f,0}(C_2H_4Cl)$ of 23.6 ± 2 kcal/mole. Within the reported limits of accuracy, all the values agree. However, since bond dissociation energies in many chlorinated ethanes depend on the heat of formation of the 2-chloroethyl radical, it will be advantageous to narrow the limits of uncertainty.

REFERENCES

1. (a)R. S. Mulliken, Phys. Rev. **50**, 1017 (1936); (b)bf 51,310 (1937); (c) **45**, 413 (1935);(d) J. Chem. Phys. **8**, 382 (1940).

2. R. A. Boschi and D. R. Salahub, Mol. Phys. **24**(2), 289 (1972).

3. D. Porret and C. F. Goodeve, Proc. Roy. Soc. Ser. A **165**, 31 (1938).

4. J. V. V. Kasper and G. C. Pimentel, Appl. Phys. Lett. **5**, 231 (1964).

5. (a) J. V. V. Kasper, J. H. Parker, and G. C. Pimentel, J. Chem. Phys. **43**, 1827 (1965) (b) M. A. Pollack, Appl. Phys. Lett. **8**, 36 (1966)

6. D. Husain and R. J. Donovan, Adv. Photochem. **8**, 1 (1971).

7. M. Dzvonik, S. Yang, and R. Bersohn, J. Chem. Phys. **61**, 4408 (1974).

8. S. Riley and K. Wilson, Discuss. Faraday Soc. **53**, 132 (1972).

9. R. K. Sparks, K. Shobatake, L. R. Carlson, and Y. T. Lee, J. Chem. **75**(8), 3838 (1981).

10. D. J. Krajnovich, Ph.D. thesis, University of California, Berkeley, 1983.

11. D. J. Krajnovich, L. J. Butler, and Y. T. Lee J. Chem. Phys. **81**, 3031 (1984).

12. R. D. Clear, S. J. Riley, and K. R. Wilson, J. Chem. Phys. **63**, 1340 (1975).

13. G. N. A. van Veen, T. Baller, A. E. de Vries, and N. J. A. van Veen, Chem Phys. **87**, 405 (1984).

14. R. J. Oldman, R. K. Sander, and K. R. Wilson, J. Chem. Phys. **54**, 4127 (1971).

15. A. Gedanken and M. D. Rowe, Chem. Phys. Lett. **34**, 39 (1975)

16. G. E. Busch, J. F. Cornelius, R. T. Mahoney, R. I. Morse, D. W. Schlosser, and K. R. Wilson, Rev. Sci. Instrum. **41**, 1066 (1970).

17. K. R. Wilson, in *Chemistry of the Excited State*, edited by J. N. Pitts, Jr. (Gordon and Breach, New York, 1970), pp. 33-55.

18. G. E. Busch and K. R. Wilson, J. Chem. Phys. **56**, 3626 (1972); (b) **56**, 3638 (1972).

19. T. F. Hunter, S. Lunt, and K. S. Kristjansson, J. Chem. Soc., Faraday Trans. 2 **79**, 303 (1983).

20. P. Brewer, P. Das, G. Ondrey, and R. Bersohn, J. Chem. Phys. **79**, 720 (1983).

21. S. L. Baughcum and S. R. Leone, J. Chem. Phys. **72**, 6531 (1980).

22. Y. T. Lee, J. D. McDonald, P. R. LeBreton, and D. R. Herschbach, Rev. Sci. Instrum. **40**, 1402 (1969).

23. R. B. Bernstein, *Chemical Dynamics via Molecular Beam and Laser Techniques* (Oxford University Press, New York, 1982) p. 30.

24. H. B. Schlegel and C. Sosa, J. Phys. Chem. **88**, 1141 (1984).

25. F. Huisken, D. Krajnovich, Z. Zhang, Y. R. Shen, and Y. T. Lee, J. Chem. Phys. **78**, 3086 (1983).

26. T. Donohue and J. R. Wiesenfeld, J. Chem. Phys. **63**, 3130 (1975).

27. T. F. Hunter and K. S. Kristjansson, Chem. Phys. Lett. **58**, 291 (1978).

28. G. B. Skinner and B. S. Rabinovitch, Bull. Soc. Chim. Belg. **82**, 305 (1973).

29. S. W. Benson, F. R. Cruickshank, D. M. Golden, G. R. Haugen, H. E. O'Neal, A. S. Rodgers, R. Shaw, R. Walsh, Chem, Rev. **69**, 279 (1969).

30. S. W. Benson, *Thermochemical Kinetics*, 2nd ed. (Wiley, New York, 1976).

31. M. Weissman and S. Benson, J. Phys. Chem. **87**, 243 (1983).

32. JANAF *Thermochemical Tables*, 2nd ed. Natl. Stand. Ref. Data Ser., U. S. Natl. Bur. Stand. **37**, (U. S. GPO, Washington D. C., 1971).

33. S. W. Benson, J. Chem. Ed. **42**, 502 (1965).

34. A. L. Castelhano, P. R. Marriott, and D. Griller, J. Am. Chem. Soc. **103**, 4262 (1981).

35. S. W. Benson and A. Amano, J. Chem. Phys. **36**, 3464 (1962).

36. J. R. Lacher, A. Amador, and J. D. Park, Trans. Faraday Soc. **63**, 1608 (1967).

37. J. Chao, A. S. Rodgers, R. C. Wilhoit, and B. J. Zwolinski, J. Phys. Chem. Ref. Data **3**, 143 (1974).

38. J. C. Traeger and R. G. McLoughlin, J. Am. Chem. Soc. **103**, 3647 (1981).

TABLE I. $I^*(^2P_{1/2})$ quantum yields for CH_3I photolysis at 266 and 248 nm.

λ(nm)	Φ_I^*	Method	Reference
266	0.70	photofragment spectroscopy	9[a]
266	~0.78	photofragment spectroscopy	8
266	0.77	optoacoustic	19[b]
248	0.81	infrared emission	21
248	0.71	photofragment spectroscopy	13
248	0.59	optoacoustic	19[b]

[a]Taken from translational energy distributions.

[b]Esitmated from plot.

TABLE II. Standard molar enthalpies of formation for some substances at 300 K and 0 K.

Species	ΔH_f°(300 K) (kcal/mole)	ΔH_f°(0 K) (kcal/mole)	Reference
Cl	28.92±0.03	28.52±0.03	32
H	52.103±0.001	51.631±0.001	32
I	25.53±0.01	25.63±0.01	32
CH_3I	3.4±0.3	5.7±0.3[a]	34
$CH_2{=}CH_2$	12.53±0.07	14.58±0.07	32
CH_3CH_3	−20.08±0.05	−16.33±0.05[a]	38
CH_3CH_2Cl	−26.83±0.18	−23.3±0.2[a]	37
CH_2ClCH_2Cl	−30.2±1	−27.1±1[a]	36
CH_3CH_2I	−2.0±0.4	1.9±0.5[a]	34
CH_2ICH_2I	15.9±0.2	19.7±0.3[a]	35
CH_2ClCH_2I	−11.37±1.2[a]	−7.8±1.0	this work
CH_3	34.4±0.4	35.2±0.4	38
CH_3CH_2	28.0±1.0	30.6±1.0[a]	34
CH_2ClCH_2	21.2±1.0[a]	23.6±1.0[b]	estimate

[a]Calculated by correcting for thermal energy (Ref. 33)

[b]Calculated assuming $D_0^\circ(CH_2ClCH_2\text{–}H) = D_0^\circ(CH_3CH_2\text{–}H)$ (see the text)

FIGURE CAPTIONS

Figure 1. Schematic diagram of the center-of-mass velocity distribution for the two recoiling photodissociation products. The shaded area depicts those C_2H_4Cl radicals with slow velocities, or low translational energies, which have enough internal excitation to dissociate into C_2H_4 and Cl. From conservation of momentum, detection of either fragment should yield the total c.m. translational energy distribution. However, because of secondary dissociation of the chloroethyl product, the iodine fragment is monitored to provide the lost information.

Figure 2. Schematic diagram of the experimental appartus. The numbers correspond to pressures in Torr for the various regions.

Figure 3. Laboratory TOF distributions of I atom product at 266 nm for five detector angles. o Experimental points; —— calculated using the $P(E_T)$ in Figure 12 and $\beta = 1.8$.

Figure 4. Laboratory TOF distributions of I atom product at 248 nm for four detector angles. o Experimental points; —— calculated using the $P(E_T)$ in Figure 12 and $\beta = 1.8$.

Figure 5. Newton diagram representing photodissociation of CH_2ClCH_2I at 248 nm with detection of iodine. Velocity vectors shown are the molecular beam velocity $\mathbf{V}_b$, the center-of-mass velocity of the I fragment $\mathbf{V}_{cm}$, and the laboratory velocity of the I fragment $\mathbf{V}_{lab}$. The relevant angles are the c.m. angle θ and the laboratory angle Θ.

Figure 6. Laboratory angular distribution of I atom product at 266 nm. ● Exper-

imental points, obtained by integrating and normalizing the TOF distributions in Figure 3 (except for the point at 35°). $\pm 2\sigma$ error bars are smaller than the symbols. —— $\beta = 1.8$; - - - $\beta = 1.7$; - - - - $\beta = 1.9$.

Figure 7. Laboratory angular distribution of I atom product at 248 nm. ● Experimental points, obtained by integrating and normalizing many different TOF distributions. $\pm 2\sigma$ error bars are smaller than the symbols. —— $\beta = 1.8$; - - - $\beta = 1.9$; - - - - $\beta = 2.0$.

Figure 8. Laboratory TOF distribution of all products detected at $m/e = 26$ at 248 nm for $\Theta = 10°$. Only the experimental points are shown.

Figure 9. Blow-up of the region including the spike in Figure 8. The peak here arises from the $m/e = 26$ fragment of the stable C_2H_4Cl radicals. o Experimental points; —— best fit calculated using the $P(E_T)$ in Figure 11 and $\beta = 1.8$. The shaded region illustrates the uncertainty in the fit to the slow tail which gives rise to an uncertainty of ± 1 kcal/mole in the low translational energy side of the $P(E_T)$ distribution.

Figure 10. Laboratory TOF distribution of C_2H_4Cl product (detected at $m/e = 26$) at 266 nm for $\Theta = 7°$. o Experimental points; —— best fit calculated using $P(E_T)$ in Figure 11 and $\beta = 1.8$. The shaded region illustrates the uncertainty in the fit to the slow tail which gives rise to an uncertainty of ±1 kcal/mole in the low translational energy side of the $P(E_T)$ distribution.

Figure 11. Laboratory TOF distribution of products detected at $m/e = 35$ at 248 nm for $\Theta = 10°$. Only experimental points are shown.

Figure 12. C.M. recoil translational energy distributions for 1,2-chloroiodoethane photodissociation at 248 and 266 nm. —— Total $P(E_T)$ derived from fitting TOF's of iodine fragment. – – – Derived from measurement of C_2H_4Cl fragment; with the exception of the low translational energy section, this curve corresponds to formation of $I^*(^2P_{1/2})$ because $I(^2P_{3/2})$formation leads to complete secondary dissociation of the radical. - - - - $P(E_T)$ for I^* subtracted from total $P(E_T)$ giving the $P(E_T)$ for ground state I formation. E_{avl} is the excess energy after breaking the C–I bond in CH_2ClCH_2I. E^*_{avl} is E_{avl} minus the I atom spin-orbit excitation (21.7 kcal/mole). Total fragment internal energy is given by E_{avl} (or E^*_{avl}) minus the c.m. translational energy. The shaded areas show the uncertainty in the low energy side of the $P(E_T)$ derived from mass 26 TOF data, which arises from the uncertainty in the fits to the slow tails in Figures 8 and 9. The resulting uncertainty in the low energy thresholds of the $P(E_T)$'s is ±1 kcal/mole.

Figure 13. Energy level diagram for the photodissociation of CH_2ClCH_2I at 248 and 266 nm.

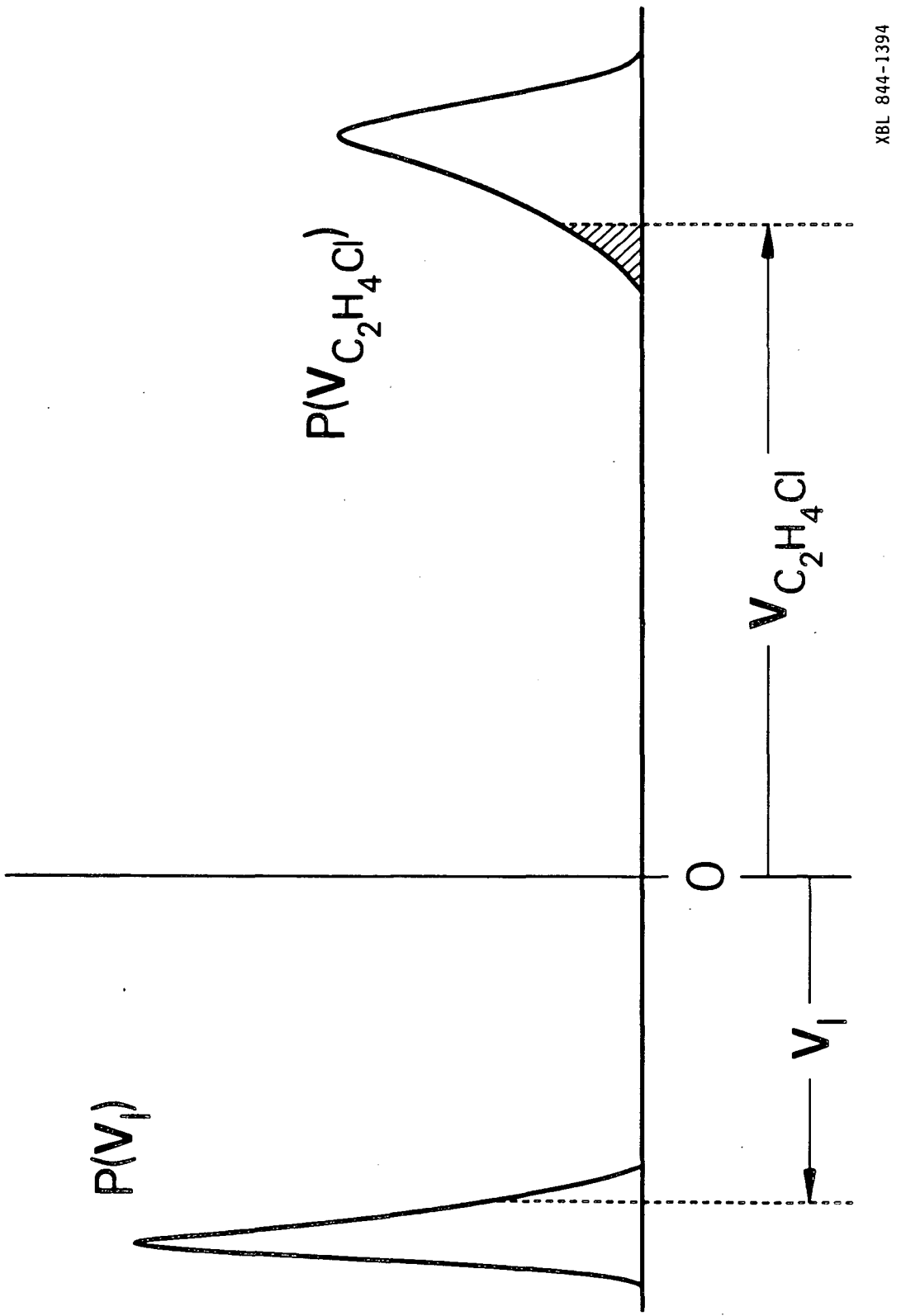

Figure 1

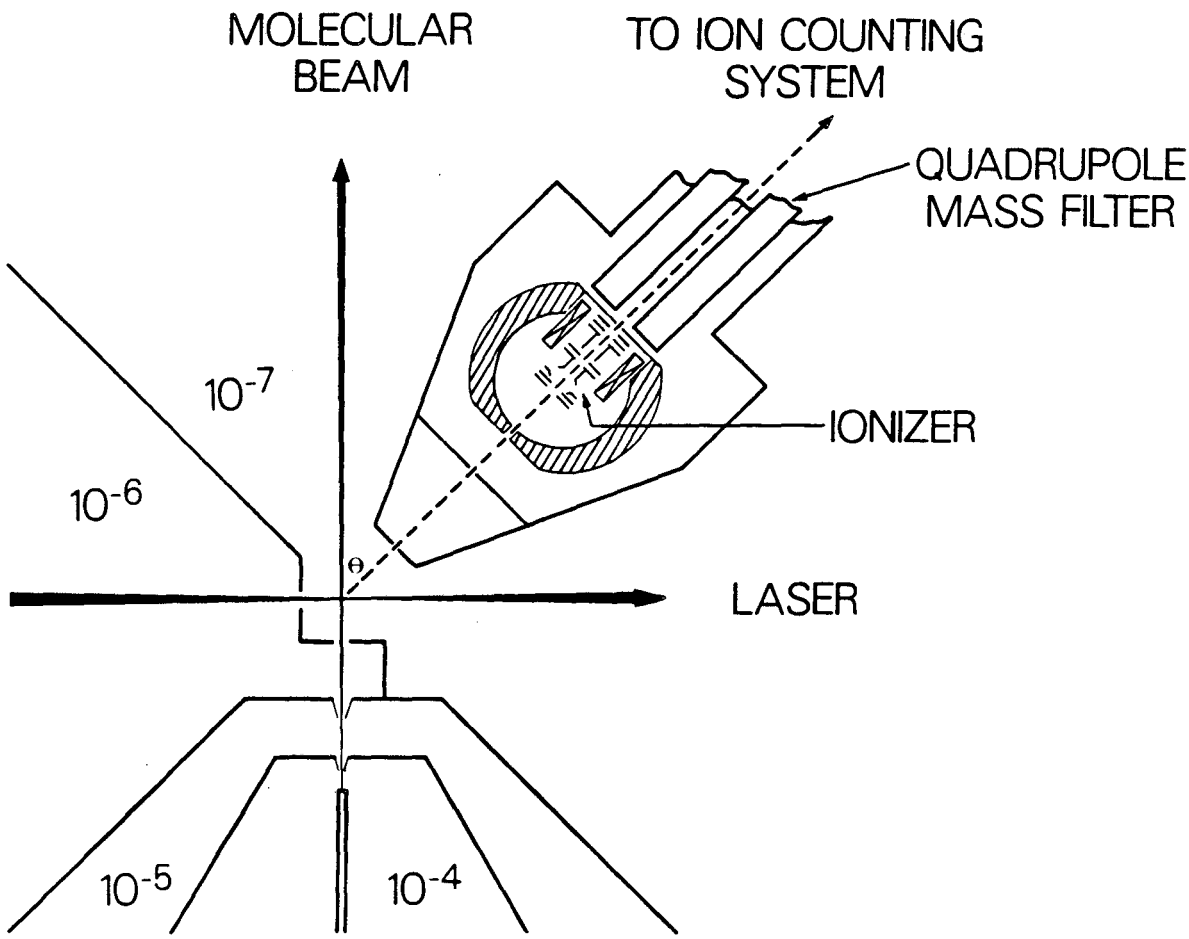

XBL 844-1401

Figure 2

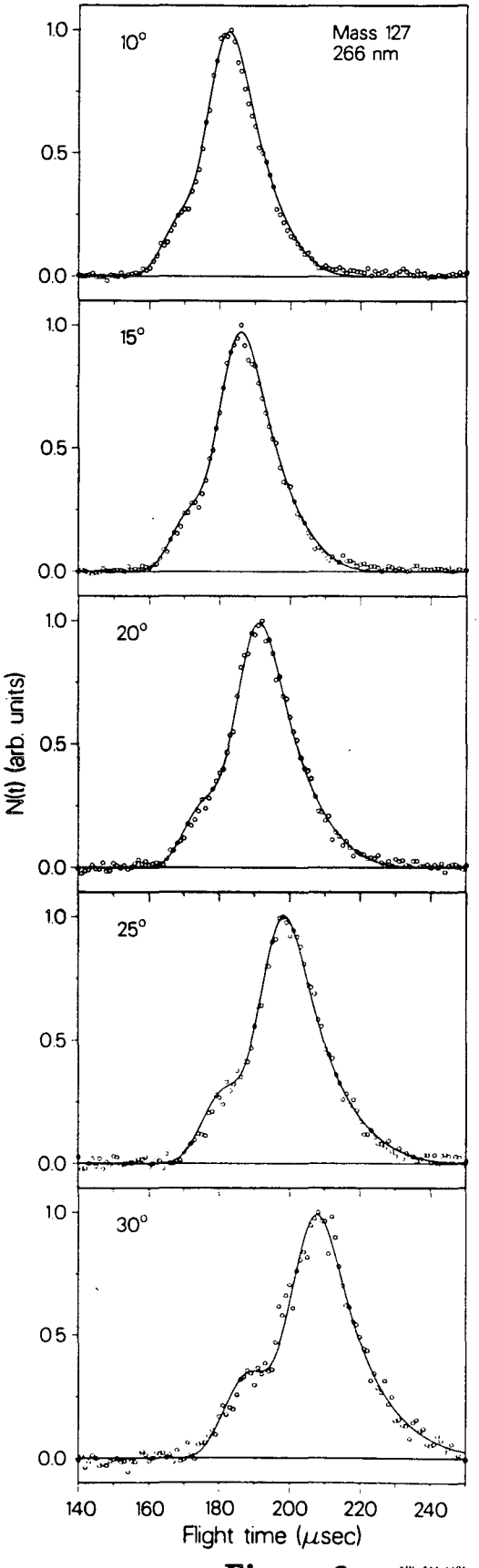
Mass 127
266 nm
10°
15°
20°
25°
30°
1.0
0.5
0.0
N(t) (arb. units)
140
160
180
200
220
240
Flight time (μsec)

Figure 3

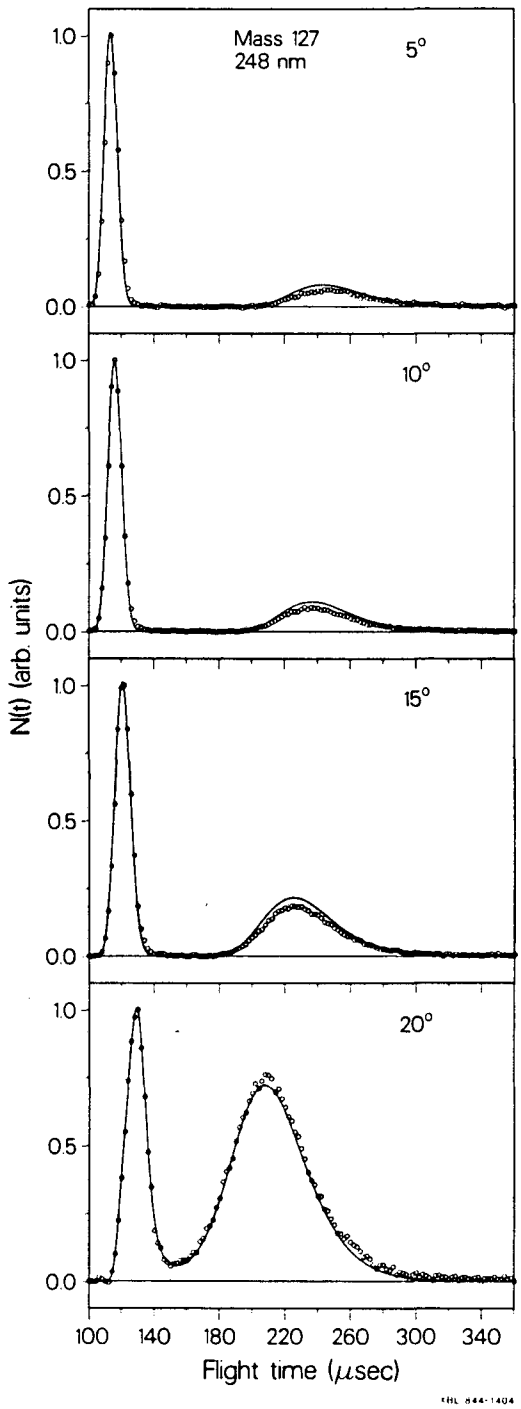
Mass 127
248 nm
5°
10°
15°
20°
1.0
0.5
0.0
N(t) (arb. units)
100
140
180
220
260
300
340
Flight time (μsec)

Figure 4

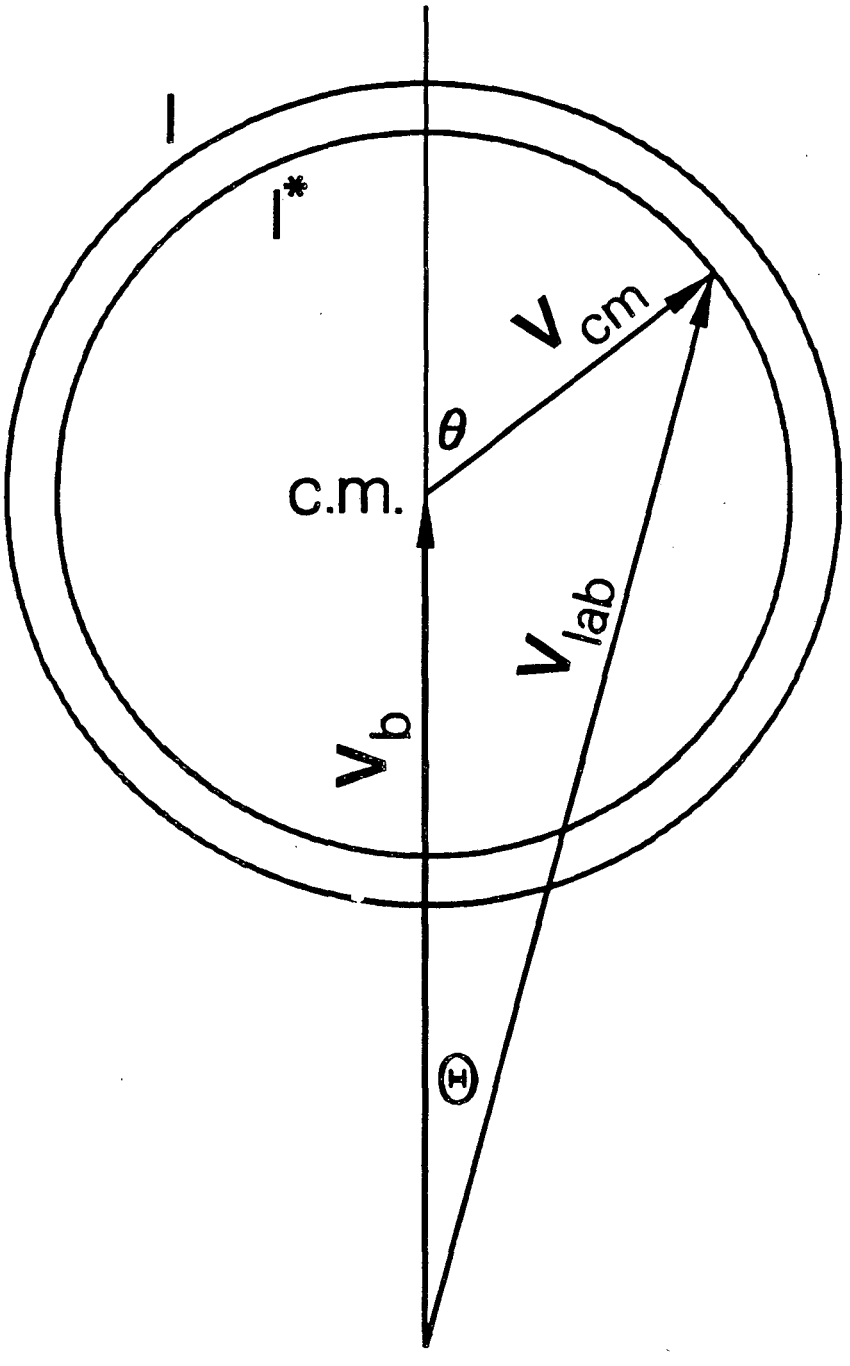

XBL 844-1402

Figure 5

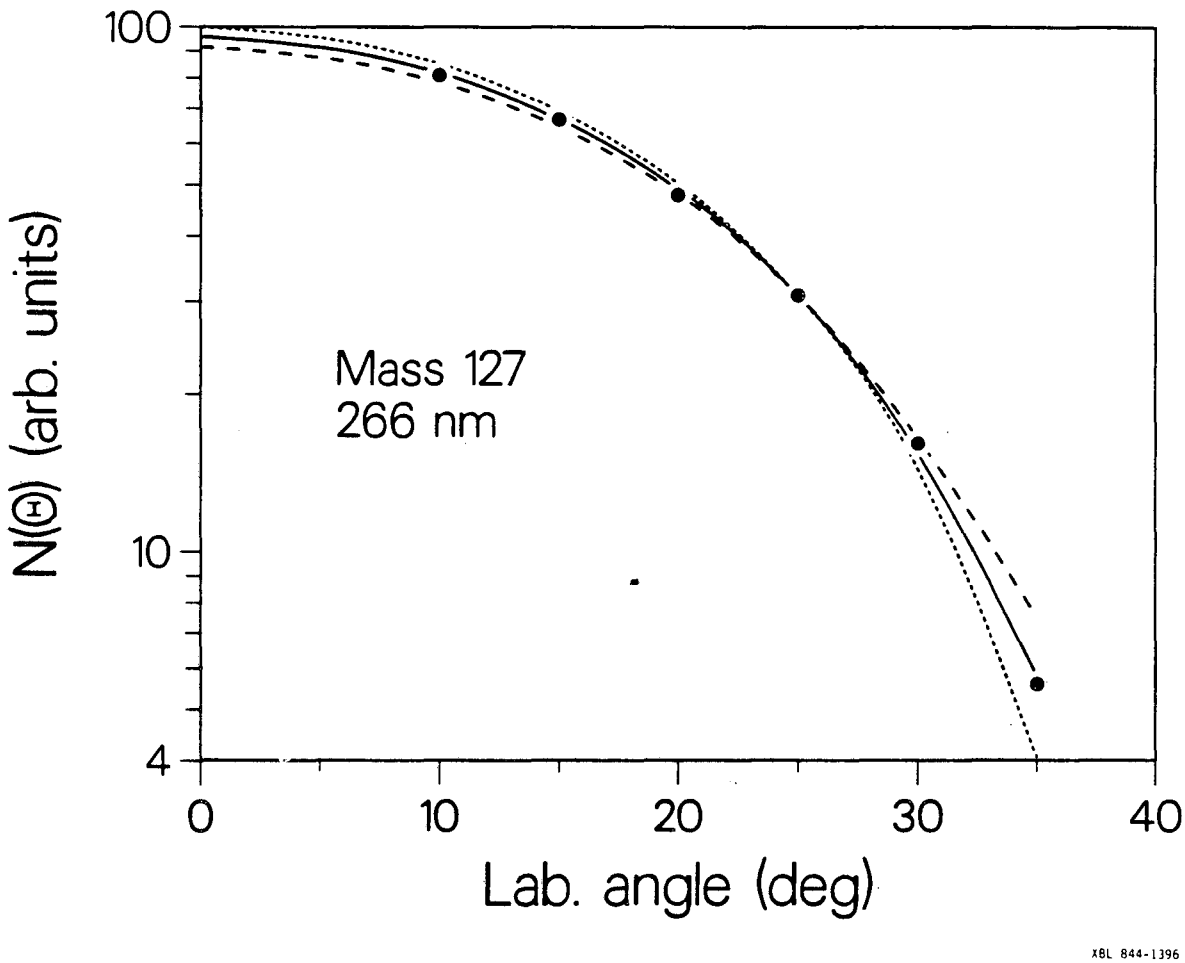
100
10
4
N(Θ) (arb. units)
Mass 127
266 nm
0
10
20
30
40
Lab. angle (deg)
XBL 844-1396

Figure 6

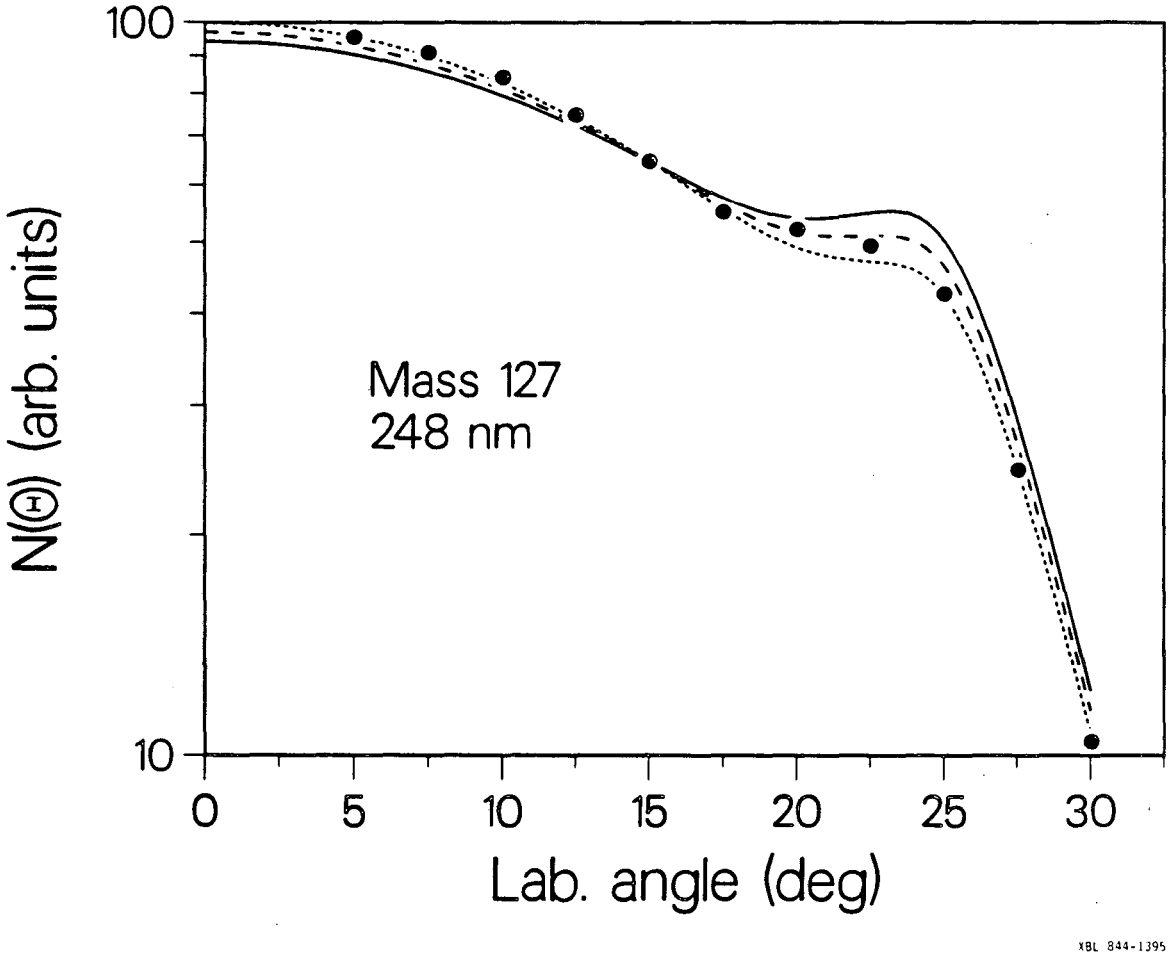
100
10
N(Θ) (arb. units)
Mass 127
248 nm
0
5
10
15
20
25
30
Lab. angle (deg)
XBL 844-1395

Figure 7

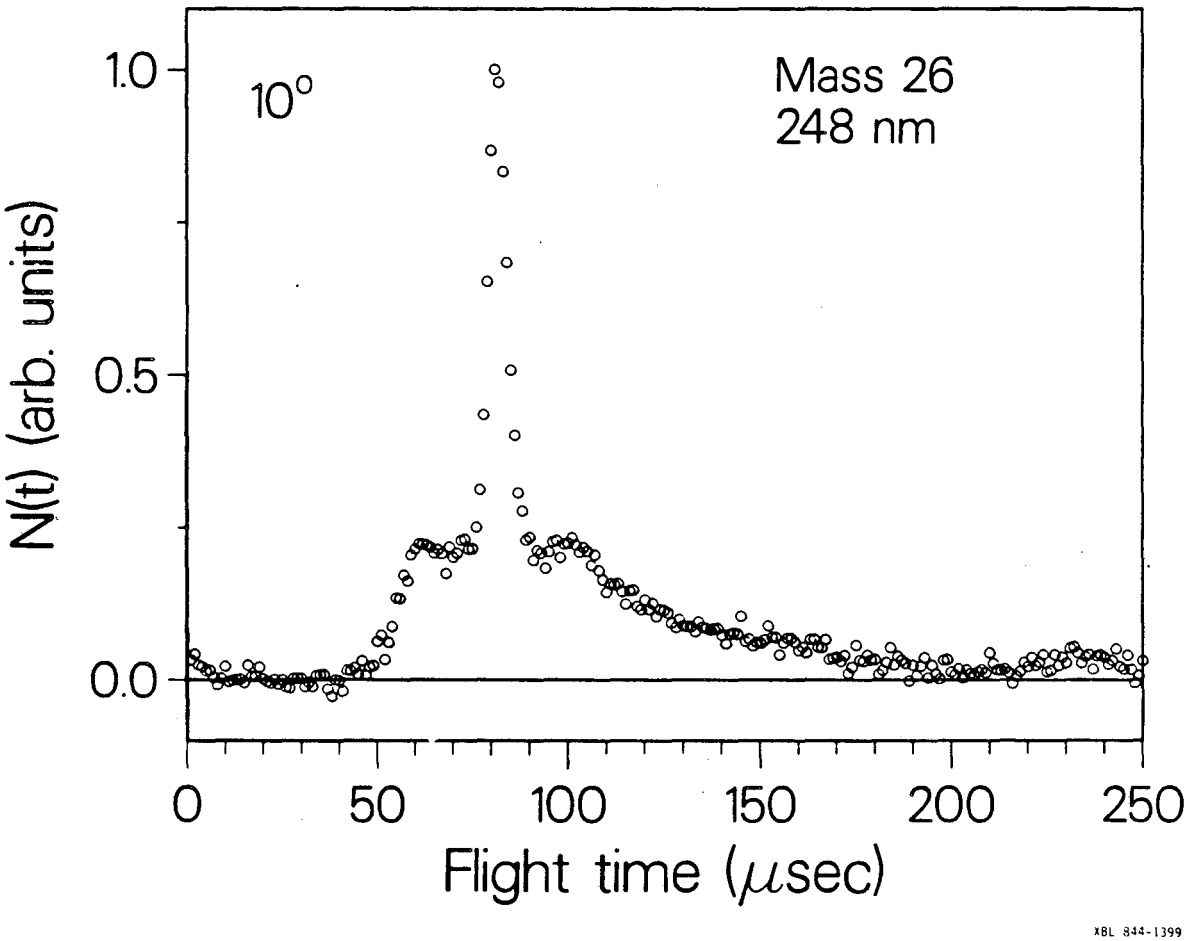
1.0
0.5
0.0
10°
Mass 26
248 nm
N(t) (arb. units)
0
50
100
150
200
250
Flight time (μsec)
XBL 844-1399

Figure 8

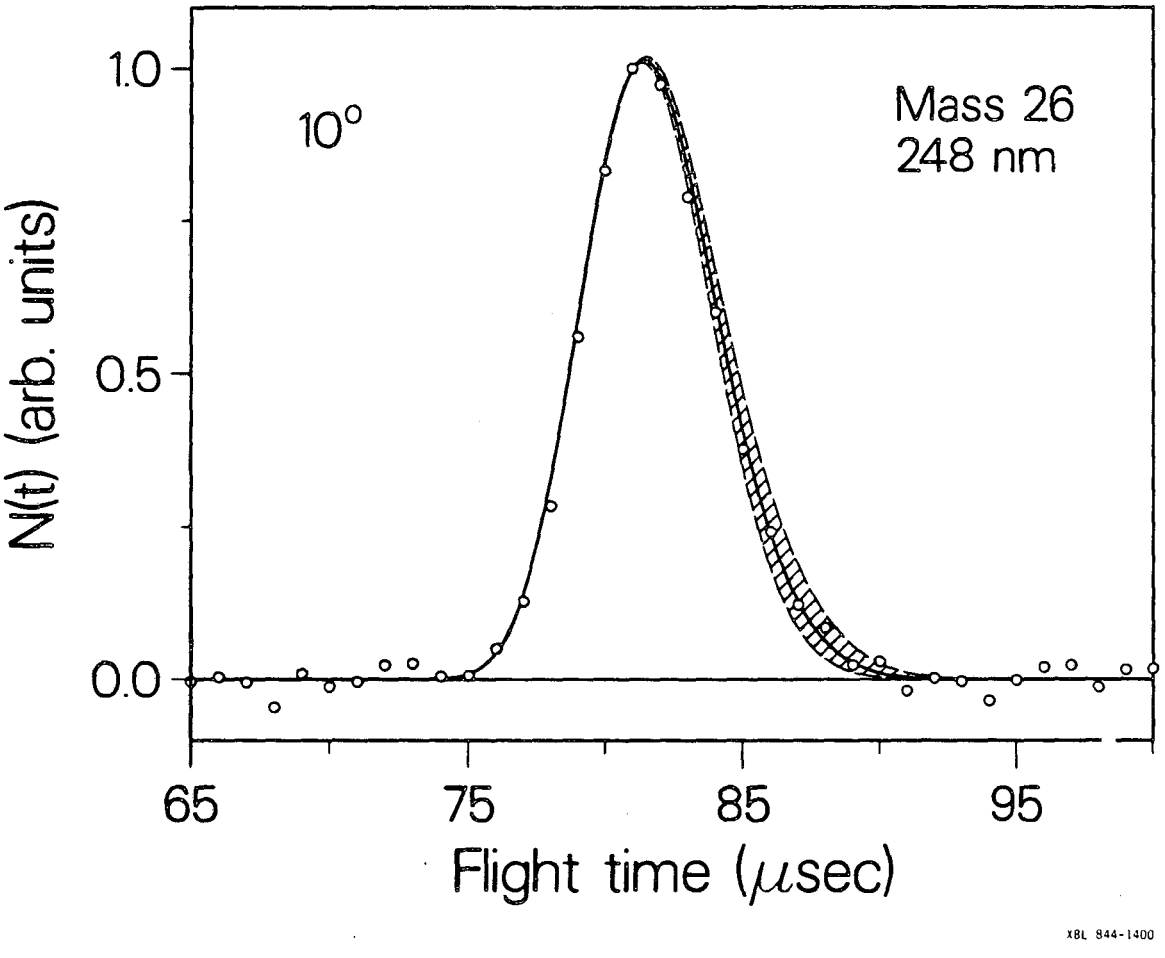
1.0
0.5
0.0
N(t) (arb. units)
10°
Mass 26
248 nm
65
75
85
95
Flight time (μsec)
XBL 844-1400

Figure 9

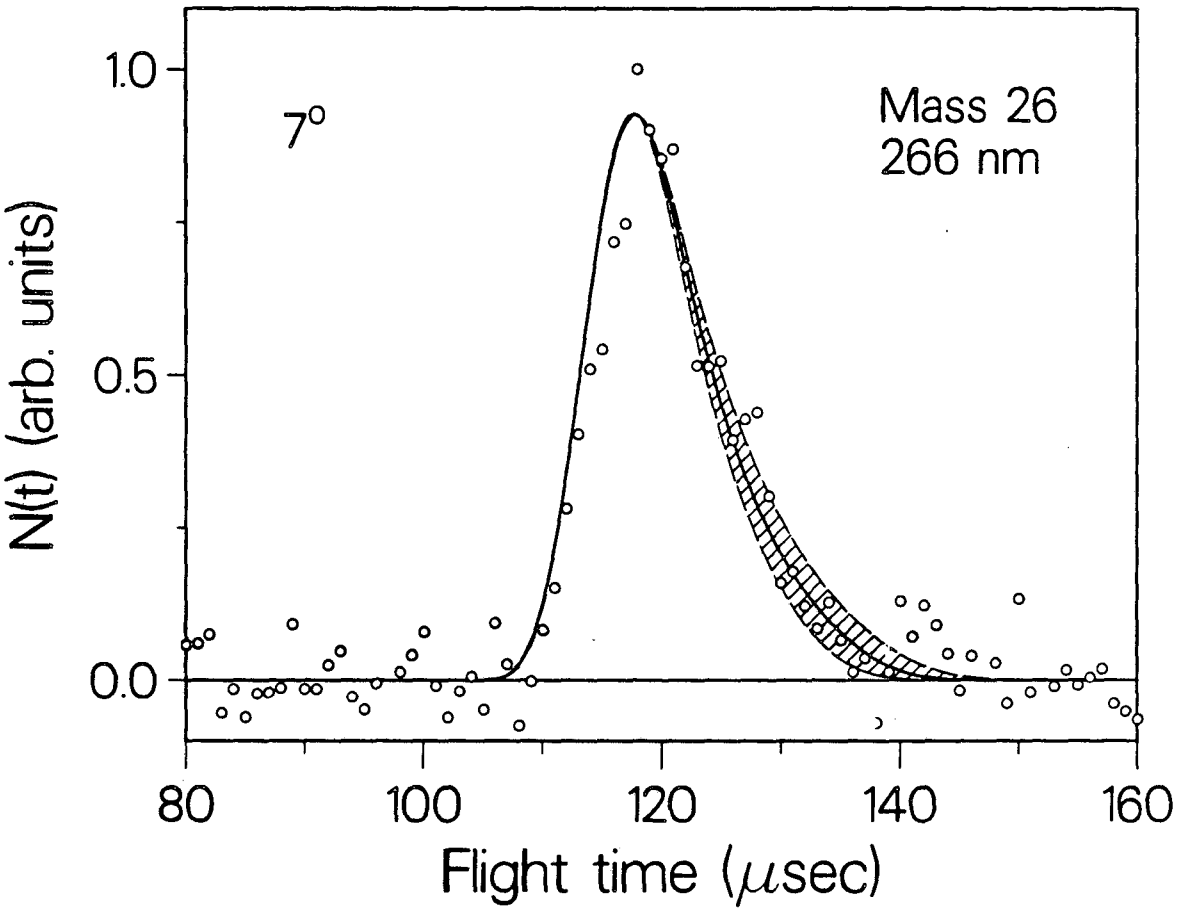
1.0
0.5
0.0
N(t) (arb. units)
7°
Mass 26
266 nm
80
100
120
140
160
Flight time (μsec)
XBL 844-1397

Figure 10

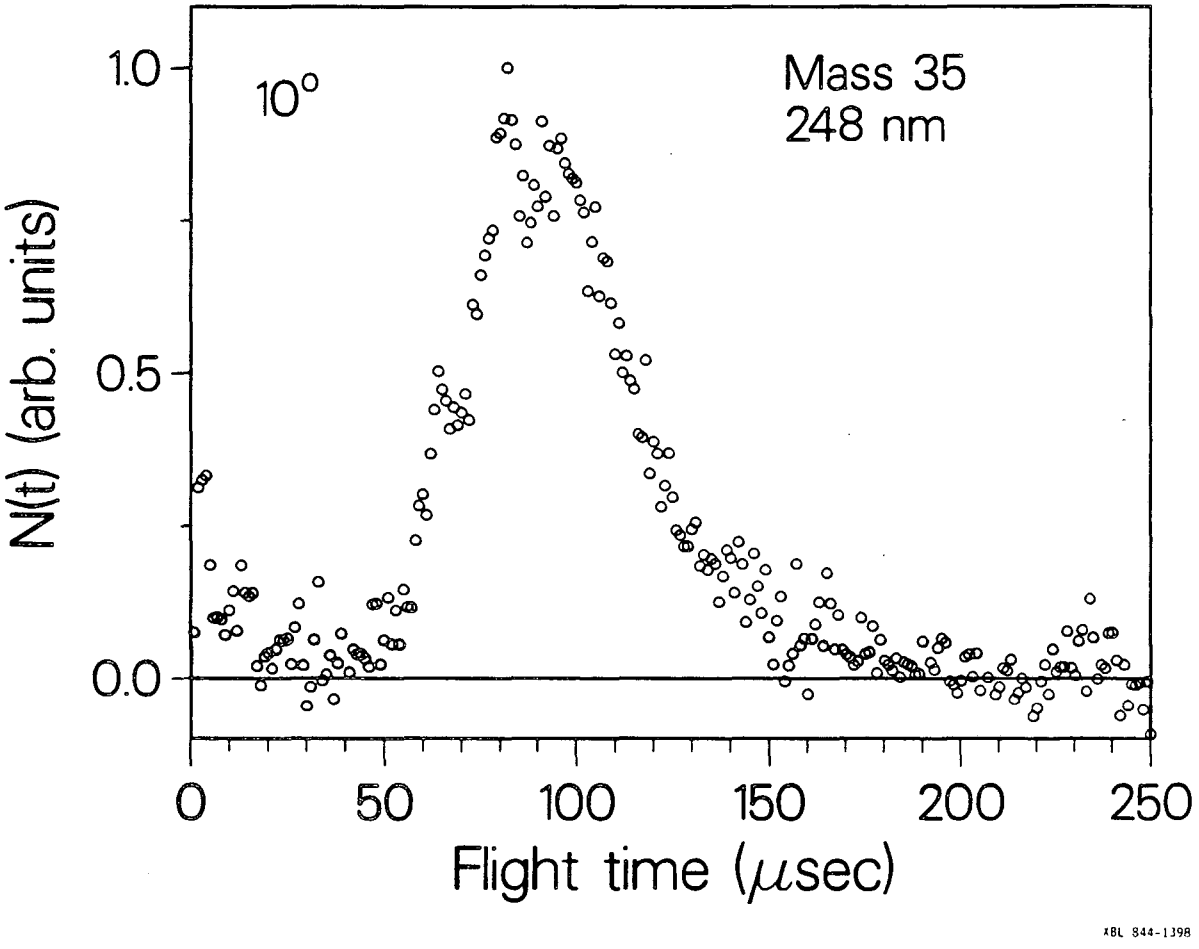
1.0
0.5
0.0
10°
Mass 35
248 nm
N(t) (arb. units)
0
50
100
150
200
250
Flight time (μsec)
XBL 844-1198

Figure 11

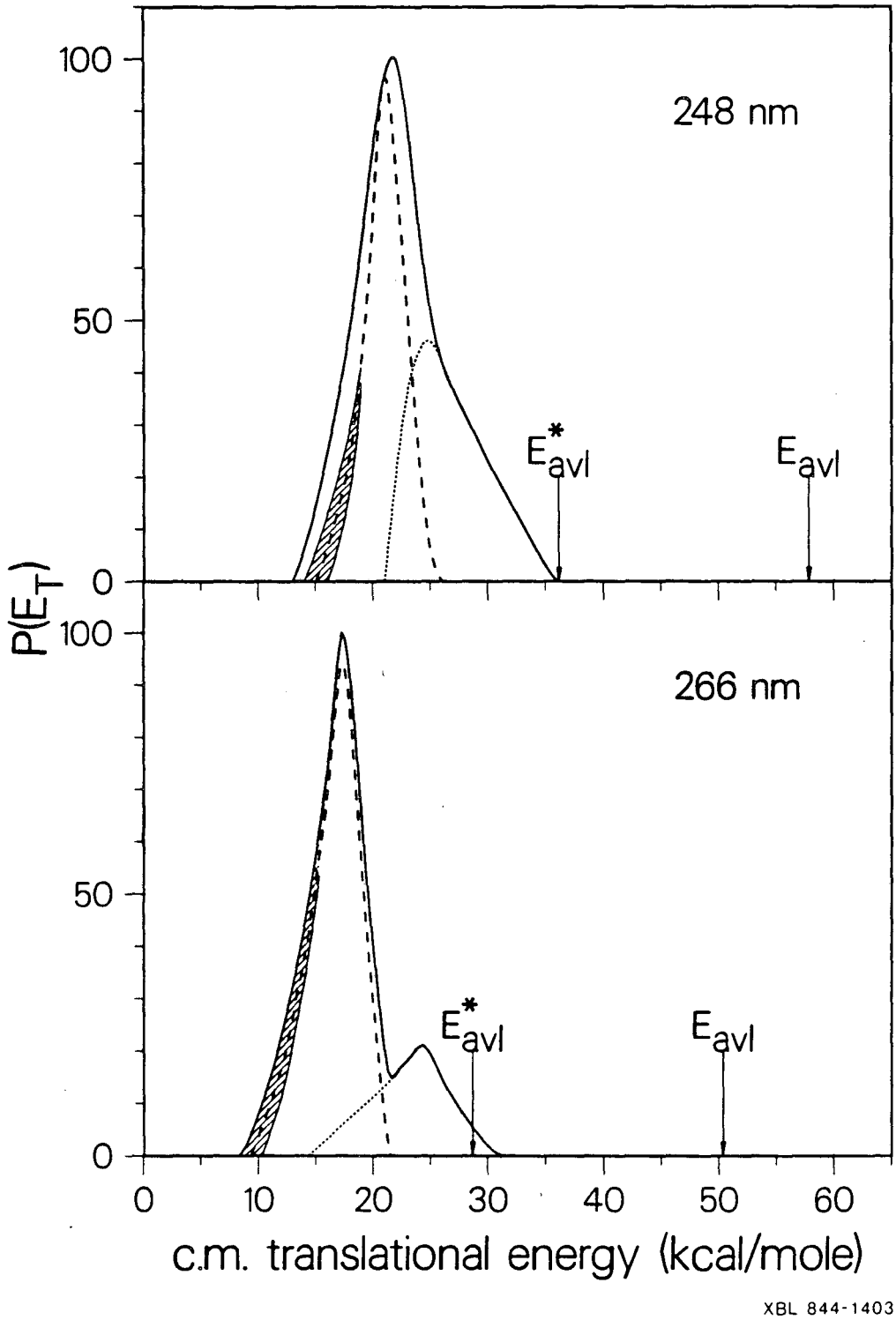
100
50
0
248 nm
E^*_{avl}
E_{avl}
$P(E_T)$
100
50
0
266 nm
E^*_{avl}
E_{avl}
0
10
20
30
40
50
60
c.m. translational energy (kcal/mole)
XBL 844-1403

Figure 12

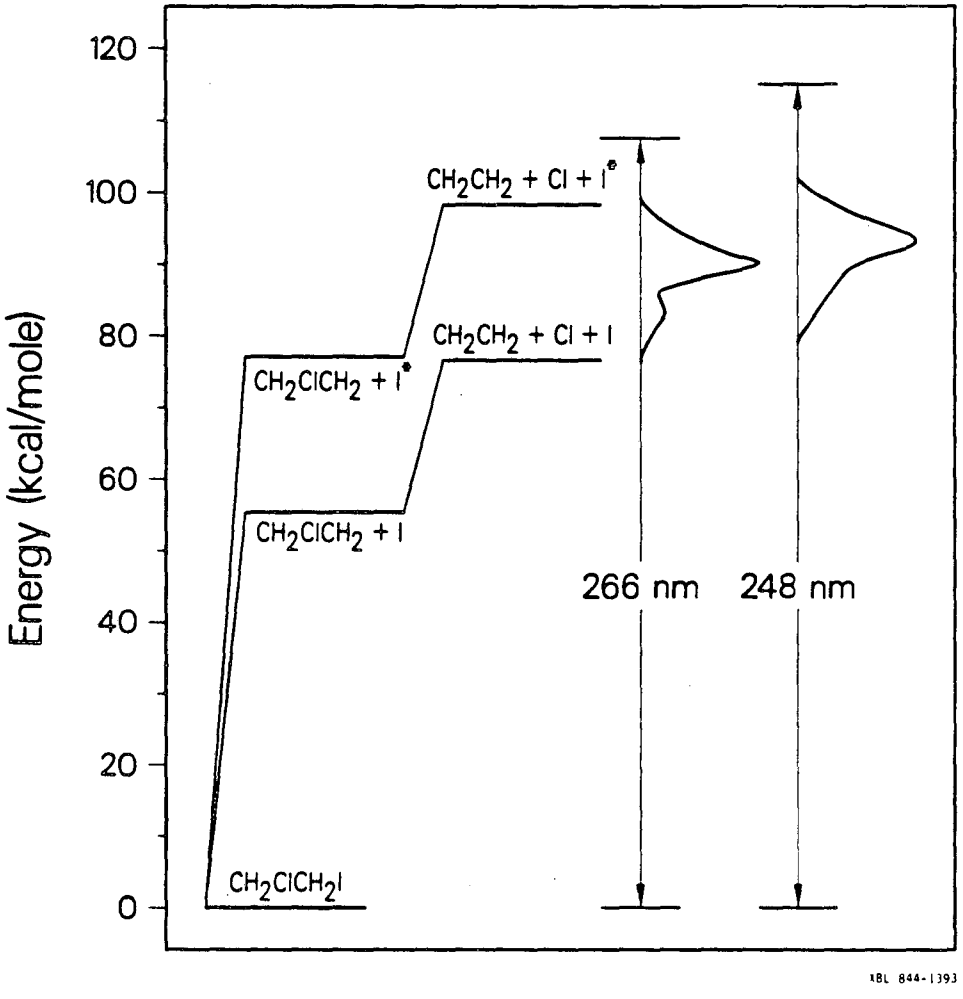
120
100
80
60
40
20
0
Energy (kcal/mole)
$CH_2CH_2 + Cl + I^*$
$CH_2CH_2 + Cl + I$
$CH_2ClCH_2 + I^*$
$CH_2ClCH_2 + I$
CH_2ClCH_2I
266 nm
248 nm
XBL 844-1393

Figure 13

Chapter 2

Photodissociation of CH_2ClCH_2I at 308 nm

I. INTRODUCTION

The photodissociation dynamics of CH_2ClCH_2I have been studied previously in our laboratory at 248 and 266 nm,[1] where an $n \longrightarrow \sigma^*$ absorption localized on the C–I bond is expected to occur. The translational energy distributions and angular distributions show that two dissociation pathways exist, leading to formation of either ground or spin-orbit excited state iodine, and that both channels at both excitation wavelengths originate from a parallel transition—i.e., the transition moment must be nearly parallel to the C–I bond. Even though the polarization dependence is the same at both wavelengths, the $I(^2P_{1/2})/I(^2P_{3/2})$ branching ratios differ significantly (1.5 at 248 nm and 3.0 at 266 nm). These observations do not fully conform to the commonly employed quasi-diatomic model,[2] which is an extension of Mulliken's description of the $n \longrightarrow \sigma^*$ absorption band in the hydrogen halides, the interhalogens, and methyl iodide.[3] This model predicts a parallel polarization dependence for the $I(^2P_{1/2})$ dissociation channel and a perpendicular dependence for $I(^2P_{3/2})$ formation. Consequently, the model provides no explanation for the different branching ratios. By investigating the photofragmentation of many iodoethanes at different wavelengths, we hope that some trends will emerge, leading to a better understanding of the $n \longrightarrow \sigma^*$ continuum in haloethanes. Accordingly, we have extended the data on CH_2ClCH_2I to include a third excitation wavelength

at the low energy (long wavelength) tail of the $n \longrightarrow \sigma^*$ continuum.[4]

II. EXPERIMENT

The experimental apparatus and conditions were virtually identical to those described elsewhere (in the next chapter), and we will only briefly describe them here. The apparatus has a rotatable molecular beam source with a fixed mass spectrometer detector. A 308 nm excimer laser beam, which was focused to a spot size of 3 mm × 0.4 mm, crossed the molecular beam perpendicularly to the plane of the molecular beam and detector. Time-of-flight (TOF) measurements of the photofragments were taken with two laser polarizations: horizontal and vertical (parallel and perpendicular, respectively, to the detector axis). Average laser pulse energies were 9.9 mJ for horizontal polarization and 15.4 mJ for vertical polarization. Laser saturation was unimportant at these energies because the absorption cross section at 308 nm is very low ($< 10^{-19}$ cm^2—see ref. 4 and the following chapter). The gas mixture for the molecular beam was formed by bubbling Ar through liquid CH_2ClCH_2I, maintained at 20°C (vapor press. = 7 Torr), to make a total stagnation pressure of 300 Torr. The mixture was allowed to expand through a 0.005 in. (0.125 mm) diameter nozzle, heated to 250°C to prevent dimer formation. Signal could only be detected at $m/e = 127$ (I^+), and TOF data at this mass were taken at source angles of 20° and 40° (horizontal polarization) with count rates of 0.052 and 0.034 counts/laser pulse, respectively. One TOF was recorded with vertical laser polarization at 20° with a count rate of 0.021 counts/pulse.

III. RESULTS AND ANALYSIS

The center-of-mass (c.m.) translational energy distribution $P(E_T)$ and the c.m. angular distribution $w(\theta)$ for the photofragments are derived from our experimental,

laboratory TOF distributions $N(t)$ and angular distributions $N(\Theta)$ by a forward convolution technique (see Chapters 1 and 3), where we assume that the c.m. flux distribution I_{cm} is given by the product, $I_{cm}(E_T, \theta) = P(E_T)w(\theta)$. The form of the c.m. angular distribution is[5]

$$w(\theta) \propto 1 + \beta P_2(\cos\theta), \tag{1}$$

where θ is the angle between the electric vector of the laser light and the c.m. recoil direction of the products. β is the anisotropy parameter, which we derive, and it is equal to 2.0 for a purely parallel transition ($w(\theta) \propto \cos^2\theta$) and −1.0 for a purely perpendicular transition ($w(\theta) \propto \sin^2\theta$).

Figure 1 shows the TOF data, along with the best fits (using the $P(E_T)$ distribution in Figure 2), for the iodine fragment. Unlike the previous CH_2ClCH_2I experiments at 248 and 266 nm,[1] these data do not exhibit two distinct components, suggesting that only one spin-orbit state of iodine is formed in the dissociation process.

The anisotropy parameter was found by two methods. First, we compared the integrated signal ratio for horizontal and vertical polarization to the ratios calculated for different β values. Second, we compared the ratio of the signals at 20° and 40° for fixed horizontal polarization to the ratios calculated for various β's. The results are summarized in Table I. The two best fit β parameters are different; however, the table shows that the horizontal/vertical angular dependence is much more sensitive to β than the 20°/40° angular scan. Therefore, using only the more reliable angular dependence, we will take as the value of the anisotropy parameter: $\beta = 1.75 \pm 0.2$. The assigned error limits are a result of the uncertainty in the $P(E_T)$ distribution used in the calculation of β.

The β parameter and the fits to the TOF distributions were calculated from the translational energy distribution shown in Figure 2. The available translational en-

ergy for each of the two possible dissociation channels is indicated in the figure (E_{avl} for ground state I($^2P_{3/2}$) formation and E^*_{avl} for excited state I($^2P_{1/2}$) formation). By energy conservation, most of the $P(E_T)$ distribution could only come from dissociation leading to ground state iodine product. Some part of the low energy tail might be caused by a small amount of I($^2P_{1/2}$) formation, but we cannot determine the magnitude of this fraction or if it is, in fact, nonzero. Assuming the whole curve to be the the result of I($^2P_{3/2}$) formation, then the average energy in translation is 0.54 of the available energy. This fraction is very close to the usual observation for photodissociation of iodoethanes that about 50% of the available energy appears in translation. The energy range of the $P(E_T)$ distribution combined with the observation of only one peak in the time-of-flight provides strong evidence that ground state iodine is the exclusive product. While we cannot rule out I($^2P_{1/2}$) formation completely, its abundance must be small (<6%), given the low E^*_{avl}.

IV. DISCUSSION

The most significant results from this study are the $P(E_T)$ distribution, which shows the overwhelming dominance of the ground state I($^2P_{3/2}$) dissociation channel, and the anisotropy parameter, which is indicative of a parallel transition—that is, one in which the transition moment is parallel to the C–I bond.

The factors that affect β are discussed in Chapter 3, but it should be noted here that the fact that β is less than 2.0 does not necessarily imply a combination of two types of transitions—parallel and perpendicular—or a transition moment which is not exactly parallel to the C–I bond. The reduction of β could be caused by distortion of the excited complex prior to dissociation, which would change the direction of fragment recoil with respect to the initial C–I bond axis. In any case, an anisotropy parameter of 1.75 implies a predominantly parallel transition.

The observation of only $I(^2P_{3/2})$ formation via a parallel polarization dependence is surprising. Using a quasi-diatomic model,[2] which assumes an $n \longrightarrow \sigma^*$ transition localized on the C–I bond, we would predict that ground state iodine formation should originate from a perpendicular transition to the $^3Q_1$ or ^1Q state. A parallel transition to the $^3Q_0$ state should correlate only to $I(^2P_{1/2})$ product. Photodissociation of many alkyl iodides has been observed [1,6–9] to produce both $I(^2P_{1/2})$ and $I(^2P_{3/2})$ products with the same, parallel polarization dependence, leading to the invocation of curve crossing to explain the results. This study of CH_2ClCH_2I, however, marks the first observation of *total* ground state formation from a parallel transition. Within the context of the diatomic model, we would be forced to conclude that curve crossing occurs 100% of the time after an initial excitation to the $^3Q_0$ state. But this explanation is unsatisfactory as curve crossing is not expected to be so efficient. The apparent failure of the simple picture suggests that a better understanding of the excitation process leading to dissociation would come from consideration of the molecule as a whole. A systematic study of the photofragmentation dynamics of many alkyl iodides in the 230-310 nm region would be an instructive link in the formulation of a successful model, which will describe the dissociation process in the $n \longrightarrow \sigma^*$ continuum.

REFERENCES

1. T.K. Minton, P. Felder, R.J. Brudzynski, and Y.T. Lee, J. Chem. Phys. **81**, 1759 (1984).

2. D. Krajnovich, L.J. Butler, and Y.T. Lee, J. Chem. Phys. **81**, 3031 (1984).

3. (a) R.S. Mulliken, Phys. Rev. **50**, 1017 (1936); (b) **51**, 310 (1937); (c) **47**, 413 (1935); (d) J. Chem. Phys. **8**, 382 (1940).

4. R.A. Boschi and D.R. Salahub, Mol. Phys. **24**, 289 (1972).

5. G.E. Busch and K.R. Wilson, J. Chem. Phys. **56**, 3638 (1972).

6. S. Riley and K.R. Wilson, Discuss. Faraday Soc. **53**, 132 (1972).

7. G.N.A. van Veen, T. Baller, A.E. Devries, and N.J.A. van Veen, Chem. Phys. **87**, 405 (1984).

8. M.D. Barry and P.A. Gorry, Mol. Phys. **52**, 461 (1984).

9. L.J. Butler, E.J. Hintsa, S.F. Shane, and Y.T. Lee, J. Chem. Phys., to be published.

TABLE I. Observed and calculated signal ratios, using various values for the anisotropy parameter β, for horizontal vs. vertical polarization at a fixed source angle of 20° and for 20° vs. 40° source angle with fixed horizontal polarization.

Trial β	Horizontal/Vertical	20°/40°	
—	4.00	1.59	observed
1.00	2.31	1.52	
1.10	2.48	1.56	
1.20	2.68	1.59[a]	
1.30	2.88	1.63	
1.40	3.10	1.67	
1.50	3.34	1.70	
1.60	3.60	1.74	
1.70	3.88	1.78	
1.75	4.03[a]	1.79	
1.80	4.18	1.81	
1.90	4.51	1.84	
2.00	4.87	1.87	

[a]best fit to β for the respective ratio

FIGURE CAPTIONS

Figure 1. Laboratory TOF distributions of I atom product. o Experimental points; —— calculated using the $P(E_T)$ in Figure 2 and $\beta = 1.75$.

Figure 2. Center-of-mass recoil translational energy distribution for CH_2ClCH_2I photodissociation at 308 nm. E_{avl} is the excess energy after breaking the C–I bond in CH_2ClCH_2I. E^*_{avl} is E_{avl} minus the I atom spin-orbit splitting (21.7 kcal/mole). Total fragment internal energy is given by E_{avl}(or E^*_{avl}) minus the c.m. translational energy. Because the curve does not show evidence of two components and because the majority of the distribution is higher in energy than E^*_{avl}, the exclusive dissociation channel must be C–I fission with ground state $I(^2P_{3/2})$ formation.

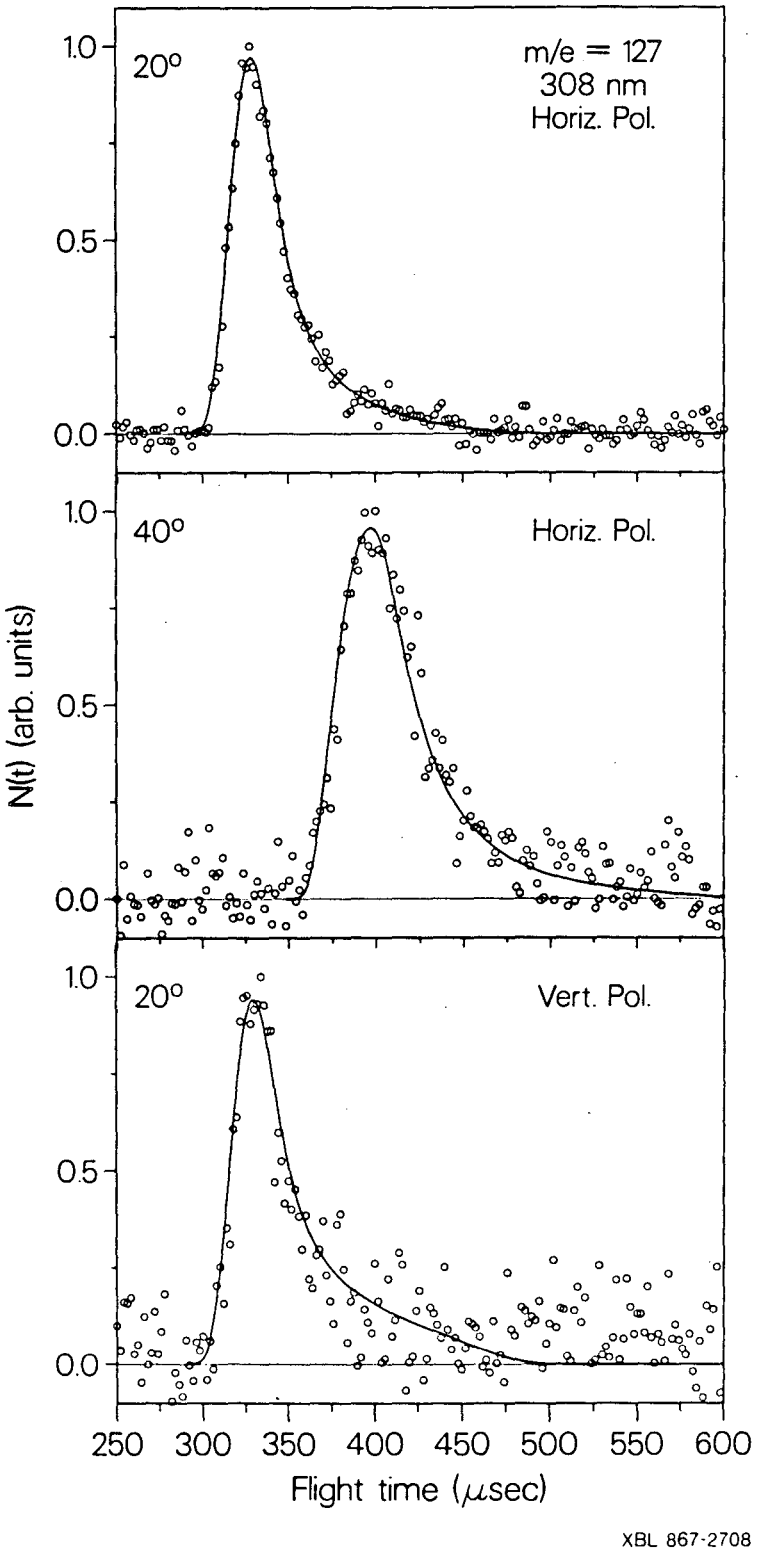
1.0
0.5
0.0
20°
m/e = 127
308 nm
Horiz. Pol.
40°
Horiz. Pol.
20°
Vert. Pol.
N(t) (arb. units)
250 300 350 400 450 500 550 600
Flight time (μsec)
XBL 867-2708

Figure 1

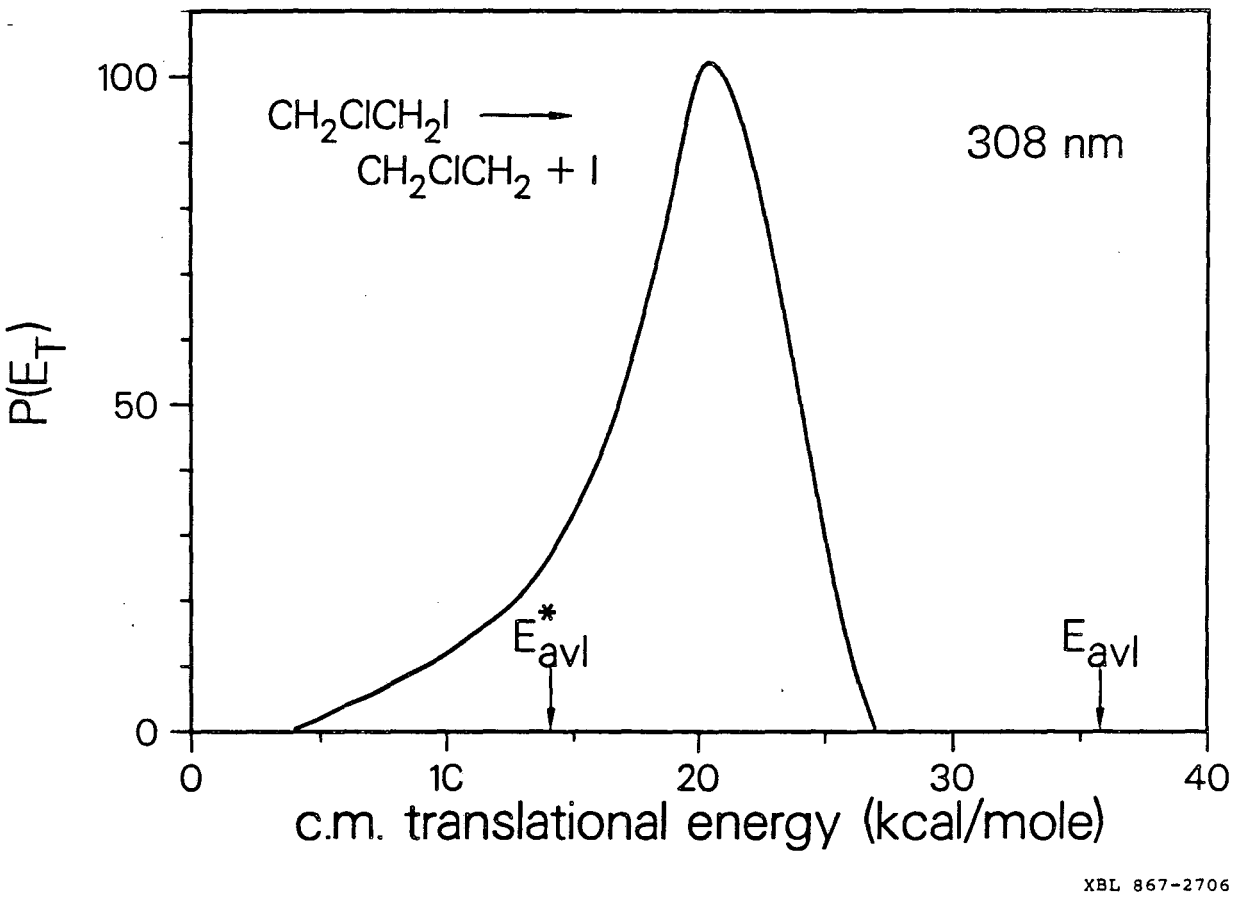
100
50
0
$P(E_T)$
$CH_2ClCH_2I \longrightarrow CH_2ClCH_2 + I$
308 nm
E^*_{avl}
E_{avl}
0
10
20
30
40
c.m. translational energy (kcal/mole)
XBL 867-2706

Figure 2

Chapter 3

Photodissociation of CF_2BrCH_2I at 248, 266, and 308 nm

I. INTRODUCTION

Photofragmentation translational spectroscopy studies of alkyl iodides[1-9] have yielded detailed information about the partitioning of energy in the photofragments, the branching ratios for the two possible product iodine states, $^2P_{1/2}$ and $^2P_{3/2}$, and the polarization dependence of the product angular distributions with respect to the electric field vector. The number of systems which have been carefully investigated is small, however, and our understanding of the alkyl iodide photodissociation process is still fragmented. Even in the case of methyl iodide, which has been studied extensively[2,3,5] as a prototypical alkyl iodide, detailed analyses have only been completed for two excitation wavelengths in the 200-300 nm region: 248 and 266 nm. Furthermore a magnetic circular dichroism (MCD) experiment,[10] which probed the underlying structure of the $n \longrightarrow \sigma^*$ absorption continuum, could not foretell the predominant spin-orbit state of the I atom product at 248 or 266 nm because of the complication of curve crossing.

According to the prevailing picture,[7] alkyl iodide photodissociation in the 230-310 nm region of the spectrum is assumed to occur via an $n \longrightarrow \sigma^*$ transition localized on the C–I bond. This transition manifests itself as a broad absorption

continuum, which was described by Mulliken[11] as consisting of three overlapping bands, with transitions from the ground N state to the ^1Q, $^3Q_1$, and $^3Q_0$ states. An alkyl bromide will exhibit an analogous $n \longrightarrow \sigma^*$ continuum, which will be shifted to shorter wavelength, although still overlapping somewhat with the C–I absorption.[12,13]

In the quest for bond selective photochemistry, photofragmentation studies of CF_2BrCF_2I[7] and CH_2BrI[8,9,13] have been performed in order to discover if excitation in the wavelength region of the C–Br continuum would result in preferential breakage of the stronger C–Br bond over the weaker C–I bond. These studies show that selective C–Br bond breakage is possible and that the ratio of C–Br to C–I bond fission is dependent on the excitation wavelength as well as the relative orientation of the C–Br bond with respect to the C–I bond in the molecule.

Another iodohaloethane, CH_2ClCH_2I, has also been studied in our laboratory[6] (Chapter 1). In addition to the commonly obtainable information (mentioned above), regarding photofragmentation dynamics, we were able to determine the heat of formation of the chloroiodoethane parent, and we could also estimate the C–Cl bond energy of the chloroethyl radical product. These thermochemical quantities could be determined because much of the CH_2ClCH_2 product remained stable after primary C–I bond fission, while a fraction of the radical product was formed with too much internal energy to remain stable and, consequently, underwent secondary decomposition. By finding the center-of-mass translational energy distribution which fitted the stable CH_2ClCH_2 radical time-of-flight signal and by observing the minimum energy in translation at which stable radical could exist, we determined the threshold energy (or reaction enthalpy ΔH) at 0 K for the reaction $CH_2ClCH_2I \longrightarrow CH_2CH_2 + Cl + I$. $\Delta H_f^\circ(CH_2ClCH_2I)$ follows directly from the ΔH for this reaction and $D_0^\circ(CH_2CH_2\text{–}Cl)$ can be inferred by estimating the C–I

bond dissociation energy.

Thus far, all the studies of iodohaloethanes have been limited to excitation wavelengths of 248 and 266 nm (except for C_2F_5I and CF_2BrCF_2I, which were also studied at 193 nm). In general ~50% of the excess energy is observed to appear in translation, and both the ground and excited state iodine (or bromine) channels show a predominantly parallel polarization dependence—i.e., the transition dipole moment must be nearly parallel to the C–I (or C–Br) bond. The branching ratios for $I(^2P_{1/2})$ to $I(^2P_{3/2})$ formation cannot be generalized, however, and they seem to be a function of the individual molecule and excitation wavelength. Besides secondary dissociation of internally excited primary products, which was discussed above, another secondary process, secondary *photo*dissociation has also been observed to occur when the radical product absorbs a photon and dissociates.[7,8]

In this paper, we report the results of a photofragmentation study of CF_2BrCH_2I in which we explore the dynamics and mechanisms of the primary and secondary photochemical processes occuring at three excitation wavelengths in the n(I)$\longrightarrow$ σ^*(C–I) continuum. A key point in this investigation will be the stability of the CF_2BrCH_2 radical product. This paper is one of several in which we will describe the details of photofragmentation for particular iodohaloethane systems at different wavelengths. After completion of a systematic study of these molecules and a comparison of our results with all the other alkyl iodide studies, we hope that some unmistakable trends will emerge and thus lead to a general understanding of the dynamics of alkyl iodide photodissociation in the $n \longrightarrow \sigma^*$ continuum.

II. EXPERIMENT

Photodissociation of CF_2BrCH_2I was studied at 248, 266, and 308 nm using an apparatus[14] which was designed specifically for the crossed laser and molecular

beam technique known as photofragmentation translational spectroscopy.

The apparatus is shown schematically in Figure 1. It consists of a rotatable molecular beam source and a fixed quadrupole mass spectrometer detector in a plane perpendicular to the propagation direction of the laser. The time-of-flight (TOF) signal of the photodissociation products is registered on a 4096 channel multichannel scaler[15] capable of a minimum dwell time of 0.15 μs. Most of our data have been recorded with a 1.0 μs dwell time. The flight path from the interaction region to the electron impact ionizer is 36.8 cm. An important feature of this apparatus is the slit mounted in the main chamber near the beam source and facing the detector. This slit is cooled to 25 K, and it reduces the detector background originating from the main chamber by a factor of 10 because condensible gases will not bounce off the cold surface that is in the viewing window of the detector.

The main resolution limit in the TOF spectra resulting only from the apparatus is determined by the ratio of the effective ionizer length to the flight path length. By observing the extremely fast and monoenergetic H atom fragment from photodissociation of HI at 248 nm and using the minimum 0.15 μs dwell time on the multichannel scaler, we were able to measure the effective ionizer length. Noting that the width in the TOF signal would only be due to the finite length of the ionizer and the laser spot size, we measured a FWHM in the TOF of 0.45 μs peaked at an arrival time of ~20 μs. Using the relation, $\Delta t/t = \Delta l/l$ (for constant velocity), and subtracting the length of the laser spot (0.3 cm), we found an effective ionizer length of ~0.5 cm. Thus, the resolution, due to the finite ionizer length, of a TOF spectrum would be about one part in 75.

In practice, the molecular beam velocity distribution is usually the major limiting factor in the TOF resolution. Our CF_2BrCH_2I beam typically had a peak velocity of 7×10^4 cm/s with a velocity spread (FWHM) of ~12%. We per-

formed velocity distribution measurements by chopping the beam with a spinning disk with four narrow slits (0.075 cm) and observing the TOF of the segments which passed through the slits to the detector. The TOF measurements were fitted with the program, KELVIN,[16] to an assumed form for the velocity distribution, $N(v) \propto v^2 \exp[-(v/\alpha - S)^2]$.[17,18] Table I shows the α and S parameters used for the experiment at each wavelength. The small variations in the velocity distributions for each wavelength were caused mostly by slight differences in the temperature of the nozzle for the different experiments.

The molecular beam was formed by bubbling Ar through liquid CF_2BrCH_2I at 14°C (vapor press. $\approx$ 8 Torr) to yield a total stagnation pressure of 300 Torr. The mixture was expanded through a 0.125 mm (0.005 in.) dia. nickel nozzle which was heated to 240° -250°C at the tip to prevent dimer formation. The molecular beam passed through two differentially pumped regions before intersecting the laser beam. A skimmer defined the beam to an angular divergence of 3°. The distance from the nozzle to the interaction region was 7.4 cm.

1-bromo-1,1-difluoro-2-iodoethane was custom synthesized by Fairfield Chemical of Blythewood, SC, and it was used without further purification. A GC-mass spectrum showed in our sample a 1% impurity of CF_2BrCH_2Br and a 3% impurity of an isomer, which was determined by NMR to be CF_2ICH_2Br. Only the isomer impurity could potentially cause a problem in the wavelength region of these studies, but we saw no evidence for any interference due to an impurity of this level.

The experiment at 266 nm used the fourth harmonic of a Quanta Ray DCR-1 Nd:YAG laser equipped with a model HG-2 harmonic generator. Following the harmonic generator, the light passed through a Pellin-Broca prism, after which the unwanted fundamental and second harmonic were directed into a beam dump. The fourth harmonic was redirected by a 90° Suprasil I prism into the machine, where

it was focused to a spot size of 2.4 mm diameter. In general, the laser output was polarized horizontally—parallel to the detector axis. Occasionally, however, we used the vertical polarization, which was achieved by rotating the harmonic generator by 90°. The laser was adjusted such that the pulse energy in the interaction region was ~30 mJ for both polarizations. At these pulse energies, the Pellin-Broca prism developed tracks, and degradation of the fourth harmonic polarization was observed to become more pronounced as the damage increased. Depolarization interferes with the anisotropy measurements, so we checked the polarization often with a calcite polarizer, and we either moved the prism or replaced it at the first sign of depolarization. We used a crystalline quartz prism and varying quality fused silica prisms during the experiment, and we found that the fused silica prism purchased from Quanta Ray lasted longest before tracking. Neither the Suprasil I right angle prism nor the MgF_2 lens ever showed any visible damage.

For both the 248 and 308 nm experiments, a Lambda Physik EMG 103 MSC excimer laser was used with the KrF and XeCl transitions, respectively. The optional ILC (Intelligent Laser Control) was used to maintain constant output power. The repetition rate was varied from 100 to 150 Hz. The optical arrangment lay in one plane. The unpolarized output of the laser was directed into a fused silica bending prism which bent the light up at the correct angle into a 60° MgF_2 prism polarizer such that the desired polarization—horizontal or vertical— would come out level and proceed into the machine through a 25 cm fl MgF_2 spherical lens, while the unwanted polarization was blocked. The two polarizations differed in direction by only a few degrees with the vertical component above the horizontal component. The prism polarizer was mounted on a rotation stage so that a simple rotation of the prism would direct the desired polarization, precisely aligned, into the machine. Typical pulse energies at the interaction region for the 308 nm experiment were

12 mJ for horizontal polarization and 18.5 mJ for vertical polarization. The 308 nm spot size was 3 mm wide and 0.4 mm high. At 248 nm, the typical pulse energies were 11 mJ for horizontal and 19 mJ for vertical polarization, and the spot size at the interaction region was 3 mm × 0.6 mm.

At 266 nm, TOF measurements were made at source angles of 10° to 50°. Signal was detected at m/e = 127, 79 (20° only), and 64 (20° only), corresponding to I^+, and Br^+, and $CF_2CH_2^+$, respectively. The respective integrated counts/laser pulse at 20° (horizontal polarization) were 5.5, 2.3, and 0.10. The number of laser pulses was 45,000 for I^+, 100,000 for Br^+, and 280,000 for $CF_2CH_2^+$.

At 248 nm, TOF measurments were made at source angles of 20° to 50°. Signal was detected at m/e = 127(I^+), 79(Br^+), and 64($CF_2CH_2^+$). I^+ TOF's were counted for 100,000 laser pulses with a count rate (horizontal pol.) at 20° of 1.3 counts/pulse. Br^+ was counted only at 20° for 200,000 pulses with a count rate of 0.81 counts/pulse. $CF_2CH_2^+$ also was counted only at 20° for 1,000,000 pulses with a count rate of 0.28 counts/pulse.

At 308 nm, signal was detected at two masses—127(I^+) and 79(Br^+). I^+ TOF's were recorded at source angles of 10° to 50° for 200,000 laser pulses with a count rate (horizontal pol.) at 20° of 0.14 counts/pulse. Br^+ was recorded only at 20° for 1,000,000 pulses with a count rate of 0.12 counts/pulse.

In all three experiments, we made an unsuccessful effort to observe the parent CF_2BrCH_2 radical at m/e = 143. The only mass which showed any evidence of stable radical was m/e = 79(Br^+). This mass is not ideal for observing stable radical (through dissociative ionization) because most of the Br^+ signal is expected to result from atomic Br, which is present at high levels because of secondary decomposition of CF_2BrCH_2 product.

In general, two types of angular distributions were performed. The signal was

monitored as a function of source angle for fixed horizontal polarization, and the signal was monitored for horizontal and vertical polarizations at a fixed angle. The exception for the latter case was at 266 nm, where the polarization could not be changed without realigning the laser beam. For both types of angular dependences, the angle or the polarization was changed often and the scan repeated many times to offset any drifts which might have occured in the laser power, the electronics, or the molecular beam intensity.

The 248 and 266 nm laser intensities were high enough that saturation could affect the angular distributions. (The effect of saturation will be discussed in Section IV.) In order to ascertain the amount of saturation, we took an absorption spectrum of gaseous CF_2BrCH_2I on a Cary 14 spectrophotometer (Fig. 2) to determine the absorption cross section. Table II gives the cross section as well as the product of the cross section and laser intensity for each wavelength studied.

III. RESULTS AND ANALYSIS

The goals of the data analysis are the center-of-mass (c.m.) product translational energy distribution $P(E_T)$ and the determination of the parameter β in the c.m. angular distribution, expressed in the form[19(b)]

$$w(\theta) \propto 1 + \beta P_2(\cos\theta), \tag{1}$$

where θ is the angle between the electric vector of the laser light and the c.m. recoil direction of the products. The calculated c.m. flux distribution is assumed to be the product $P(E_T)w(\theta)$. The primary data, from which the $P(E_T)$ and β are derived, are the laboratory TOF distributions $N(t)$ and the laboratory angular distributions $N(\Theta)$. For a single photon dipole transition to a repulsive state in a diatomic molecule, the anisotropy parameter β is related to the angle α between

the transition moment and the bond dissociation coordinate according to [19(b)]

$$\beta = 2P_2(\cos\alpha). \tag{2}$$

For a purely parallel transition, $\alpha = 0°$, $\beta = 2$, and $w(\theta)$ is a $\cos^2\theta$ distribution, while for a purely perpendicular transition, $\alpha = 90°$, $\beta = -1$, and $w(\theta)$ is a $\sin^2\theta$ distribution. For polyatomic molecules, however, several physical effects, involving motion of the excited molecule prior to dissociation, are often imbedded in β. Saturation in the laser excitation can also affect β, and this saturation effect is taken into account in the analysis using a model first proposed by Ling and Wilson[20] (see Discussion).

The $P(E_T)$ and β are determined by a forward convolution technique in which a $P(E_T)$ distribution and a β are guessed and then convoluted with the beam velocity distribution, ionizer length, and laser spot size. A c.m. to lab transformation is then performed, yielding a calculated $N(t)$ distribution which is compared to the observed TOF. The $P(E_T)$ and β are refined until a satisfactory fit is simultaneously obtained for all TOF and angular distributions. We have found empirically that including in our fitting routine the 3° angular divergence of the molecular beam and the 1.5° angular divergence of the detector aperature will only negligibly narrow the fitted $P(E_T)$ distribution.

The TOF distributions presented here show the total time for a fragment to go from the interaction region to the ionizer, and after ionization, through the quadrupole mass filter to the Daly-type ion counter. The true flight time from the interaction region to the ionizer is found by subtracting the ion flight time from the observed total arrival time. The ion flight time for a singly charged ion of mass m has been found experimentally, and it can be expressed in μs by the formula $\alpha\sqrt{m}$ where the parameter α is a function of the ion energy, the resolution, and other mass spectrometer parameters. α was equal to 3.96 for all of the data reported here

with the exception of the iodine TOF's at 266 nm, where α was determined to be 2.64.

A. TOF and angular distributions

1. 266 nm

Figure 3 shows the iodine fragment TOF data for horizontal polarization at various angles along with the best calculated fits using the $P(E_T)$ in Figure 15. (The two components fit separately were deconvoluted such that the two curves would be smooth and unimodal.) Three components are definitely present in the TOF. Based on previous alkyl iodide studies,[1-9,22-24] we would have expected two components arising from two dissociation pathways: one yielding faster, ground state $I(^2P_{3/2})$, and the other yielding slower, spin-orbit excited $I(^2P_{1/2})$. Indeed, the two most prominent peaks in the TOF are consistent with the previous observations[6,7] that about half the available energy for each channel appears in translation—see the $P(E_T)$ in Figure 15. The third slow component is associated with primary C–Br bond fission and originates from the CF_2CH_2I fragment (see below and part B).

The angular distribution for fixed horizontal polarization is shown in Figure 4. For reference, two fits are shown for different values of β. It is apparent that the angular distribution is not very sensitive to β, although the range of β's that fit the angular distribution is indicative of a predominantly parallel transition. Figure 5 shows a kinematic diagram for CF_2BrCH_2I photodissociation with I atom detection, where it can be seen that the recoil velocities are large enough compared to the beam velocity that $\cos^2\theta$ does not change much over the range of c.m. angles sampled for a given laboratory angle (when using horizontal polarization). Thus, the shape of the calculated $N(t)$ distribution is mostly sensitive to the $P(E_T)$ distribution, while the shape of the calculated $N(\Theta)$ distribution is mostly sensitive

to β. It is a fortunate circumstance that the $P(E_T)$ and β can be optimized almost independently. As is also seen in Figure 5, when the laser polarization is vertical, $\cos^2\theta$ for the complementary c.m. angle does change significantly over the range of a TOF distribution. Consequently, fitting a vertical polarization TOF after finding the correct $P(E_T)$ from a horizontal polarization TOF provides a double check on β. Experience has shown that we can only expect to be accurate to about ± 0.3 in β with the fixed polarization method of measuring the angular dependence. A rotating detector machine, which has been used in our laboratory for other similar experiments,[6,7] is much better suited for such angular studies, as the c.m. angle changes dramatically over the range of a typical angular distribution. On the other hand, the geometry of the rotating source apparatus is much better (in fact necessary) for angular distributions obtained by rotating the laser polarization at fixed beam angles, which provide, in theory, a very sensitive determination of β.

We did perform a fixed beam angle, horizontal/vertical polarization dependence at 266 nm, but we were not able to repeat the measurement over and over to average out drifts. As mentioned in Section II, when we rotated the polarization, the laser had to be realigned. Nevertheless, we were careful to use the same alignment, laser power, and experimental conditions for measuring the signal with each polarization. The anisotropy parameter given by this angular dependence was 1.6. Table III shows the sensitivity of the calculated horizontal to vertical polarization signal ratio in the determination of β.

A final test of β comes from fitting the vertical polarization, iodine TOF at 20°. Figure 6 shows the data with the calculated fits for a given $P(E_T)$ and three different β parameters. $\beta = 1.6$ gives the best fit, but the other fits are not bad. Based on the preponderance of the evidence, we will take $\beta = 1.6 \pm 0.2$ as the anisotropy parameter for the 266 nm photodissociation process. It should be noted

that we tried fitting the data using two and three different β values for the different components in the TOF (by arbitrarily deconvoluting the $P(E_T)$), and we were forced to conclude that all three components have the same anisotropy.

An incidental feature in Figure 6 is the long slow tail, which was not present in the horizontal polarization TOF data. This tail is caused by a small amount of clusters in the beam. Vertical polarization (i.e., when the electric vector is perpendicular to the detector axis) accentuates signal from clusters because their slow c.m. velocities make their detection possible only at large c.m. angles; thus, assuming a parallel transition, the more favorable polarization would be vertical. Apparently, even the heated nozzle did not prevent some clusters from forming.

We observed a TOF spectrum at $m/e = 79(Br^+)$ in addition to the iodine data. Figure 7 shows this TOF distribution along with a section of the same distribution on an expanded scale. Included also is the calculated fit for the stable CF_2BrCH_2 fragment assuming it would be seen at $m/e = 79$. Based on CH_2ClCH_2I photodissociation,[6] the radical fragments are expected to be internally hot, with a large fraction of the CF_2BrCH_2 radicals undergoing secondary dissociation into CF_2CH_2 and Br. The observed broad TOF is suggestive of secondary dissociation, while the fast feature probably contains an additional contribution from primary C–Br bond fission. At ~300 μs, a small peak is discernable, and because it falls in the range of the calculated CF_2BrCH_2 TOF, it is probably an indication of a small amount of stable CF_2BrCH_2 product.

With the observation of stable difluorobromoethyl product as a goal, we searched in vain for signal at the parent mass, 143. Apparently, even if stable radical were formed, it did not survive electron bombardment in the ionizer. Another possible mass for observing the stable CF_2BrCH_2 product was $m/e = 64(CF_2CH_2^+)$. The measured TOF in Figure 8 does not exhibit any definite feature at the expected

stable radical arrival time, although there is a hint of a peak at ~300 μs, which corresponds exactly to the arrival time of the small, stable radical peak in the Br^+ TOF (when the proper correction for ion flight time is made). Unfortunately, the signal-to-noise ratio of the data is not very good because we had to increase the mass spectrometer resolution to filter out the I^{++} signal at $m/e = 63.5$. Nevertheless, the characteristically broad secondary dissociation signal is present as well as a fast peak, which, by conservation of energy, must result from secondary *photo*dissociation, where the radical has absorbed another photon and fallen apart with a large translational energy release. The Br^+ TOF distribution should also show this fast, secondary photodissociation signal, and we can estimate by conservation of momentum that secondary dissociation accounts for the signal under the fast edge of the sharp feature in the Br^+ TOF.

2. 248 nm

The iodine TOF spectra, shown in Figure 9, from 248 nm photodissociation are similar to those seen at 266 nm. As before, three components are clearly visible, with the fast ground state iodine peak more prominent in the 248 nm TOF's. While the ground and excited state iodine channels could not be resolved completely in the time-of-flight, we separated the $P(E_T)$ into two components, as we did for the 266 nm data (see Figure 15), and the fits are shown in Figure 9.

As usual for the experiments on the rotating source apparatus, the fixed polarization-rotating source angular dependence did not give a distribution which was very sensitive to the β parameter, and we could find one $P(E_T)$ along with a range of β values, from 1.0-2.0, which would satisfactorily fit all the iodine TOF's as well as the angular distribution. However, at 20° we collected I^+ data at both horizontal and vertical (Figure 10) polarizations, and a simultaneous fitting of the shape of

the two TOF spectra was very dependent on the β parameter as well as the $P(E_T)$ distribution. We were able to fit the horizontal and vertical polarization TOF's simultaneously, provided the I($^2P_{1/2}$) fraction in the $P(E_T)$ was 0.77 and the I($^2P_{3/2}$) fraction was 0.23 *and* provided the ground state β was 0.35 lower than the excited state β. We also tried arbitrarily separating the $P(E_T)$ to give a third component, corresponding to the slow shoulder, but we concluded that it must have the same anisotropy as the excited state iodine channel. The relation between the two β values was thus established, but their actual values could still not be resolved.

The horizontal/vertical polarization dependence on the integrated signal furnished the final constraint needed to determine the anisotropy paramenters. Table IV shows the calculated horizontal to vertical polarization signal ratios for selected β values in addition to the experimental ratio. (Note that all the ratios in Table IV include the effect of laser saturation.) The best fit β pair is $\beta^* = 1.6$ and $\beta = 1.25$, and these are the parameters used in the fits in Figures 9 and 10.

Figure 11 shows the bromine TOF distributions recorded for both horizontal and vertical polarizations. The two TOF's are strikingly different in the intensity of the fast feature with respect to the broad secondary background. This fast peak is presumably a combination of Br^+ arising from secondary photodissociation of the CF_2BrCH_2 radical and, more importantly, primary photodissociation resulting in C–Br bond cleavage. The peak of the fast feature in both the 248 and 266 nm Br^+ TOF distributions occurs at an arrival time which can be explained by assuming Br formation with $\sim 1/2$ the available energy going into translation—a common observation in C–I bond fission.

The fact that the fast bromine peak decreases markedly, relative to the broad background, on going from horizontal to vertical polarization is suggestive of a primary process with a parallel polarization dependence. The secondary signal origi-

nates from decomposition of the relatively slow CF_2BrCH_2 radical, which will show a less sensitive polarization dependence than the fast Br product from C–Br bond dissociation, because the c.m. angle changes less between horizontal and vertical polarization for a slower product than for a faster product (at a given laboratory angle).

From the fast secondary photodissociation peak in the $CF_2CH_2^+$ TOF (Figure 12), the peak arrival time of the complementary bromine signal can be estimated to be ~235 μs. Thus, the secondary photodissociation signal is under the fast side of the prominent peak in the Br^+ TOF. This conclusion is consistant with the observation that, when going from horizontal to vertical polarization, the faster side of the fast peak decreases more than the slower side, as evidenced by the apparent shift in the peak to a slower arrival time. The secondary photodissociation signal should have a two photon polarization dependence of approximately $[w(\theta)]^2$ (if β for both processes is similar), so it is reduced drastically when changing from horizontal to vertical polarization. Also contributing (but to a lesser extent) to the apparent peak shift is the fact that the faster signal depends more strongly on the laser polarization than the slower signal.

Given the analogous nature of the data at 266 and 248 nm, the basic processes occurring at the two wavelengths must be similar, including the CF_2CH_2I product origin of the slow shoulder.

3. 308 nm

The I^+ TOF spectra at 308 nm (Figure 13) are strikingly different from those at 248 or 266 nm. At 308 nm, the faster, $I(^2P_{3/2})$ channel dominates and there is no evidence for a slow shoulder. The fits in Figure 13 come from a bimodal $P(E_T)$ (Figure 15), which has been deconvoluted into a ground and an excited state iodine

component. While this deconvolution is an estimate, the high energy side of the $P(E_T)$ for the $I(^2P_{1/2})$ channel is limited by the available energy.

The anisotropy parameter for 308 nm photodissociation was most sensitive to the horizontal/vertical polarization dependence at 20° (see Table 5). The fixed polarization/source rotation angular dependence was inconclusive and the vertical polarization data was too noisy for a sensitive fit to the shape of a vertical polarization TOF. The agreement between the calculated horizontal/vertical polarization signal ratio and the experimental ratio was best for $\beta = 1.2$. As before, we attempted to fit all the data using different β values for each component in the TOF, and we concluded that both photodissociation channels must have approximately the same anisotropy. It is conceivable, but unlikely, that the two channels could have β's differing by as much as 0.2; however, they would both be around 1.2, i.e., mostly parallel in character.

Figure 14 shows the $m/e = 79(Br^+)$ TOF distribution. It is generally noisy, broad, and featureless, except for a hint of a sharp peak at ~280 μs arrival time. The lack of a large fast peak, as seen in the 248 and 266 nm TOF's, implies that primary C–Br bond fission is not occuring here, which is not surprising given the absorption spectrum (Figure 2). We are unable to assign unambiguously any of the fast bromine signal to secondary photodissociation because it is energetically possible for *spontaneous* secondary dissociation to give the fastest observed signal and because the signal-to-noise ratio was too low at $m/e = 64$ to have a chance of observing a fast, two-photon peak, similar to that seen in the 248 and 266 nm data. Probably, the majority of the Br^+ TOF is a result of Br atoms coming from secondary dissociation of internally excited CF_2BrCH_2 radical product.

The small sharp peak, mentioned above, is evidence for stable radicals. Included in Figure 14 is the calculated temporal distribution of the CF_2BrCH_2 fragment,

which uses the $P(E_T)$ derived from fitting the I^+ TOF's and assumes no secondary dissociation takes place. It is perplexing that the observed peak appears to stem from the ground state iodine channel rather than from the excited state channel, which would leave much less energy available for internal excitation of the radical. Nevertheless, within the error limits of the data, the position of the peak is energetically consistent with endoergicity of the reaction, $CF_2BrCH_2I \longrightarrow CF_2CH_2 + Br(^2P_{3/2}) + I(^2P_{3/2})$ (see part B), derived from the 266 nm Br^+ TOF distribution. The stable radical signal from the $I(^2P_{1/2})$ channel must be buried in the noise.

B. Product translational energy distributions and branching ratios

The fits to the TOF and angular distributions were calculated using the $P(E_T)$ distributions shown in Figure 15. In each case, the $P(E_T)$'s for the ground and excited state iodine dissociation channels were not completely resolved, so the dashed curves represent our best estimates for their separation. It is more difficult to separate the slow shoulder from the $I(^2P_{1/2})$ $P(E_T)$ for 248 and 266 nm photodissociation, but we have done so in order to illustrate the approximate shape of the excited state iodine component.

An energy level diagram for C–I and C–Br bond fission in CF_2BrCH_2I is shown in Figure 16. The energy available for translation and internal excitation of the products (E_{avl} for $^2P_{3/2}$ and E^*_{avl} for $^2P_{1/2}$ formation) is given by the energy conservation expressions,

$$\begin{aligned} E_{avl} = h\nu + E^P_{int} \;\; - \;\; D^\circ_0(\text{C–I[Br]}) &= E_T + E^R_{int} \\ E^*_{avl} \;\; = \;\; E_{avl} - E_{so}, & \end{aligned} \tag{3}$$

where E^P_{int} is the part of the initial internal energy, which is stored in the vibrational degrees of freedom of the CF_2BrCH_2I parent that are directly coupled to the

dissociation coordinate, and E_{int}^{R} is the internal energy of the radical fragment after photodissociation. D_0°(C–I) is estimated to be 55.8 ± 1.5 kcal/mole, and D_0°(C–Br) is estimated to be ~68 kcal/mole (see Discussion, part B). The photon energy $h\nu$ is 115 kcal/mole at 248 nm, 107.5 kcal/mole at 266 nm, and 92.8 kcal/mole at 308 nm. E_{so}, the $^2P_{3/2}$ - $^2P_{1/2}$ spin-orbit splitting is 21.7 kcal/mole for I and 10.59 kcal/mole for Br.

As mentioned in part A, a small peak attributable to stable CF_2BrCH_2 radical is observed in the bromine TOF at 266 nm. Unfortunately, the stable CF_2BrCH_2 radical peak was of much too poor quality to fit (unlike the analogous stable CH_2ClCH_2 radical peak in the previous CH_2ClCH_2I experiment[6]), so we performed a simple calculation of the translational energy with the use of a kinematic (Newton) diagram (e.g., Figure 5) and the assumption of a monoenergetic molecular beam and infinite detector resolution. By carrying out this calculation for various points over the range of the peak, we obtained an idea of the accuracy of our method. Fortunately, the peak was very narrow, and over half the width of it (the slow half), the c.m. translational energy changed from 16.5 to 20 kcal/mole. Because the peak is so narrow, all the CF_2BrCH_2 radicals formed must be near their maximum internal energy (i.e., near the C–Br bond dissociation limit). Thus, we take the midpoint, 18.3±2 kcal/mole, as the translational energy threshold.

This threshold energy provides the information necessary to calculate the change in enthalpy ΔH for the reaction,

$$CF_2BrCH_2I \longrightarrow CF_2CH_2 + Br + I. \tag{4}$$

From Equation (3), ΔH for this reaction can be determined [assuming E_{int}^{P} is equal to zero (see Section IV. B.)] as follows:

$$D_0^\circ(CF_2BrCH_2 - I) + D_0^\circ(CH_2CF_2 - Br) = h\nu - E_{so} - E_T(\text{min}), \tag{5}$$

where $D_0^\circ(CH_2CF_2\text{–Br})$ has been used instead of $E_{int}^R(max)$. ΔH (at 0 K) for reaction 4 is then 67.5 ± 2 kcal/mole.

The slowest component in the iodine TOF at 248 and 266 nm can be understood in light of the result above. Based on C–Br bond energies for similar bromoethanes (see Table VII), we know that ΔH (at 0 K) for the reaction,

$$CF_2BrCH_2I \longrightarrow CF_2CH_2I + Br, \qquad (6)$$

is 67-68 kcal/mole. Since the C–Br bond dissociation energy is almost the same as the energy required to break both the C–Br and C–I bonds, $D_0^\circ(CF_2CH_2\text{–I})$ must be approximately 0 kcal/mole. If we assume that primary C–Br bond fission occurs and that the slow shoulder is the result of the CF_2CH_2I product, and if we assume that Br is formed in the spin-orbit excited state, then the energy available for translation at 248 nm is 115 – 69 – 10.6 = 35.4 kcal/mole, and at 266 nm, the available energy is 107.5 – 69 – 10.6 = 27.9 kcal/mole. The peak of the slow bump corresponds to a c.m. translational energy of ~32.5 kcal/mole at 248 nm and ~27 kcal/mole at 266 nm. Therefore, the CF_2CH_2I internal energy is about 3 kcal/mole at 248 nm and about 1 kcal/mole at 266 nm. These values are, of course, subject to error because of the uncertainty in the peak position and in the C–Br bond energy; nevertheless, they fall in the range of the expected bond energy of the radical. Whether the CF_2CH_2I radical is stable or not, it can account for the slow bump because even if it is unstable by one or two kcal/mole, the iodine will be recoiling from the CF_2CH_2 relatively slowly compared to the initial velocity of the CF_2CH_2I product. Hence, the I^+ TOF signal from secondary dissociation of slightly unstable CF_2CH_2I would appear similar to the I^+ TOF signal from a slightly stable CF_2CH_2I product. Ground state Br formation would not lead to a distinct bump in the TOF, because the higher available energy would cause the two secondary fragments to recoil from each other with a broad range of velocities.

In summary, the slow bump is consistent with a $D_0^\circ(CF_2CH_2\text{–}I)$ of approximately 0 kcal/mole, but we cannot conclude from our data whether or not the CF_2CH_2I radical is weakly chemically bound.

From the areas under the $P(E_T)$ distributions, we can estimate branching ratios for the formation of the two electronic states of iodine. The $I(^2P_{1/2})/I(^2P_{3/2})$ ratios are 3.3, 9.0, and 0.5, respectively for 248, 266, and 308 nm. These results do contain uncertainties, mainly resulting from the deconvolution of the curves. Other errors can arise from the noise in the data, which leads to ambiguities in the fits. Despite the uncertainties, our ratios are probably accurate to 10%.

Finally, we compare the fraction of the available energy that went into translation for the average E_T and the extremes in the $P(E_T)$ distribution. The results are summarized in Table VI.

IV. DISCUSSION

A. Anisotropy and polarization

The polarization dependences of both the ground and excited state iodine channels at all three wavelengths studied suggest a predominantly parallel transition for every photodissociation process observed. However, the anisotropy parameter β is, in every case, less than 2, the expected β value for a purely parallel transition. We will examine below the factors that can reduce β, and we will estimate the relative importance of each.

Rotation of the excited complex prior to dissociation would cause a reduction in β if the excited state lifetime were long enough to allow the molecule to rotate such that the recoil direction of the products differed significantly from the initial orientation of the C–I bond. Following a derivation by Jonah[21] and also Busch and Wilson,[19(b)] the angular distribution arising from dissociating molecules with a

random distribution of lifetimes is

$$w(\theta) \propto 1 + \beta_{true}\left[\frac{1+(\omega\tau)^2}{1+4(\omega\tau)^2}\right] P_2(\cos\theta), \tag{7}$$

where the observed β_{obs} would be the true β_{true} reduced by the factor $[1+(\omega\tau)^2]/[1+4(\omega\tau)^2]$, and $\omega\tau$ is the angle through which a molecule with angluar velocity ω and lifetime τ would rotate before dissociating. Rearranging,

$$\omega\tau = \left[\frac{1-\beta_{obs}/\beta_{true}}{4(\beta_{obs}/\beta_{true})-1}\right]^{1/2}. \tag{8}$$

Thus, to explain a reduction in β from 2.0 to 1.5 ($\beta_{obs}/\beta_{true} = 1.5/2.0$), a rotation of 20° would be required.

The degree to which rotation of excited CF_2BrCH_2I plays a role in reducing the anisotropy can be ascertained from the knowledge of the rotational temperature of the molecule. The rotational temperature in the molecular beam can be estimated by assuming it is equal to the terminal longitudinal translational temperature in the beam, which is related to the α parameter in the form for the velocity distribution (see Section II) by[18]

$$\alpha = \left(\frac{2kT}{m}\right)^{1/2}. \tag{9}$$

For our beam conditions, T is ~35 K, which corresponds to a rotational period of approximately 40 ps for CF_2BrCH_2I. The amount of time required to rotate 20° would be ~2.2 ps—much longer than the expected lifetime of < 400 fs[23,25] of the repulsive state. Given the short lifetime, the excited complex would rotate only a few degrees or less before dissociating, and the anisotropy parameter would change by no more than one percent. Rotation of the excited complex has been observed to reduce the anisotropy in a photofragmentation study[3] of CH_3I, where the sample was near room temperature. Evidently, it is prudent to take advantage of the efficient rotational cooling in a molecular beam in order to render this effect negligible.

The initial tangential velocity component of the dissociating fragment in the excited complex could lead to a resultant fragment velocity oriented along a different direction than the initial C–I bond axis (when the photon was absorbed), thus causing an apparent reduction in the anisotropy parameter. Assuming a fixed rotational (or tangential) velocity, the form for the c.m. angular distribution would be,[19(b)]

$$w(\theta) \propto 1 + \beta_{true} P_2(\cos\gamma) P_2(\cos\theta), \tag{10}$$

where γ is the angle between the initial orientation of the C–I bond and the resultant direction of the fragment velocity. The observed β_{obs} would be the true, or otherwise unperturbed, β reduced by $P_2(\cos\gamma)$. For a CF_2BrCH_2I rotational temperature of 35 K, the tangential velocity of the I fragment would be ~3000 cm/s, and for a typical iodine recoil velocity of 7×10^4 cm/s, the angle γ would be ~2.5°. Consequently, β_{obs} would differ from β_{true} by a fraction of one percent.

Laser saturation of the exctation is another possible reason for an apparently low anisotropy, and its effect has been modeled by Ling and Wilson.[20] Using their model, we derive a slightly more general equation than they reported for the angular distribution,

$$w(\theta) \propto [1 + \beta P_2(\cos\theta)] \int_0^{2\pi} \frac{1 - \exp\{-\sigma F[1 - \frac{\beta}{2} P_2(\sin\theta\cos\chi)]\}}{1 - \frac{\beta}{2} P_2(\sin\theta\cos\chi)} d\chi, \tag{11}$$

where we see that the simple form of the angular distribution is modified by an integral which cannot be solved analytically. σF is the product of the absorption cross section and the integrated photon flux for the laser pulse. χ is the angle between the angular momentum vector **J** for the rotating parent molecule and the projection of the electric vector **E** onto the plane containing **J**. The fragments seen at the detector do not come from molecules with a single angular momentum orientation, but from molecules with any **J** lying in a plane that is perpendicular

to the dissociation coordinate.

This saturation model is really only valid for a diatomic molecule, but CF_2BrCH_2I is sufficiently prolate (the ratio of rotational constants is $A/\overline{B} \approx 11$) that the diatomic model can be used to estimate the effect of saturation. We have incorporated Equation (11) into our data analysis program, and we have concluded that for σF values of ~0.4, for example, the anisotropy parameter, fit without taking into account saturation, would be about 0.2 too low. Nevertheless, as noted previously, only at 248 and 266 nm could saturation effects be important, and they have been taken into account in the data analysis, so our reported β values should be free from saturation lowering.

It is plausible that the parent molecules could be excited either by a parallel transition to the $^3Q_0$ state or by a perpendicular transition to the ^1Q state. Allowing for curve crossing from either state to the other, then the anisotropy parameter for a particular dissociation channel could fall in between –1.0 and 2.0. The problem with this reasoning is that the experimental results for 266 and 308 nm photodissociation show the same anisotropy for both ground and excited state iodine channels, and it would be highly unlikely that the probability for curve crossing from $^3Q_0$ to ^1Q could be exactly complemented by the probability for curve crossing from ^1Q to $^3Q_0$ such that both channels would have equal β values. Much more reasonable is the explanation that both dissociation channels originate from the same excited state—$^3Q_0$. At 248 nm, the ground state I channel had a slightly lower β than the excited state channel, so it is possible that two excited states could be responsible for dissociation, with the ground state I($^2P_{3/2}$) channel having more perpendicular character than the excited state I($^2P_{1/2}$) channel, but the similarity of the two β values makes this possibility suspect.

A likely explanation for the reduction of β from 2 is distortion of the excited

complex before dissociation, which could easily change the direction of fragment recoil with respect to the initial C–I bond axis. This effect is difficult to model quantitatively, but we do have reason to believe it is important. Assuming a rigid radical impulsive model,[1,26] the fraction of the available energy in translation is given by

$$\frac{E_T}{E_{avl}} = \left[1 + \frac{\mu b^2}{I}\right]^{-1}, \tag{12}$$

where μ is the reduced mass of the two fragments R and I, b is the exit impact parameter, and I is the moment of inertia for the radical R. For CF_2BrCH_2I, these quantities are 67.5 amu, ~1.5 Å, and 249 amu·Å^2, respectively, where the impact parameter is derived from the equilibrium structure of the molecule. Using these values, the expected fraction of available energy in translation would be 0.62. This fraction should reflect the maximum energy that could appear in translation—assuming no distortion—because a softer radical would channel energy into vibration and reduce this ratio. Table 6 shows that the observed ratios, $E_T(\text{max})/E_{avl}$, can be explained for some cases without invoking distortion, while in other cases, they cannot. Most notably, at 308 nm the maximum energy in translation is much higher than expected if the molecule dissociated from its equilibrium configuration. A ratio of 0.73, for example, would require a b of ~1.17, and in order to measure a translational energy equal to the available energy, b would have to be zero. The large deformations which must be occuring at 308 nm probably account for the fact that the β value at 308 nm was the lowest observed.

While the rigid radical model is useful for predicting when distortion must occur, distortion might still occur if the translational energy is less than or equal to that predicted by the model. A deformation of the molecule could result in vibrational excitation of the radical; then the rigid radical picture would not apply. For example, bending of the Br–C–C–I skeleton toward lower exit impact parameter leads

to lower rotational excitation and thus greater vibrational excitation, for a given translational energy release. Therefore, even at 248 and 266 nm, where the maximum energy in translation is not much different than the rigid radical prediction, β could be reduced because of bending in the complex. A point not to be overlooked, however, is that the impulsive model should more accurately describe the dissociation process at higher excitation energies (such as 266 and 248 nm), where a steeper part of the dissociative surface is reached. At a lower energy excitation to a more level part of the potential, the C–I bond might not break as fast, allowing more time for the radical fragment to distort. In addition, bending does not have to happen only in the excited complex. Depending on the wavelength, Franck-Condon factors might favor absorption from a distorted ground state.

The implications of the anisotropy parameter take on meaning insofar as we understand the nature of the electronic transitions involved in the photodissociation process. A quasi-diatomic picture,[7,11,26] which assumes an $n \longrightarrow \sigma^*$ transition localized on the C–I[Br] bond, predicts ground state iodine formation arising from a perpendicular transition to the $^3Q_1$ or ^1Q states, and spin-orbit excited state iodine is predicted to correlate to the $^3Q_0$ state reached by a parallel transition. Within the context of this picture, our observation of ground state I($^2P_{3/2}$) product with a parallel polarization dependence can only be explained by an initial transition to the $^3Q_0$ state and subsequent curve crossing to the ^1Q (or possibly the $^3Q_1$) state.

The quasi-diatomic model is credible because the UV absorption spectrum of CF_2BrCF_2I, for example, resembles closely the sum of the separate CF_3CF_2Br and CF_3CF_2I absorption spectra.[12] In addition, the position and shape of the C–I absorption continuum in CH_3CH_2I is virtually unchanged when a β-hydrogen is substituted with a Cl of Br. Further evidence for localized transitions comes from Butler, *et al.*,[8,9,26] who showed that excitation near the peak of the supposed C–Br absorp-

tion continuum in CH_2BrI resulted in simple bond fission of only the stronger C–Br bond. (3-center IBr elimination was also observed, but it was a minor channel.) The demonstration of bond-selective photochemistry helps reinforce our desire to view the C–X chromophores in alkyl halides as local diatomic entities.

Unfortunately, some experimental results exist which must cloud our view. In a photodissociation study of CF_2BrCF_2I,[7] whose aim was bond-selective photochemistry, C–I bond breakage was almost twice as probable as C–Br bond fission even though only the C–Br $n \longrightarrow \sigma^*$ transition should have been pumped. This observation was rationalized within the quasi-diatomic framework as a local C–Br bond absorption and a high probability for fast resonant electronic energy transfer to the C–I bond. Recent results in our laboratory show that at 308 nm, photodissociation of both CH_2ClCH_2I and CH_2BrCH_2I, yield only ground state iodine product with a *parallel* polarization dependence. It is difficult to imagine that curve crossing could be as efficient as 100 percent. Quite possibly, the assumed $n \longrightarrow \sigma^*$ absorption spectrum of haloethanes (especially *di*haloethanes) is more complicated than our satisfyingly simple diatomic picture, and the transition moment might not be simply parallel (or perpendicular) to the C–X bond. In such a case (see Eq. (2)), the anisotropy parameter would be less than 2.

The $I(^2P_{1/2})/I(^2P_{3/2})$ branching ratios reported here can also not be explained under the quasi-diatomic assumption. The large ground state iodine component at 308 nm might be interpreted as arising from a slow velocity through the curve crossing, thereby increasing the curve crossing probability, but this interpretation fails to explain why a greater fraction of $I(^2P_{3/2})$ is observed at 248 nm than at 266 nm. Furthermore, it is well known[7,12,26,27–32] that halogen substitution of hydrogens in alkyl iodides changes the $I(^2P_{1/2})$ quantum yield dramatically. Clearly, a complete understanding of the branching ratios requires consideration of the whole molecule.

B. Thermochemistry

The observation of stable CF_2BrCH_2 radical product in the midst of spontaneous secondary dissociation enables the derivation of the energy threshold for breaking both the C–I and C–Br bonds in CF_2BrCH_2I. The precision in the measured ΔH for Reaction (4) is low because the stable radical peak was too small to allow a careful threshold determination in a manner similar to the previous CH_2ClCH_2I analysis.[6] Other factors, which could affect the accuracy of ΔH, must also be considered.

If initial parent internal energy could not be neglected, then Equation (5) would predict a ΔH that is too low by the amount E_{int}^{P}. While the rotational energy of the parent CF_2BrCH_2I molecules in the molecular beam is negligible, vibrations are not cooled nearly so well, and the average vibrational energy could be 2.0-2.5 kcal/mole. In photodissociation from a repulsive surface, only a fraction of the vibrational energy (specifically that associated with the C–I bond) can couple to the dissociation coordinate. This fraction should average less than 0.5 kcal/mole. The contribution from internal energy will therefore be small; moreover, at low excitation levels on the order of a few kcal/mole, the vibrational energy distribution must be roughly exponential with a significant fraction in the ground vibrational state, so the observed threshold will arise from molecules with no initial internal excitation.

A potentially more serious inaccuracy in ΔH could result from an exit channel barrier in CF_2BrCH_2 decomposition. The maximum internal energy $E_{int}^{R}(\max)$ at which stable radical can still exist can be found from Equation (5), where the minimum energy in translation $E_T(\min)$, derived from the stable CF_2BrCH_2 radical peak, is subtracted from the available energy E_{avl}^{*}. The presence of a barrier would make $E_T(\min)$ too low by an amount equal to the barrier height because decomposition of the CF_2BrCH_2 radicals would only occur above the endoergic limit, where they contain the extra internal energy required to overcome the barrier.

Two barrier types could exist: an intrinsic barrier for the addition of Br to the double bond and a centrifugal barrier generated by the necessity of conserving angular momentum when the product radicals fall apart. The intrinsic barrier should be small or nonexistent (if Br addition to the double bond is similar to Cl addition[33]), but even a small barrier of one or two kcal/mole would be near the uncertainty level of our measurement. The centrifugal barrier could be several kcal/mole for some CF_2BrCH_2 radicals because the exit impact parameter for primary C–I fission is high (when dissociation occurs from the equilibrium configuration), leaving the radical with a large angular momentum (perhaps as high as $150\hbar$).

The measured $E_T(\text{min})$ will be too low only if the CF_2BrCH_2 radicals, created with internal energies greater than the C–Br bond energy, do not decompose because of a barrier. While an intrinsic barrier cannot be circumvented, it is plausible that, during the long transit time from the interaction region to the ionizer, the radical will distort and stretch to a geometry where the centrifugal barrier will be minimal, allowing dissociation to take place. Thus, our analysis assumes that nearly all the CF_2BrCH_2 radicals formed with an internal energy above the C–Br endoergicity will dissociate before they can be detected.

A recent photofragmentation study in our laboratory of CF_2BrCF_2I at 266 and 308 nm (see Chapter 4) lends more credence to the unimportance of the centrifugal barrier in the threshold determination. At 266 nm, the low translational energy threshold for existence of stable radical (arising from $I(^2P_{1/2})$ formation) was 13 kcal/mole. At 308 nm, the threshold was observed to be 19.5 kcal/mole when ground state was formed. Analysis of both thresholds produced virtually the *same* value of ΔH for $CF_2BrCF_2I \longrightarrow CF_2CF_2 + Br + I$ (73.3 ± 1 kcal/mole). Given the different translational energies, the angular momenta of the radical fragments should differ by $\sim [E_T(308)/E_T(266)]^{1/2} = 1.23$ in the rigid radical limit

($E_{rot} = L^2/2I_R = E_T\mu b^2/I_R$), and the ratio of barrier heights would be the square of this number, or ~1.5. If a centrifugal barrier were important, we would have expected a higher ΔH from the 308 nm experiment. The CF_2BrCF_2 radical is not an ideal test case, however, because its large size and moment of inertia would result in relatively low levels of rotational excitation—around 3 kcal/mole. And if the centrifugal barrier were to occur at about twice the C–Br bond length, its height would only be ~0.8 kcal/mole, which is within our uncertainty limits. Hence, even though the CF_2BrCF_2 radical data do not necessarily point to the general unimportance of a centrifugal barrier, such a barrier will be unimportant if the moment of inertia of the radical is large.

The secondary dissociation threshold for CH_2ClCH_2I was also determined at two excitation wavelengths, 248 and 266 nm (see Chapter 1), and in this case, the two thresholds differed by ~2 kcal/mole. The 248 nm experiment, where the average E_T was greater, yielded the higher value. The chloroethyl radical is substantially smaller than CF_2BrCF_2 and could be formed with as much as 8 kcal/mole in rotation (with dissociation from the equilibrium configuration), which might lead to a centrifugal barrier height of ~2 kcal/mole. The discrepancy between the two experiments was rationalized as experimental error, but the existence of a centrifugal barrier is possibly a better explanation. If a centrifugal barrier were important, even the threshold energy from the 266 nm experiment could be high.

As stated above, any barrier would cause the apparent minimum energy in translation to be too low by an amount equal to the barrier height, making ΔH for Reaction (4) too high by that amount. Because we cannot rule out a barrier entirely, we must ultimately conclude that, rigorously, our result (and any other obtained by the same method) for the reaction enthalpy is an upper limit.

The heat of formation $\Delta H_f^\circ(0)$ of CF_2BrCH_2I follows directly from our result

for the ΔH of Reaction (4): $\Delta H^{\circ}_{f,0}(CF_2BrCH_2I)$ = –92.6 ± 2 kcal/mole (refer to Table 7). The credibility of this result can be confirmed by examining the following scheme:

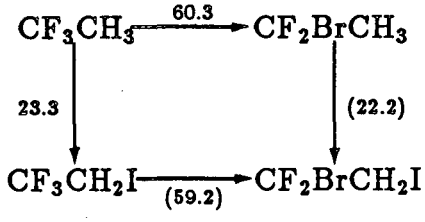

(13)

The numbers are the changes in $\Delta H^{\circ}_{f}(0)$ for each step in units of kcal/mole. Without our experiment result, the values in parentheses would have to be approximated by using the analogous change in $\Delta H^{\circ}_{f}(0)$ for the known, less substituted species, in which case the estimated $\Delta H^{\circ}_{f}(0)$ of CF_2BrCH_2I would be –91.5 ± 1.5 kcal/mole. Thus, our result is quite reasonable.

If the C-I bond energy of CF_2BrCH_2I were known, then the C–Br bond energy of the CF_2BrCH_2 radical could easily be calculated. Although $D^{\circ}_{0}(CF_2BrCH_2\text{–I})$ is not known exactly, a good assumption would be to set it equal to $D^{\circ}_{0}(CF_3CH_2\text{–I})$ = 55.8 ± 1.7 kcal/mole. Then $D^{\circ}_{0}(CH_2CF_2\text{–Br})$ would equal 67.5–55.8 = 11.7 ± 2.5 kcal/mole. An alternative method of obtaining $D^{\circ}_{0}(CH_2CF_2\text{–Br})$ is to assume that ΔH for $CF_3CH_3 \longrightarrow CF_3CH_2 + H$ is the same as ΔH for $CF_2BrCH_2 \longrightarrow CF_2BrCH_2 + H$. $\Delta H^{\circ}_{f,0}(CF_2BrCH_2)$ would then equal 61.3 ± 2.0 kcal/mole and the C–Br bond energy in the radical would be 10.6 ± 2.5 kcal/mole. Both estimates are fairly close; nevertheless, a 5 kcal/mole range of uncertainty is unsatisfactory. If either the C–I bond energy of the parent or the R–X radical bond energy were measured for CF_2BrCH_2I and other similar compounds for which ΔH°_{f} is known, then the thermochemical picture of these iodoethanes would be complete. The effect of substitution in iodoethanes as well as the substitution effect on the bromo(chloro)ethyl radical C–X bond energy would then become clear.

REFERENCES

1. S. Riley and K.R. Wilson, Discuss. Faraday Soc. **53**, 132 (1972).

2. R.K. Sparks, K. Shobatake, L.R. Carlson, and Y.T. Lee, J. Chem. Phys. **75**, 3838 (1981).

3. G.N.A. Van Veen, T. Baller, A.E. De Vries, and N.J.A. Van Veen, Chem. Phys. **87**, 405 (1984).

4. G.N.A. Van Veen, T. Baller, A.E. De Vries, and M. Shapiro, Chem. Phys. **93**, 277 (1985).

5. M.D. Barry and P.A. Gorry, Mol. Phys. **52**, 461 (1984).

6. T.K. Minton, P. Felder, R.J. Brudzynski, and Y.T. Lee, J. Chem. Phys. **81**, 1759 (1984).

7. D. Krajnovich, L.J. Butler, and Y.T. Lee, J. Chem. Phys. **81**, 3031 (1984).

8. L.J. Butler, E.J. Hintsa, S.F. Shane, and Y.T. Lee, J. Chem. Phys., to be published.

9. L.J. Butler, E.J. Hintsa, and Y.T. Lee, J. Chem. Phys. **84**, 4104 (1986).

10. A. Gedanken and M.D. Rowe, Chem. Phys. Lett. **34**, 39 (1975).

11. (a) R.S. Mulliken, Phys. Rev. **50**, 1017 (1936); (b) **51**, 310 (1937); (c) **47**, 413 (1935); (d) J. Chem. Phys. **8**, 382 (1940).

12. W.H. Pence, S.L. Baughcum, and S.R. Leone, J. Phys. Chem. **85**, 3844 (1981).

13. S.J. Lee, and R. Bersohn, J. Phys. Chem. **86**, 728 (1982).

14. A.M. Wodtke and Y.T. Lee, J. Phys. Chem. **89**, 4744 (1985).

15. P.S. Weiss, Ph.D. thesis, University of California, Berkeley, 1986.

16. M. Vernon, "KELVIN Rare Gas Time-of-Flight Program," Lawrence Berkeley Laboratory Report No. 12422, 1981.

17. D.J. Krajnovich, Ph.D. thesis, University of California, Berkeley, 1983.

18. R.B. Berstein, *Chemical Dynamics via Molecular Beam and Laser Techniques* (Oxford University, New York, 1982), p. 30.

19. (a) G.E. Busch and K.R. Wilson, J. Chem. Phys. **56**, 3626 (1972); (b) **56**, 3638 (1972).

20. J.H. Ling and K.R. Wilson, J. Chem. Phys. **65**, 881 (1976).

21. C. Jonah, J. Chem. Phys. **55**, 1915 (1971).

22. D. Porret and C.F. Goodeve, Proc. R. Soc. London Ser. A **165**, 31 (1938).

23. M. Dzvonik, S. Yang, and R. Bersohn, J. Chem. Phys. **61**, 4408 (1974).

24. (a) J.V.V. Kasper, J.H. Parker, and G.C. Pimentel, J. Chem. Phys. **43**, 1827 (1965); (b) M.A. Pollack, Appl. Phys. Lett. **8**, 36 (1966).

25. A. Zewail (private communication).

26. L.J. Butler, Ph.D. thesis, University of California, Berkeley, 1985.

27. C.A. Wight and S.R. Leone, J. Phys. Chem. **87**, 5299 (1983).

28. T. Donohue and J.R. Wiesenfeld, J. Chem. Phys. **63**, 3130 (1975).

29. W.L. Ebstein, J.R. Wiesenfeld, and G.L. Wolk, Chem. Phys. Lett. **53**, 185 (1978).

30. J.B. Koffend and S.R. Leone, Chem. Phys. Lett. **81**, 136 (1981).

31. J.E. Smedley and S.R. Leone, J. Chem. Phys. **79**, 2687 (1983).

32. E. Gerck, J. Chem. Phys. **79**, 311 (1983).

33. H. B. Schlegel and C. Sosa, J. Phys. Chem. **88**, 1141 (1984).

34. *JANAF Thermochemical Tables*, 2nd ed. Natl. Stand. Ref. Data Ser., U.S. Natl. Bur. Stand **37** (U.S. GPO, Washington, D.C., 1971).

35. J.D. Cox and G. Pilcher, *Thermochemistry of Organic and Organometallic Compounds*, Academic Press, New York, N.Y., 1970.

36. J.C. Traeger and R.G. McLoughlin, J. Am. Chem. Soc. **103**, 3647 (1981).

37. A.L. Castelhano, P.R. Marriott, and D. Griller, J. Am. Chem. Soc. **103**, 4262 (1981).

38. S.W. Benson and A. Amano, J. Chem. Phys. **36**, 3464 (1962).

39. A.S. Rodgers and W.G.F. Ford, Int. J. Chem. Kinet. **5**, 965 (1973).

40. J.M. Pickard and A.S. Rodgers, Int. J. Chem. Kinet. **9**, 759 (1977).

41. S.S. Chen, A.S. Rodgers, J. Chao, R.C. Wilhoit, and B.J. Zwolinski, J. Phys. Chem. Ref. Data **4**, 441 (1975).

42. G.S. Buckley, W.G.F. Ford, and A.S. Rodgers, Thermochim. Acta **42**, 349 (1980).

43. E.C. Wu and A.S. Rodgers, J. Phys. Chem. **78**, 2315 (1974).

44. S.S. Chen, A.S. Rodgers, J. Chao, R.C. Wilhoit, and B,J, Zwolinski, Natl. Stand. Ref. Data Ser., Natl. Bur. Stand. **No. 3-35706** (Jan. 1974).

45. G.S. Buckley, W.G.F. Ford, and A.S. Rodgers, Thermochim. Acta **49**, 199 (1981).

46. E.C. Wu, J.M. Pickard, and A.S. Rodgers, J. Phys. Chem. **79**, 1078 (1975).

47. T.K. Minton, G.M. Nathanson, and Y.T. Lee, unpublished (Chapter 4).

48. J.M. Pickard and A.S. Rodgers, J. Am. Chem. Soc. **99**, 691 (1977).

49. E.C. Wu and A.S. Rodgers, J. Am. Chem. Soc. **98**, 6112 (1976).

50. S.W. Benson, J. Chem. Ed. **42**, 502 (1965).

TABLE I. Parameters obtained by fitting measured beam number density distributions to the form: $N(v) \propto v_2 \exp[-(v/\alpha - S)^2]$. The peak (most probable) velocity is given by $v_{PK} = \frac{1}{2}\alpha S[1 + \sqrt{1 + 4/S^2}]$. α and v_{PK} are in units of cm/sec.

	Calibration		
Wavelength	α	S	v_{PK}
266 nm	4272[a]	16.87[a]	72,320[a]
	4829[b]	14.43[b]	70,020[b]
248 nm	5039	13.93	70,550
308 nm	4998	13.96	70,130

[a] I^+ TOF data

[b] all other TOF data at 266 nm

TABLE II. Absorption cross section σ and product of cross section and laser intensity F for the three wavelengths studied. Estimated errors in the two quantities are $\pm 10\%$ and $\pm 20\%$, respectively.

		σF	
Wavelength	$\sigma(\times 10^{-19}$ cm$^2)$	Horizontal polarization	Vertical polarization
248 nm	3.2	0.27	0.45
266 nm	5.2	0.42	0.42
308 nm	0.32	0.057	0.087

TABLE III. Observed and calculated horizontal/vertical polarization signal ratios for 266 nm photodissociation at a source angle of 20°.

trial β	Horizontal/Vertical	
—	4.11	observed
1.5	3.73	
1.6	4.05	best
1.7	4.43	

TABLE IV. Observed and calculated horizontal/vertical polarization signal ratios for 248 nm photodissociation at a source angle of 20°. β^* refers to the I($^2P_{1/2}$) component and β refers to the I($^2P_{3/2}$) component.

trial β (β^*, β)	Horizontal/Vertical	
———	4.50	observed
1.3, 0.95	3.38	
1.5, 1.15	4.11	
1.6, 1.25	4.54	best
1.7, 1.35	5.03	

TABLE V. Observed and calculated horizontal/vertical polarization signal ratios for 308 nm photodissociation at a source angle of 20°.

trial β	Horizontal/Vertical	
—	3.00	observed
1.0	2.56	
1.1	2.79	
1.2	3.04	best
1.3	3.32	
1.4	3.63	

TABLE VI. Fraction of available energy in translation for each iodine dissociation channel [I($^2P_{3/2}$) and I*($^2P_{1/2}$)] for the minimum, maximum, and average translational energy in each $P(E_T)$.

	E_T/E_{avl}			E_T^*/E_{avl}^*		
Wavelength	E_T(min)	E_T(max)	$< E_T >$	E_T^*(min)	E_T^*(max)	$< E_T^* >$
248 nm	0.28	0.59	0.41	0.15	0.61	0.41
266 nm	0.35	0.58	0.45	0.17	0.73	0.46
308 nm	0.27	0.73	0.51	0.13	1.0	0.65

TABLE VII. Standard molar enthalpies of formation for some substances at 300 K and 0 K.

Species	ΔH_f°(300 K) (kcal/mole)	ΔH_f°(0 K) (kcal/mole)	Reference
H	52.103±0.001	51.631±0.001	34
F	18.86±0.40	18.36±0.40	34
Br	26.74±0.07	28.19±0.07	34
I	25.53±0.01	25.63±0.01	34
$CH_2=CH_2$	12.53±0.07	14.58±0.07	34
$CF_2=CH_2$	−80.5±1.0	−78.9±1.2[a]	35
$CF_2=CF_2$	−157.4±0.7	−156.6±0.7	34
CH_3CH_3	−20.08±0.05	−16.33±0.05[a]	36
CH_3CH_2Br	−15.2±0.5	−10.0±0.5	35
CH_3CH_2I	−2.0±0.4	1.90±0.5[a]	37
CH_2ICH_2I	15.9±0.2	19.7±0.3[a]	38
CH_3CF_3	−178.2±0.4	−175.1±0.6[a]	39
CH_3CF_2Br	−114.2±1.5	−109.3±1.5[a]	40
CH_3CF_2I	−98.9±1.5	−95.9±1.6[a]	41
CF_3CH_2Br	−166.0±0.5	−161.6±0.7[a]	42
CF_3CH_2I	−154.3±0.7	−151.8±1.0[a]	43
CF_2BrCH_2I	−96.9±2.0[a]	−92.6±2.0	this work
CF_3CF_3	−320.9±0.8	−318.9±0.8[a]	44
CF_3CF_2Br	−254.4±1.0	−251.0±1.0[a]	45
CF_3CF_2I	−240.0±1.0	−238.0±1.0[a]	46
CF_2BrCF_2I	−179.5±1.0[a]	−176.1±1.0	47
CF_2ICF_2I	−167.4±1.0[a]	−165.4±1.0	47
$CH_3CH_2\cdot$	28.0±1.0	30.6±1.0[a]	37
$CH_3CF_2\cdot$	−72.3±1.8	−70.0±2.0[a]	48
$CF_3CH_2\cdot$	−123.6±1.2	−121.6±1.4[a]	43
$CF_3CF_2\cdot$	−213.0±1.3	−211.6±1.3[a]	49

[a]Calculated by correcting for thermal energy (Ref. 50)

FIGURE CAPTIONS

Figure 1. Rotating molecular beam source photofragmentation apparatus. 1. Nozzle assembly; 2. Nozzle heating; 3. Cryostatic collimation slit; 4. Laser focussing lens; 5. Laser/molecular beam crossing point; 6. LN cooled panels; 7. Dectector gate valve; 8. Retractable chopping wheel; 9. Main chamber diffusion pump; 10. Source chamber diffusion pump; 11. Electron-impact ionizer; 12. Q-pole mass spectrometer; 13. Magnetically suspended turbopump; 14. Exit ion optics; 15. Ion target; 16. Scintillator; 17. Detector grease-sealed turbopumps; 18. Photomultiplier tube; 19. LN Dewars. The time-of-flight (TOF) spectra of the photoproducts are measured by firing a pulsed ArF laser at point 5 and measuring the time required for the signal at a defined m/e to appear at the detector, 11. The calibrated flight length allows the determination of the lab-frame velocity. By vectorially subtracting the parent beam velocity, measured with the retractable chopping wheel at 8, the center-of-mass (c.m.) velocity distributions of the photoproducts are obtained.

Figure 2. UV absorption spectrum of gaseous CF_2BrCH_2I measured with a Cary 14 spectrophotometer. The broad absorption peak centered at 263 nm is attributed to excitation of a nonbonding 5pπ iodine electron to a σ^* molecular orbital localized on the C–I bond. An analogous absorption also exists for the C–Br chromophore and occurs at shorter wavelengths. In this figure, the low energy tail of the C–Br absorption is observed.

Figure 3. Laboratory TOF distributions of I atom product at 266 nm (horizontal laser polarization) for five source angles. o Experimental points; —— overall fit calculated using the total $P(E_T)$ distribution in Fig. 15 and $\beta = 1.6$; - - - - calculated

fits using the component $P(E_T)$'s in Fig. 15.

Figure 4. Laboratory angular distribution of I atom product at 266 nm (horizontal polarization). ● Experimental points obtained by integrating and normalizing the TOF distributions in Fig. 3. $\pm 2\sigma$ error bars (statistical counting error) are smaller that the symbols. —— $\beta = 1.5$; - - - - $\beta = 2.0$.

Figure 5. Kinematic diagram showing the relationship between the molecular beam velocity v_b, the center-of-mass recoil velocity v_{cm}, and the laboratory velocity flux distribution, I(v). The laboratory (source) angle Θ, and the c.m. angles, $\theta_\parallel$ and $\theta_\perp$, are also shown. The c.m. angle θ is the angle between the electric vector of the laser light and the c.m. recoil direction of the products. $\theta_\parallel$ is the c.m. angle when the laser is polarized parallel (horizontal polarization) to the detector axis, and $\theta_\perp$ is the c.m. angle when the laser is polarized perpendicular (vertical polarization) to the detector axis. θ(min) refers to the minimum c.m. angle in the range of the I(v) distribution. The curves depicting the ratios, $\cos^2\theta/\cos^2[\theta(\text{min})]$, show that $\cos^2\theta_\perp$ changes almost a factor of 5 more than $\cos^2\theta_\parallel$ over the range of I(v). Thus, when the transition moment is approximately parallel to the C–I bond (i.e., $w(\theta) \sim \cos^2\theta$), the fits to the data will be much more sensitive to the angular distribution when the laser polarization is vertical rather than horizontal.

Figure 6. Laboratory TOF distribution of I atom product with vertical laser polarization at 266 nm and a source angle of 20°. The calculated fits all use the same $P(E_T)$ distribution (Fig. 15) but different β parameters in order to illustrate the sensitivity of the fit to β.

Figure 7. (a) Laboratory TOF distribution of products detected at $m/e = 79$

at 266 nm (horizontal polarization) for $\Theta = 20°$. Only the experimental points are shown. The arrow points to a small peak resulting from stable CF_2BrCH_2 radical product which is detected at the bromine mass. The sharp fast feature is mostly due to primary C–Br bond fission, with some of the fastest signal coming from secondary *photo*dissociation. The broad background arises from spontaneous secondary dissociation of the internally excited CF_2BrCH_2 primary product. (b) Blow-up of (a) in the region of the stable radical peak with the calculated TOF of the CF_2BrCH_2 fragment if it had all been stable (and able to be detected at $m/e = 79$). As expected, the stable radical peak corresponds in arrival time to the fast edge of the calculated excited state $I(^2P_{1/2})$ TOF.

Figure 8. Laboratory TOF distribution of products detected at $m/e = 64$ at 266 nm (horizontal polarization) for $\Theta = 20°$. The sharp fast peak arises from secondary photodissociation, while the broad background comes from spontaneous secondary dissociation of the internally hot radical photofragment. The arrow at 300 μs marks the expected arrival time of the stable CF_2BrCH_2 radical product based on its position in the $m/e = 79$ TOF.

Figure 9. Laboratory TOF distributions of I atom product at 248 nm (horizontal polarization) for four source angles. o Experimental points; ——overall fit calculated using the total $P(E_T)$ distribution in Fig. 15 with $\beta = 1.25$ for the $I(^2P_{3/2})$ channel and $\beta = 1.6$ for the $I(^2P_{1/2})$ channel. - - - - calculated fits using the component $P(E_T)$'s in Fig. 15 with their respective β parameters.

Figure 10. Laboratory TOF distribution of I atom product with vertical laser polarization at 248 nm and a source angle of 20°; ——, - - - - calculated fits from the total and component $P(E_T)$ distributions , respectively, in Fig. 15. $\beta = 1.25$

for the faster I($^2P_{3/2}$) channel and $\beta = 1.6$ for the slower I($^2P_{1/2}$) channel.

Figure 11. Laboratory TOF distribution of products detected at $m/e = 79$, $\Theta = 20°$, and λ =248 nm for both horizontal and vertical laser polarizations. Only the experimental points are shown. The horizontal polarization TOF is qualitatively similar to that at 266 nm (see Fig. 7).

Figure 12. Laboratory TOF distribution of products detected at $m/e = 64$ at 248 nm (horizontal polarization) for $\Theta = 20°$. Only the experimental points are shown. The most prominent peak, occurring at ~300μs, is contamination in the TOF from $m/e = 63.5$ (I^{++}). The smaller, faster peak comes from secondary photodissociation (see Fig. 8). The broad background is, as usual, the result of spontaneous secondary dissociation.

Figure 13. Laboratory TOF distributions of I atom product at 308 nm (horizontal polarization) for four source angles. o Experimental points; —— overall fit calculated using the total $P(E_T)$ distribution in Fig. 15 and $\beta = 1.2$; - - - - calculated fits using the component $P(E_T)$'s in Fig. 15.

Figure 14. Laboratory TOF distribution of products detected at $m/e = 79$ at 308 nm (horizontal polarization) for $\Theta = 20°$. The experimental points are shown along with a calculated TOF, which assumes that all the CF_2BrCH_2 photoproduct is stable and detectable at $m/e = 79$.

Figure 15. Center-of-mass recoil translational energy distributions for CF_2BrCH_2I photodissociation at 248, 266, and 308 nm. The *solid* curve shows the total $P(E_T)$ derived from fitting the time-of-flight data of the iodine fragment. The *dashed* curves depict the estimated deconvolution of the total $P(E_T)$ into the distributions for each

of the two possible dissociation channels. The relative probability of each channel is shown under the product iodine state. The low energy shoulder in the 248 and 266 nm $P(E_T)$'s is a result of I atom detection following primary C–Br bond fission (see text); thus, the shoulder is not part of the photodissociation process represented here, and the curve for the excited state iodine channel has been smoothly extended such that is does not include the shoulder.

Figure 16. Energy level diagram for photodissociation of CF_2BrCH_2I at 248, 266, and 308 nm. The total $P(E_T)$ distributions are shown in order to illustrate the relationship between the translational energy distributions and the energy available for translation. The asterisk (*) refers to the spin-orbit excited state $^2P_{1/2}$ of the atom.

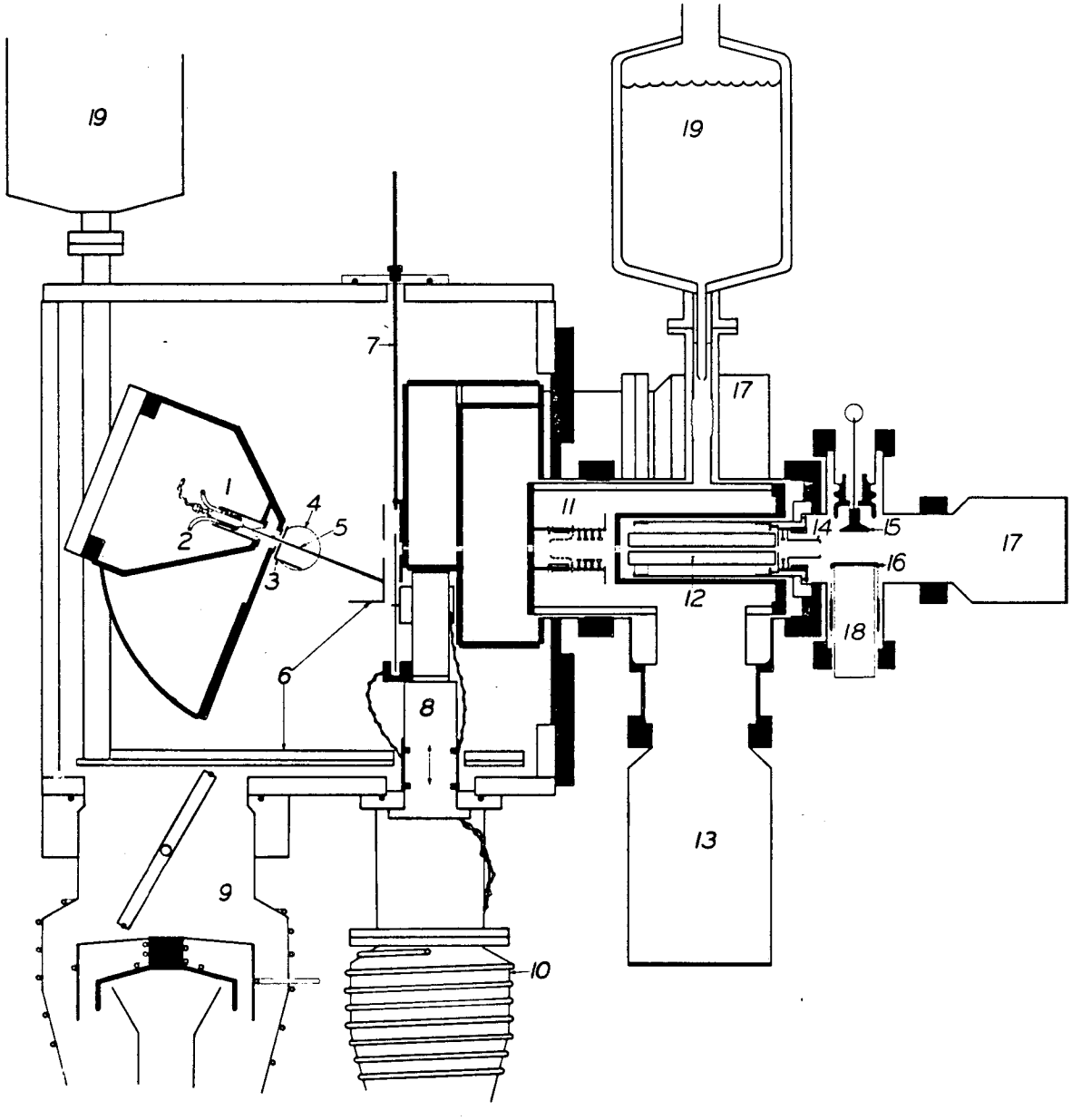

XBL 862-713

Figure 1

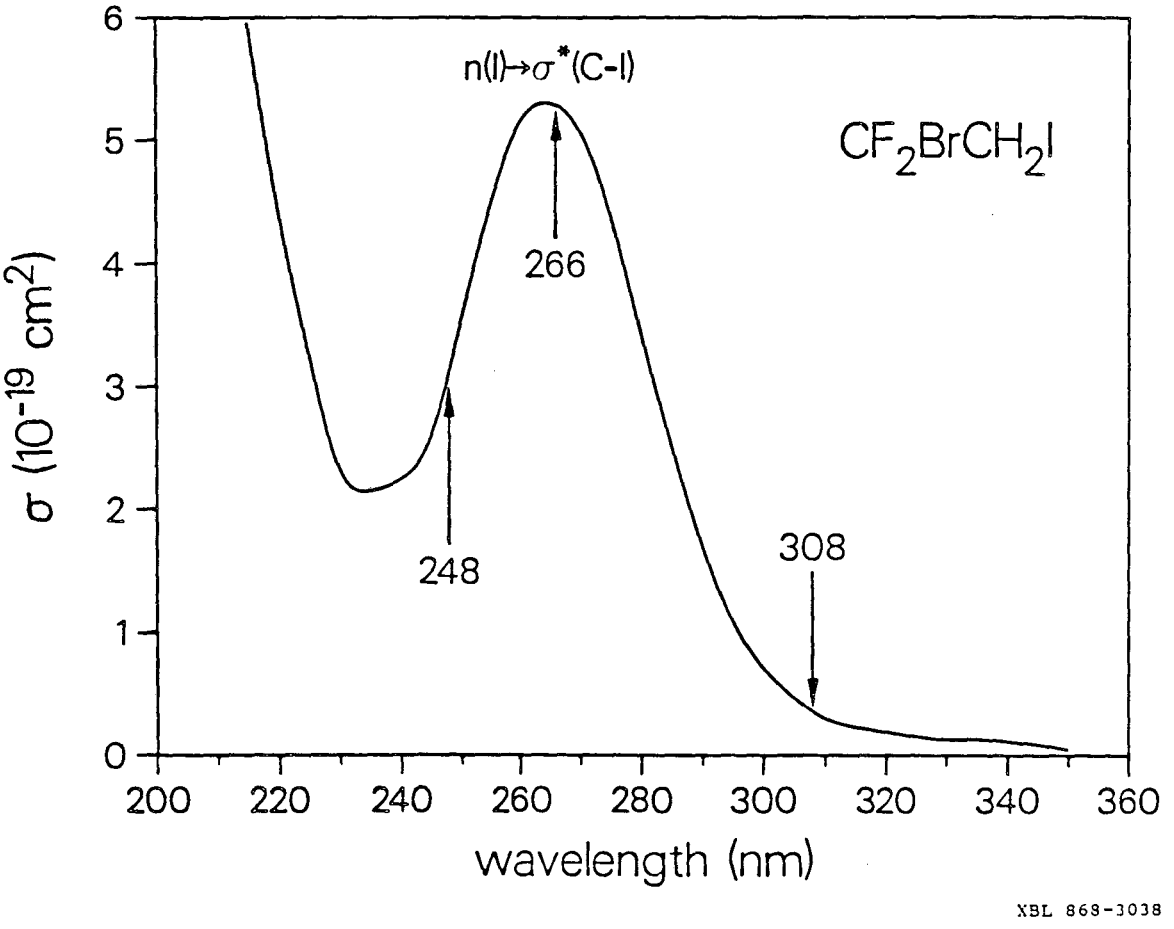
n(I)→σ*(C-I)
CF2BrCH2I
266
248
308
σ (10-19 cm2)
wavelength (nm)
0
1
2
3
4
5
6
200
220
240
260
280
300
320
340
360
XBL 868-3038

Figure 2

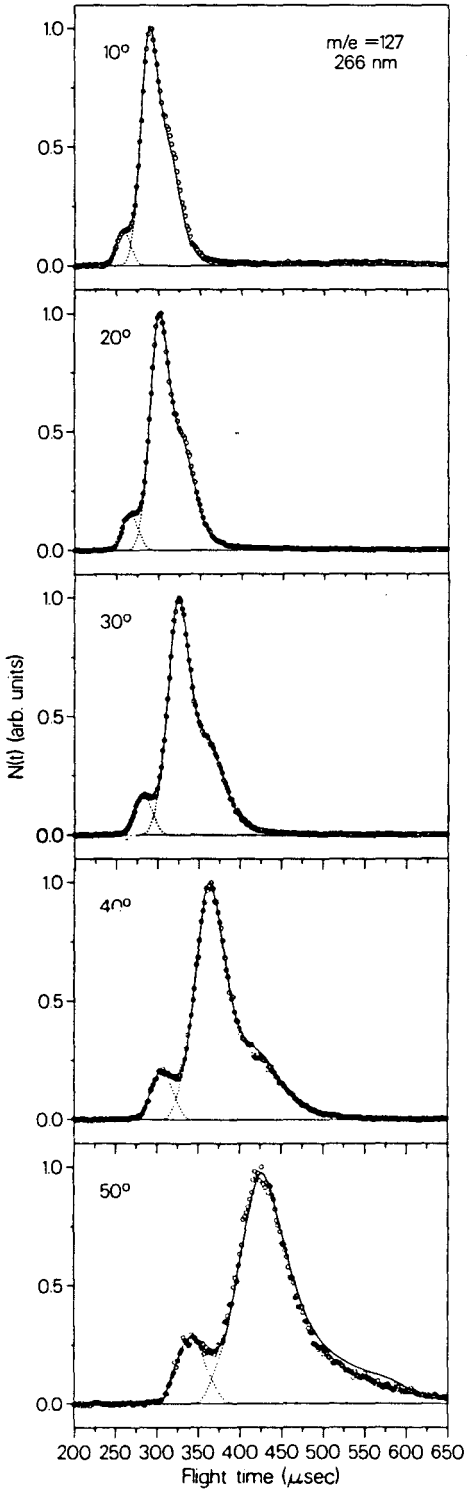
10°
m/e =127
266 nm
20°
30°
40°
50°
1.0
0.5
0.0
N(t) (arb. units)
200 250 300 350 400 450 500 550 600 650
Flight time (μsec)
XBL 867-2707

Figure 3

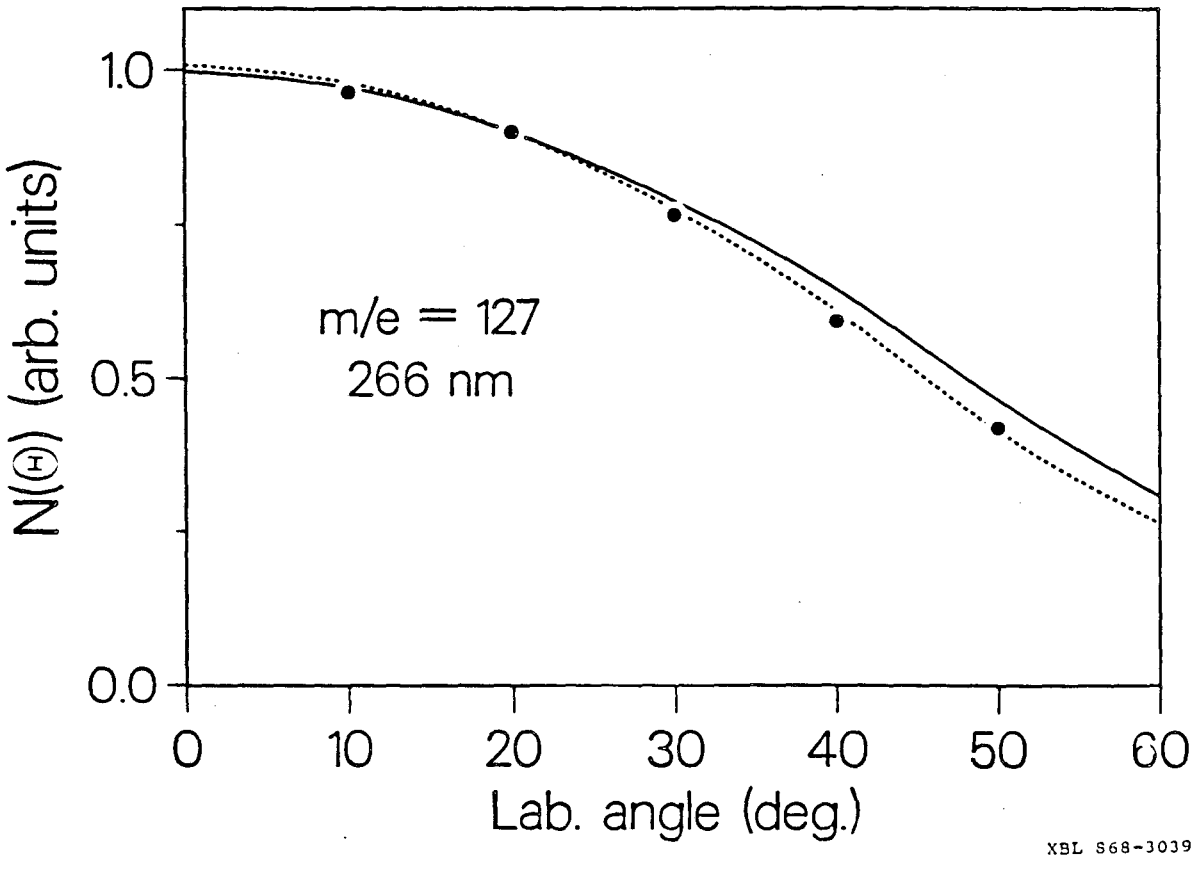
1.0
0.5
0.0
N(H) (arb. units)
m/e = 127
266 nm
0
10
20
30
40
50
60
Lab. angle (deg.)
XBL 868-3039

Figure 4

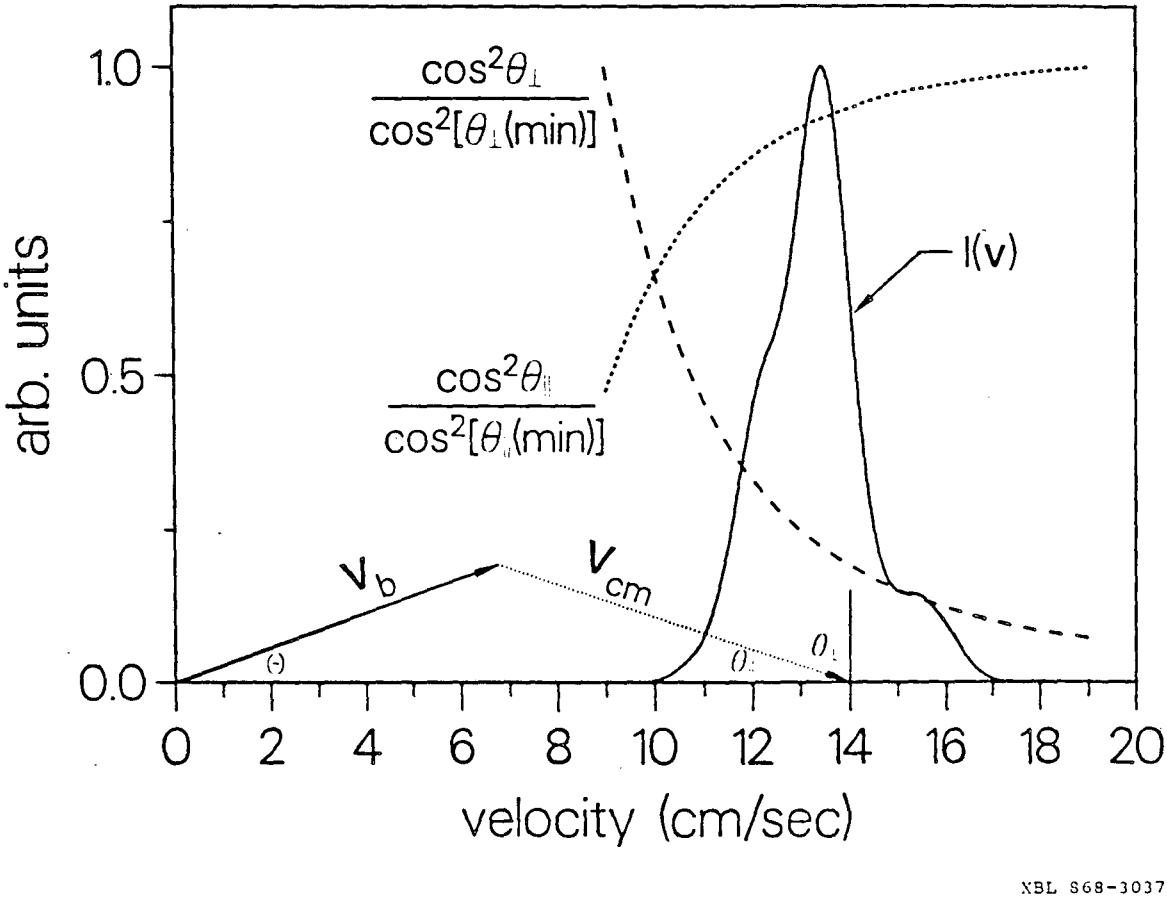
1.0
0.5
0.0
arb. units
$\frac{\cos^2\theta_\perp}{\cos^2[\theta_\perp(\min)]}$
$\frac{\cos^2\theta_\parallel}{\cos^2[\theta_\parallel(\min)]}$
I(v)
v_b
v_{cm}
θ
$\theta_\parallel$
$\theta_\perp$
0 2 4 6 8 10 12 14 16 18 20
velocity (cm/sec)
XBL 868-3037

Figure 5

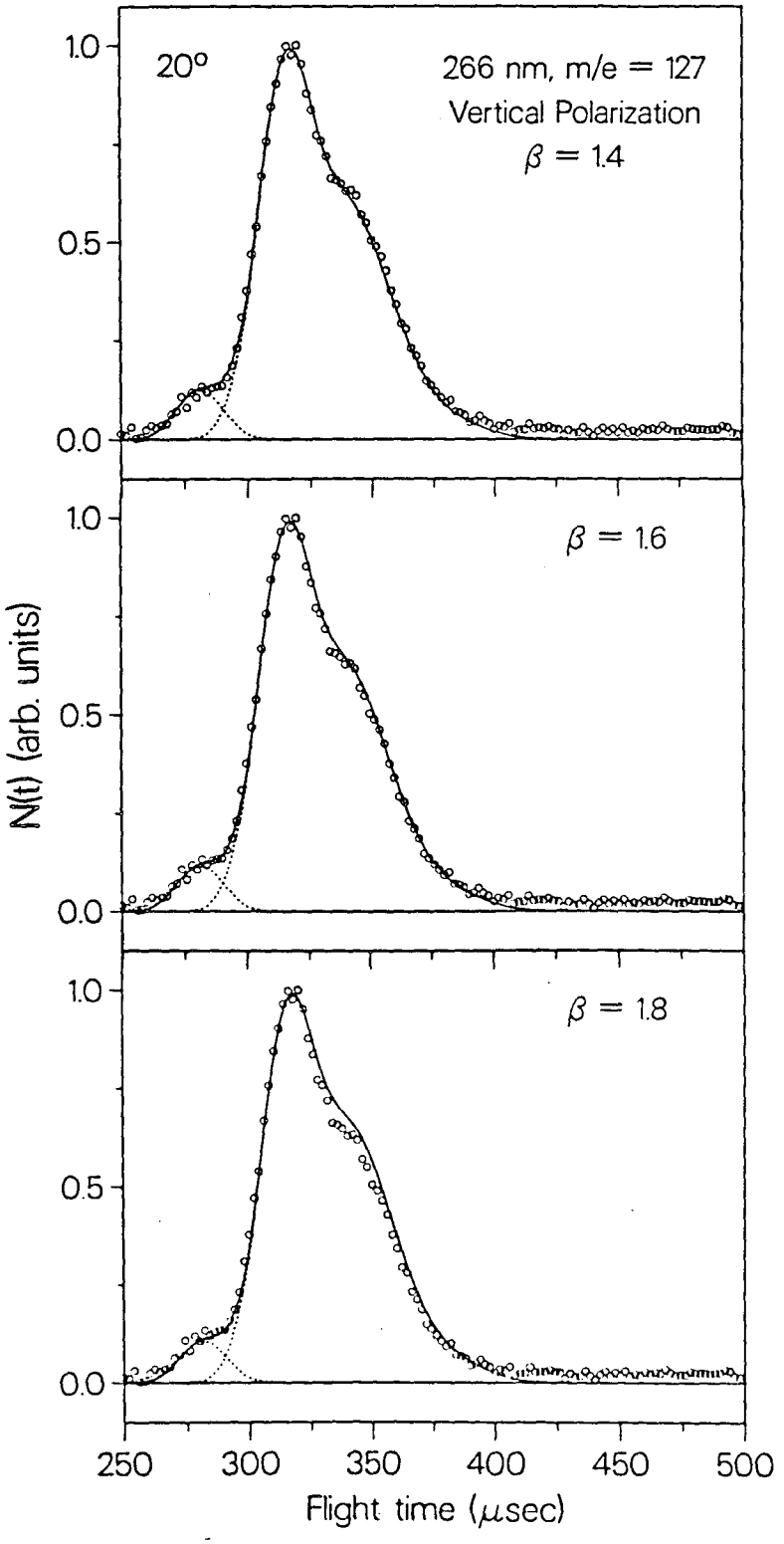
20°
266 nm, m/e = 127
Vertical Polarization
β = 1.4
β = 1.6
β = 1.8
N(t) (arb. units)
1.0
0.5
0.0
250
300
350
400
450
500
Flight time (μsec)
XBL 868-3031

Figure 6

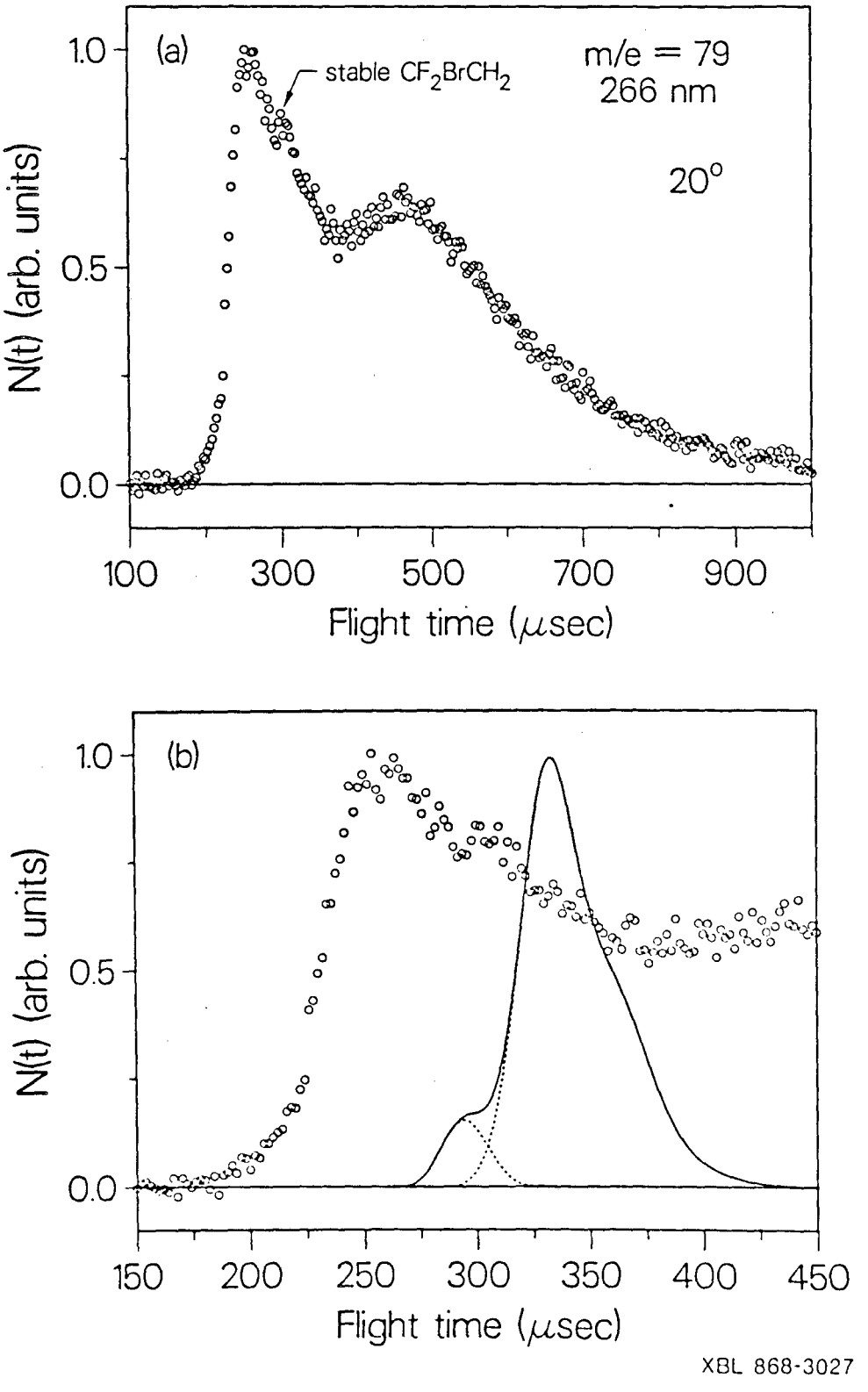
(a)
stable CF_2BrCH_2
m/e = 79
266 nm
20°
1.0
0.5
0.0
N(t) (arb. units)
100
300
500
700
900
Flight time (μsec)
(b)
1.0
0.5
0.0
N(t) (arb. units)
150
200
250
300
350
400
450
Flight time (μsec)
XBL 868-3027

Figure 7

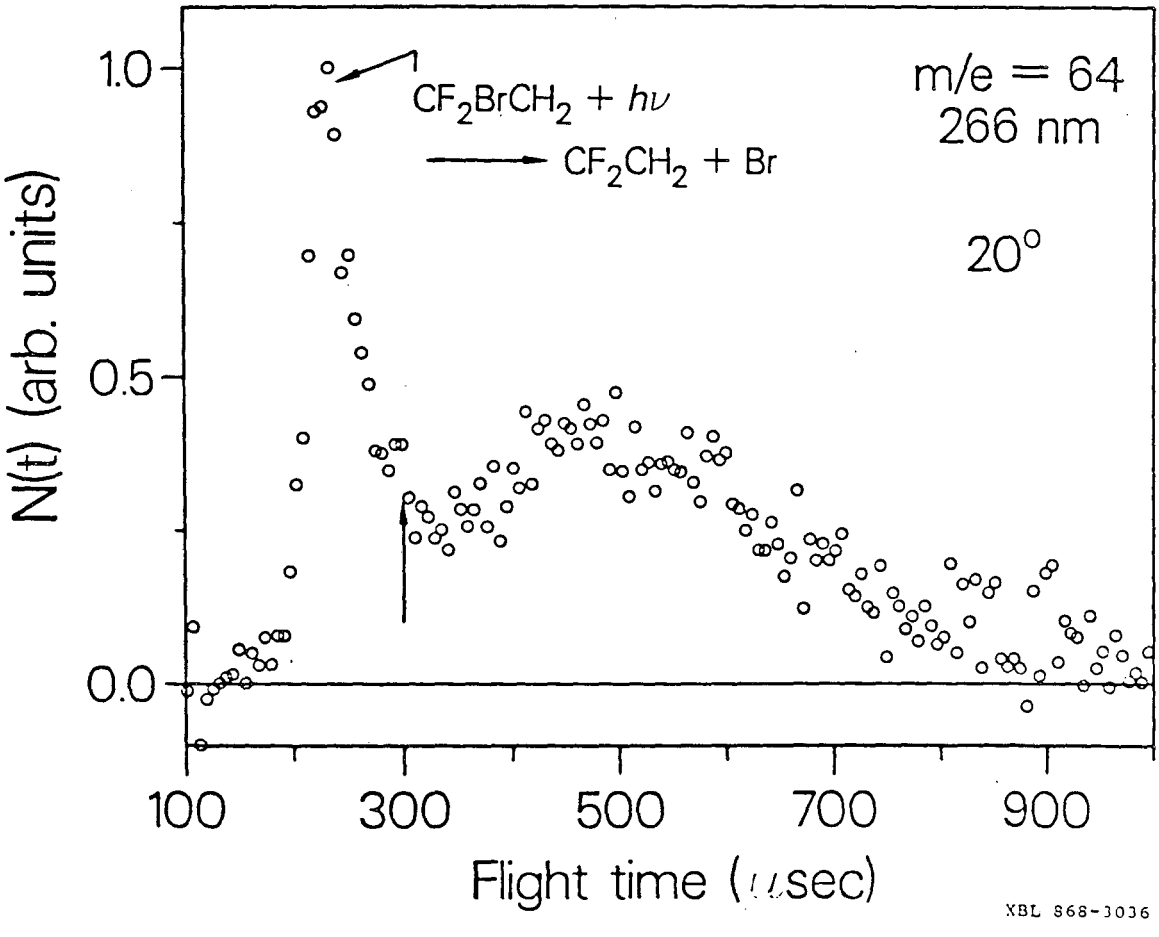
1.0
0.5
0.0
N(t) (arb. units)
$CF_2BrCH_2 + h\nu$
$\longrightarrow CF_2CH_2 + Br$
m/e = 64
266 nm
20°
100
300
500
700
900
Flight time (μsec)
XBL 868-3036

Figure 8

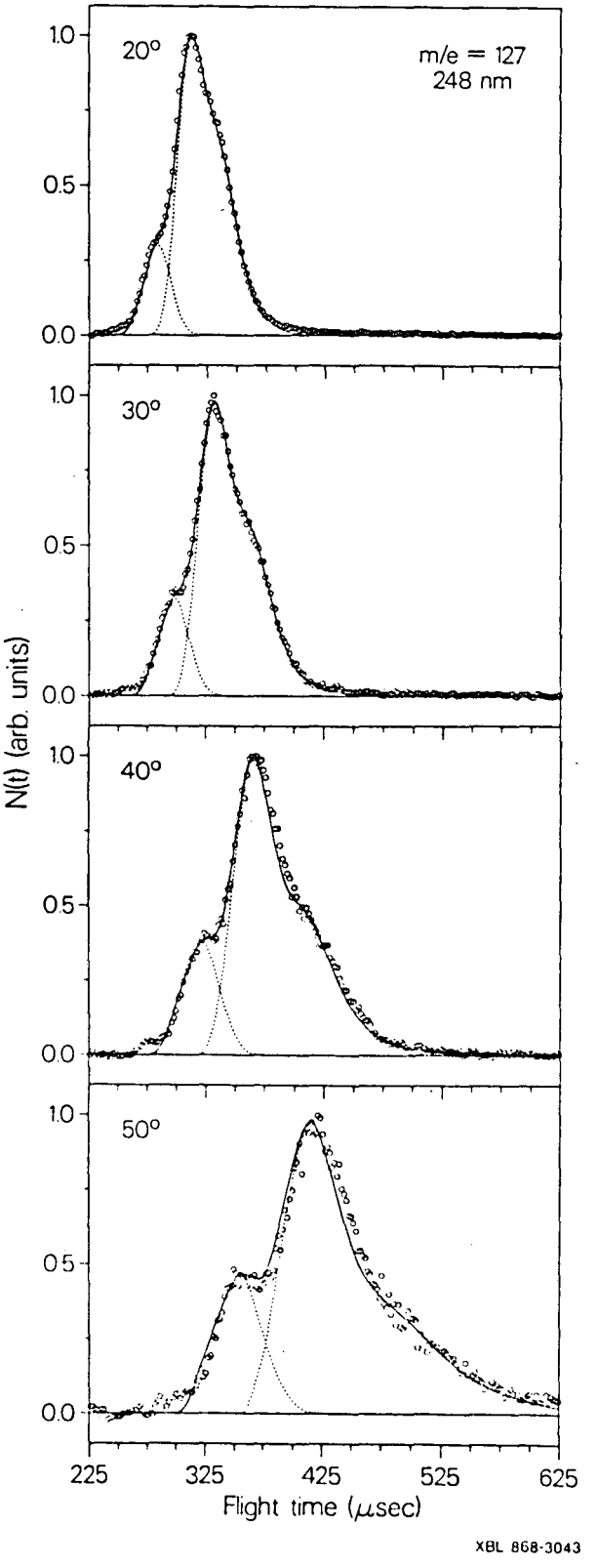
20°
m/e = 127
248 nm
30°
40°
50°
1.0
0.5
0.0
N(t) (arb. units)
225
325
425
525
625
Flight time (μsec)
XBL 868-3043

Figure 9

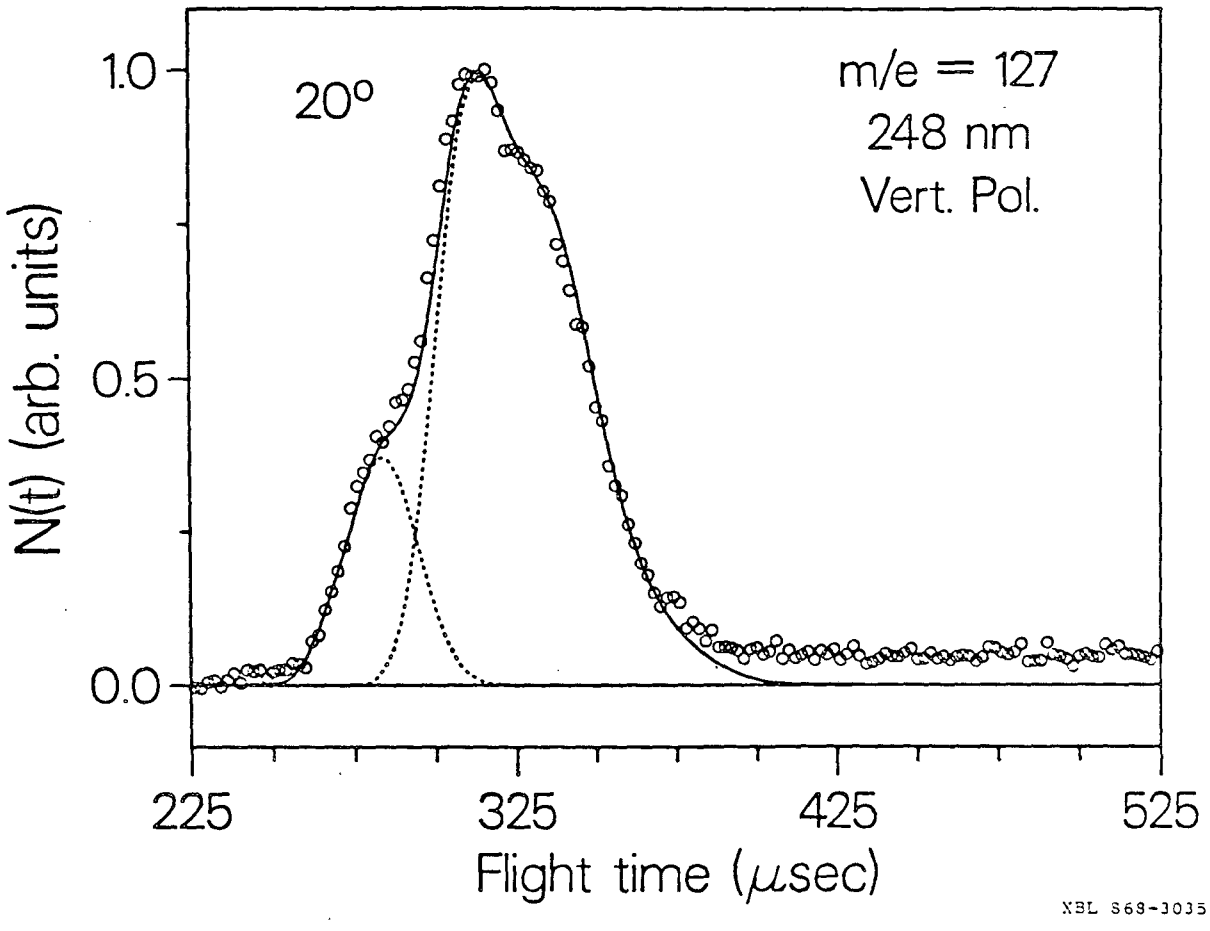
1.0
0.5
0.0
N(t) (arb. units)
20°
m/e = 127
248 nm
Vert. Pol.
225
325
425
525
Flight time (μsec)
XBL 868-3035

Figure 10

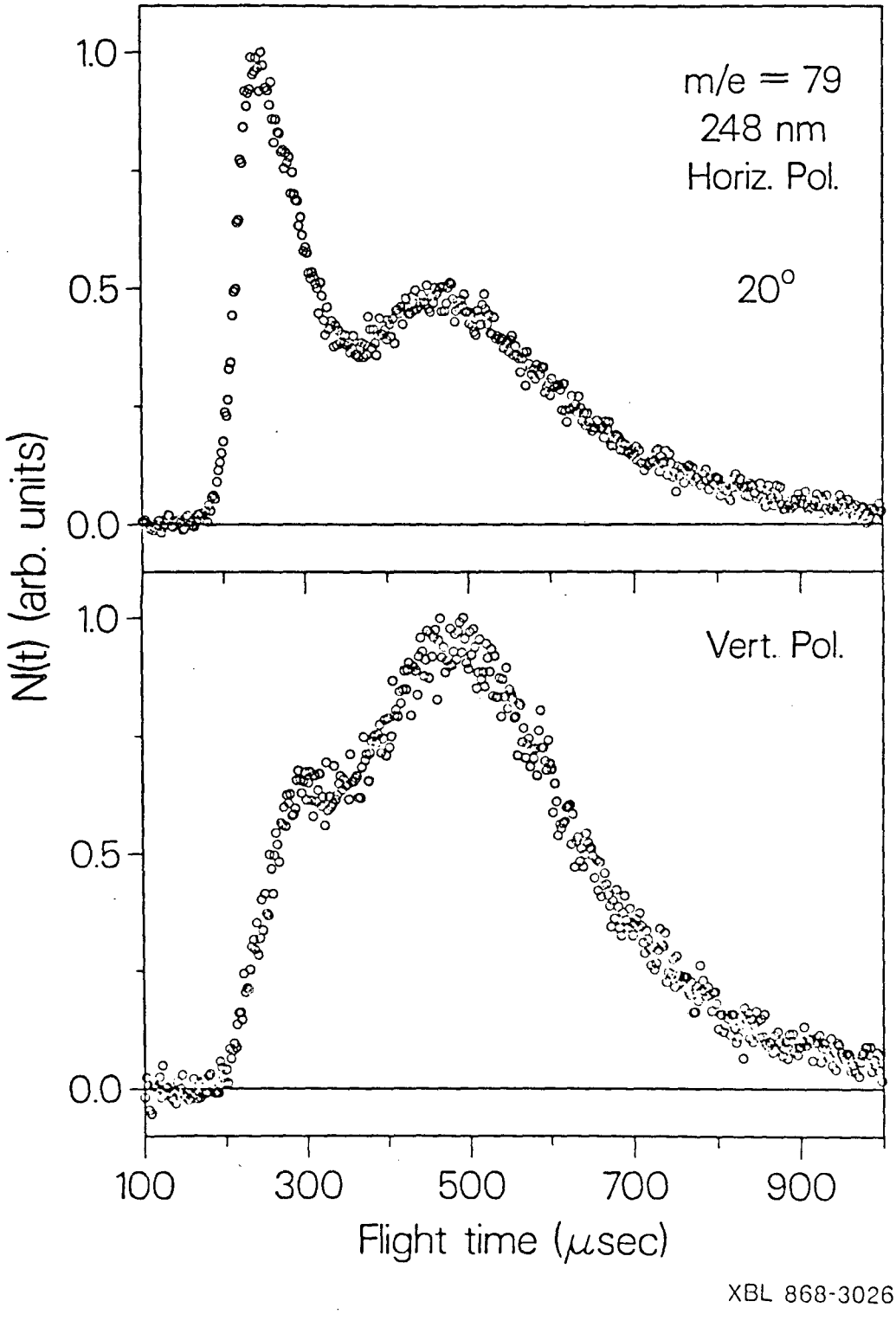
m/e = 79
248 nm
Horiz. Pol.
20°
Vert. Pol.
N(t) (arb. units)
1.0
0.5
0.0
1.0
0.5
0.0
100
300
500
700
900
Flight time (μsec)
XBL 868-3026

Figure 11

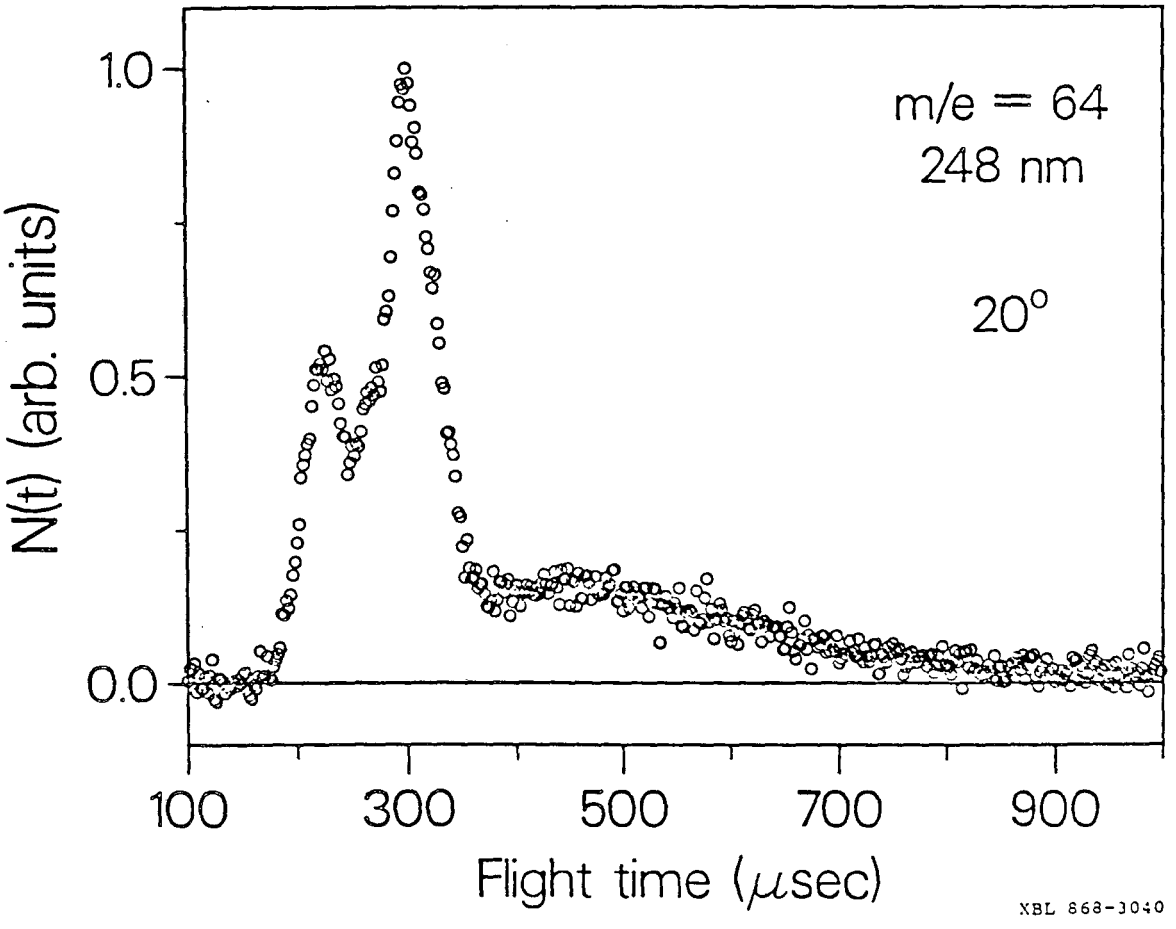
1.0
0.5
0.0
N(t) (arb. units)
m/e = 64
248 nm
20°
100
300
500
700
900
Flight time (μsec)
XBL 868-3040

Figure 12

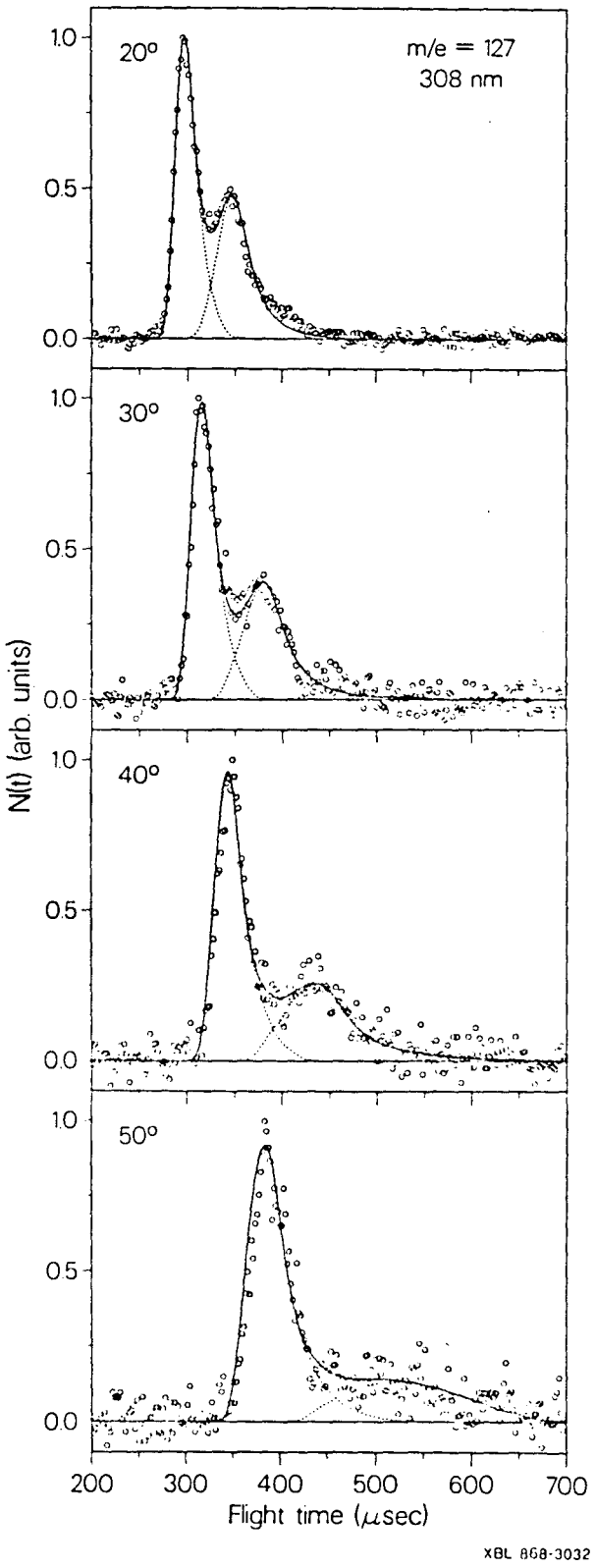
20°
m/e = 127
308 nm
30°
40°
50°
1.0
0.5
0.0
N(t) (arb. units)
200
300
400
500
600
700
Flight time (μsec)
XBL 868-3032

Figure 13

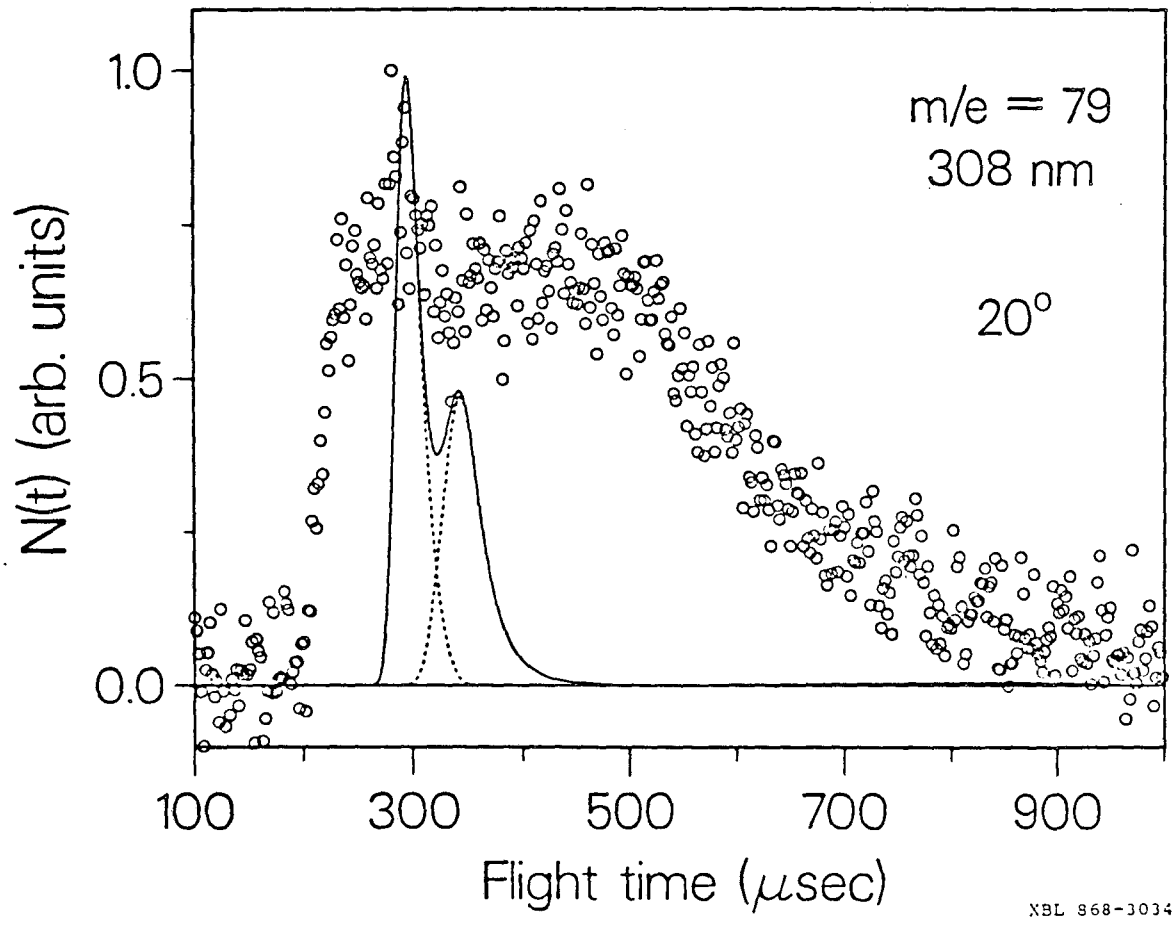
1.0
0.5
0.0
N(t) (arb. units)
m/e = 79
308 nm
20°
100
300
500
700
900
Flight time (μsec)
XBL 868-3034

Figure 14

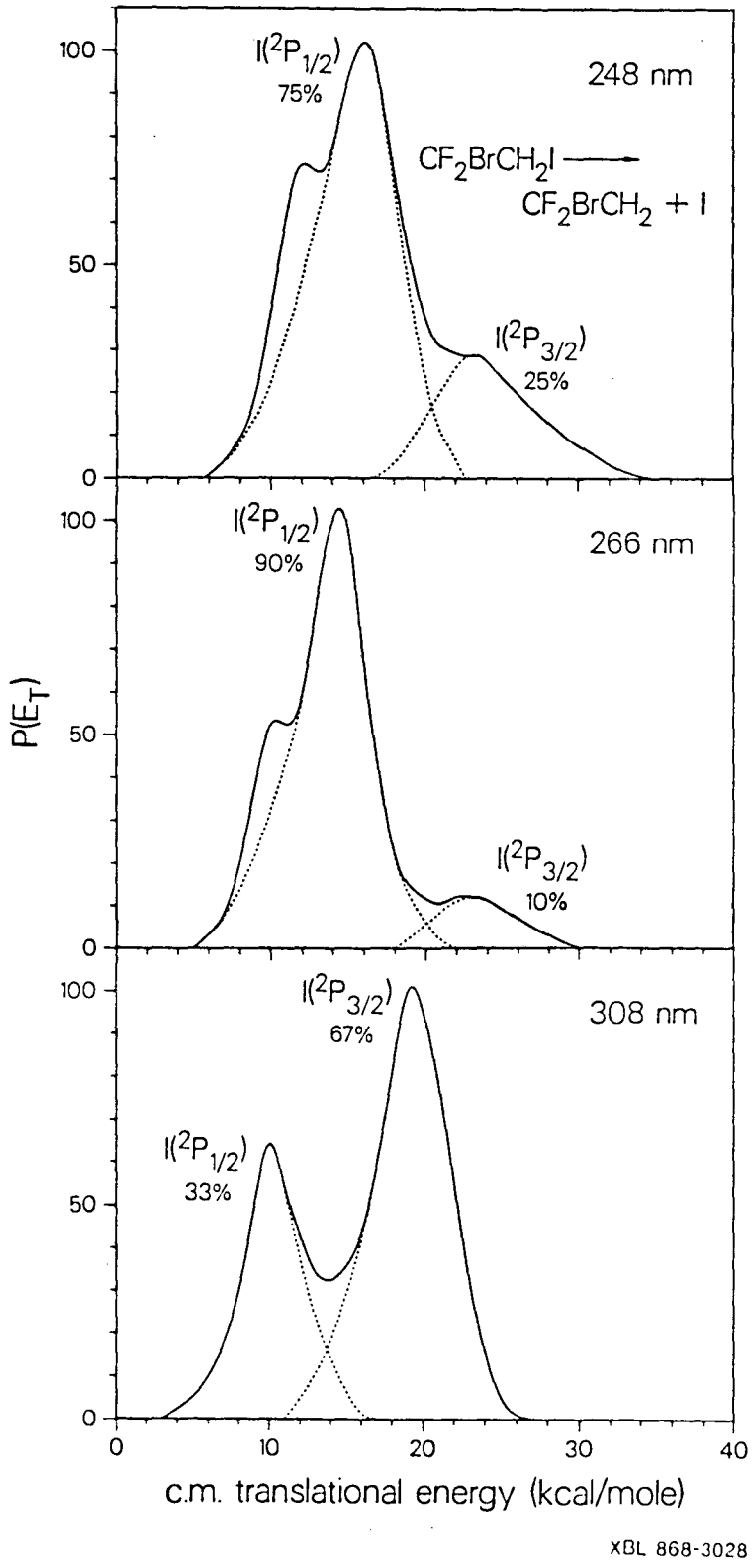
100
50
0
I(2P1/2)
75%
248 nm
CF2BrCH2I ⟶
CF2BrCH2 + I
I(2P3/2)
25%
I(2P1/2)
90%
266 nm
I(2P3/2)
10%
P(ET)
I(2P3/2)
67%
308 nm
I(2P1/2)
33%
0
10
20
30
40
c.m. translational energy (kcal/mole)
XBL 868-3028

Figure 15

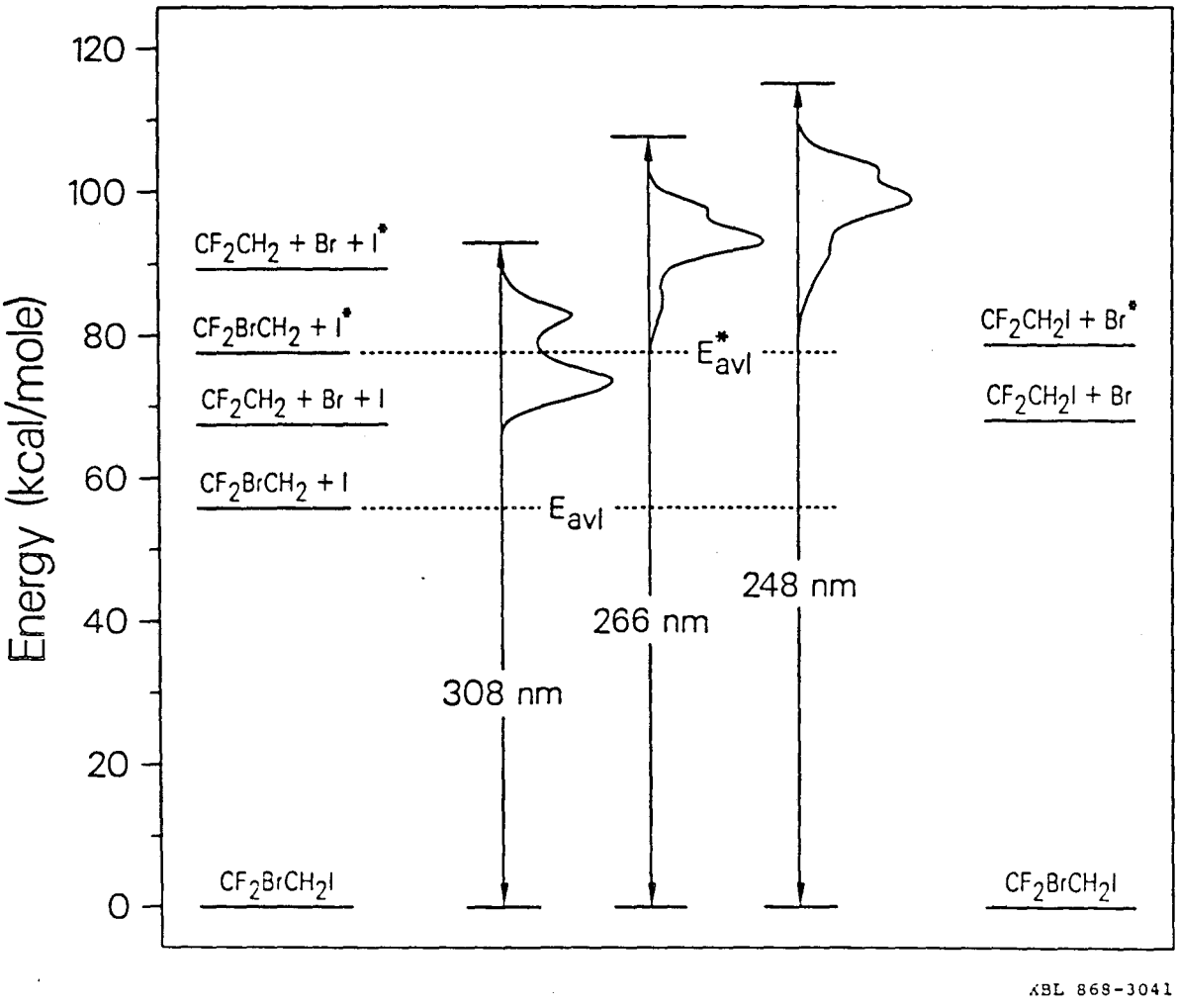
120
100
80
60
40
20
0
Energy (kcal/mole)
$CF_2CH_2 + Br + I^*$
$CF_2BrCH_2 + I^*$
$CF_2CH_2 + Br + I$
$CF_2BrCH_2 + I$
CF_2BrCH_2I
E^*_{avl}
E_{avl}
308 nm
266 nm
248 nm
$CF_2CH_2I + Br^*$
$CF_2CH_2I + Br$
CF_2BrCH_2I
XBL 868-3041

Figure 16

Chapter 4

Summary of Photofragmentation Data for Iodoethanes, Including New Results for CH_2BrCH_2I, CF_2BrCF_2I, and CF_2ICF_2I

I. INTRODUCTION

The previous chapters have dealt with the detailed analyses of photofragmentation in the n(I)$\longrightarrow\sigma^*$(C–I) continuum for two different iodoethanes, CH_2ClCH_2I and CF_2BrCH_2I. The aim of the present chapter is to present a summary of the principal results for these systems and for the five other iodoethanes (CH_3CH_2I, CF_3CF_2I, CH_2BrCH_2I, CF_2BrCF_2I, and CF_2ICF_2I), which have been studied by the same technique. New results for three of these molecules will be shown: CF_2ICF_2I at 308 nm, CF_2BrCF_2I at 266 and 308 nm,[1] and CH_2BrCH_2I at 248, 266, and 308 nm; however, as the methodology of photofragmentation translational spectroscopy of iodohaloethanes is now well established, no primary data for these newly studied systems will be given.

All the results to be presented here will be based upon the c.m. translational energy distributions $P(E_T)$ and the anisotropy parameters β. Specifically, only the $P(E_T)$'s and β's for C–I bond fission will be considered. Even though primary C–Br bond fission sometimes occurs in the region of the n(I)$\longrightarrow\sigma^*$(C–I) continuum, it is very difficult to deconvolute this process from secondary processes also taking

place—i.e., spontaneous and stimulated secondary dissociation of the RBr radical (see Chapter 3).

The $P(E_T)$ distributions for CH_2BrCH_2I, CF_2BrCF_2I, and CF_2ICF_2I are shown in Figures 1-3, and the principal results for all the iodoethanes that have been studied are summarized in Table I. In this table, no attempt has been made to include error estimates, although some values are certainly more precise than others. In particular, the ethyl iodide numbers are fairly crude, as they were taken from the $P(E_T)$ plot (except for $<E_T>$ and β) in Riley and Wilson's paper.[2] Moreover, their method was less sophisticated than that used to study the other molecules in the table. Generally, E_{avl} probably has about a ± 1 kcal/mole error (but it could be as high as ± 2 kcal/mole) because most cases required the estimation of the C–I bond energy by comparison with a similar compound (e.g., $D_0^\circ(CF_2BrCH_2\text{–I})$ was assumed to equal $D_0^\circ(CF_3CH_2\text{–I})$). The quantities derived directly from the $P(E_T)$ distribution—$E_T(\text{min})$, $E_T(\text{max})$, $<E_T>$, and FWHM —are probably only in error by ± 1 kcal/mole. These errors will, of course, be transferred to the E_T/E_{avl} ratios. The relative probability for each dissociation channel at a given wavelength should be accurate to 10%. Finally, the anisotropy parameters are imprecise to about ± 0.2 in β, unless otherwise specified by the given range.

II. DISCUSSION

A. Photofragmentation trends

1. anisotropy and branching ratios

The most striking trend in the results is the fact that every dissociation channel has a parallel polarization dependence (as evidenced by the β parameters) regardless of the molecule or the excitation wavelength. Thus, the primary excitation

process in every case must result from a transition dipole moment that is parallel to the C–I bond. As discussed in earlier chapters and elsewhere,[3] the quasi-diatomic model predicts that spin-orbit excited state $I(^2P_{1/2})$ should be formed via a parallel transition to the $^3Q_0$ repulsive state, while the only possibility of producing ground state $I(^2P_{3/2})$ by a parallel transition would be the occurrence of a curve crossing between the $^3Q_0$ and ^1Q (or $^3Q_1$) states. This explanation seems plausible, but it does have some pitfalls (see Chapter 3, Sect. IV.A.).

Related to the anisotropy are the $I(^2P_{1/2})/I(^2P_{3/2})$ branching ratios, which do not show such an apparent trend. The only certainty is that for a given molecule, 308 nm excitation produces a higher percentage of ground state iodine than does 266 or 248 nm. Possibly, the part of the potential energy surface reached at low energy excitations is not as steep as the part accessible at higher energies, then recoil resulting from absorption at longer wavelengths would be slower, allowing more time for curve crossing. This reasoning cannot be extended to the difference between the branching ratios at 266 and 248 nm, however, because the CH_2ClCH_2I and CF_2BrCH_2I systems show a higher fraction of $I(^2P_{3/2})$ at 248 nm than at 266 nm. A possibility exists that at 248 nm, a small portion of the ground state iodine product originates from a direct perpendicular transition to the ^1Q state, which is consistent with the observation of a slightly lower β value for the $I(^2P_{3/2})$ channel than for the $I(^2P_{1/2})$ channel in CF_2BrCH_2I photodissociation. While β seems to be the same for both channels in CH_2ClCH_2I, the data are not necessarily good enough to show a small difference of $\sim$0.3. Nevertheless, why CH_2BrCH_2I should exhibit such a different $I(^2P_{1/2})/I(^2P_{3/2})$ branching ratio than CH_2ClCH_2I at 248 nm is still unclear, particularly since the absorption spectra of the two molecules in the 230-310 nm region are virtually indentical.[4]

Butler[5] has discussed the relationship between the ionization potential of the

R radical (in the RI molecule) and the iodine product state branching ratio. She has concluded that a lower ionization potential of R will increase the effective spin-orbit interaction and thus the curve crossing probability, so the $I(^2P_{1/2})$ quantum yield will be lower. This conclusion can explain the rough trend that fluorinated alkyl iodides have a higher $I(^2P_{1/2})/I(^2P_{3/2})$ branching ratio than their hydrogenated analogues for a given excitation wavelength, but it cannot explain the difference in the branching ratios for CH_2ClCH_2I and CH_2BrCH_2I. Furthermore, CF_2BrCH_2I produces a higher fraction of $I(^2P_{3/2})$ at 248 nm than does CH_2BrCH_2I. Considering the lack of any definite trends, a *simple*, general picture for predicting branching ratios might not be possible, especially since it appears that even such a seemingly minor substitution as Br for Cl alters the relative probability of product states dramatically.

2. translational energy distributions

Generally, the maximum energy in translation should be less than the available energy because the geometry of an iodoethane will force the exit impact parameter to be large, and in order to conserve angular momentum, the radical fragment will have to be rotationally excited. The quantities in the "rigid radical prediction" column in Table I give the expected fraction of the available energy in translation if the molecule dissociates from its equilibrium geometry and if the radical fragment is rigid (see Chapter 3 for the applicable equations). These quantities represent the maximum fraction in translation as long as the molecule does not distort before dissociating. Evidently, distortion must occur in many cases.

The maximum release of translational energy is seldom as large as the available energy, but all the excess energy does occasionally appear in translation when the lowest energy excitation wavelength, 308 nm, is used (except for the CH_3CH_2I sys-

tem, where the quality of the data makes close scrutiny unjustifiable). In addition, the I($^2P_{1/2}$) channel tends to leave a higher fraction of the available energy in translation than does the ground state I($^2P_{3/2}$) channel. Hence, lower excess energy seems to favor a higher maximum fraction in translation. This result can be explained by noting that at lower excess energies, the dissociation might not be describable as an impulsive process, so that bending in the excited complex could take place before C–I bond fission, giving rise to a range of exit impact parameters, some of which would be small enough to allow a higher E_T/E_{avl} fraction than that predicted by the rigid radical model with dissociation from the equilibrium configuration. A broad range of exit impact parameters should result in a lower β parameter, but there is no clear correlation between high $E_T(\max)/E_{avl}$ and low β. On the other hand, the uncertainty in the β values could make this correlation moot.

The full width at half maximum (FWHM) of the $P(E_T)$ distributions might be expected to be broad if the range of exit impact parameters were large, but there is no indication of a relationship between a wide FWHM and a high fraction of available energy in translation or a low anisotropy parameter β. Some $P(E_T)$'s are significantly wider than others even for similar systems. For example, the FWHM of the CF_2BrCF_2I distribution is ~60% wider than the FWHM of the CF_3CF_2I distribution for the same dissociation channel (there is only one) at 248 nm excitation. A possible explanation would be that CF_2BrCF_2I dissociates with a wider range of exit impact parameters b with the same average b; however, as discussed above, this effect should be reflected in the anisotropy parameter and in the ratio $E_T(\max)/E_{avl}$, but these two quantities are essentially identical for both cases. The presence of more low frequency modes in CF_2BrCF_2I might be construed as a reason for a wider translational energy distribution. Another consequence of more low frequency modes would be to decrease the average recoil energy. A decrease of

~7% in $< E_T >$ (at 248 nm) was observed between CF_3CF_2I and CF_2BrCF_2I, but it would be surprising that such a small change could be reflected so dramatically in the shape of the $P(E_T)$ distribution. Since these kinematic models cannot satisfactorily explain the differences between the two $P(E_T)$'s, maybe the important factor in the width of the $P(E_T)$ distribution is the overlap of the wavefunctions between the ground and excited electronic states.

A final observation from Table I is that even though $E_T(\text{min})/E_{\text{avl}}$ and $E_T(\text{max})/E_{\text{avl}}$ differ considerably from system to system, the average energy in translation is a relatively constant fraction (~50%) of the available energy. In general, this fraction is lower than the rigid radical model prediction, suggesting that vibrational excitation of the radical fragment is significant. Nevertheless, simple explanations attempting to relate the number of low frequency modes in the R radical (or its "softness") to the fraction $< E_T > /E_{\text{avl}}$ would be questionable because the molecules with "softer" R groups, such as CF_2BrCF_2I do not, on the average, necessarily leave a smaller fraction of the excess energy in translation than molecules with "harder" R groups, such as CF_2BrCH_2I and CF_3CF_2I (although $< E_T > /E_{\text{avl}}$ for CH_3CH_2I is considerably higher than that fraction for the other iodoethanes studied at 266 nm).

B. Thermochemistry

Both Chapters 1 and 3 discuss the method by which the ΔH (at 0 K) for a reaction of the type RXI $\longrightarrow$ R + X + I can be measured by studying the photofragmentation dynamics of iodohaloethanes. In addition to the CH_2ClCH_2I and CF_2BrCH_2I systems, analogous thermochemical information has been determined for CF_2BrCF_2I and CF_2ICF_2I. Unfortunately, a third molecule, CH_2BrCH_2I did not show any stable CH_2BrCH_2 radical peak in the time-of-flight, so we were

unable to derive the energy threshold for breaking both the C–I and C–Br bonds.

Table II shows a summary of the thermochemical data obtained from these investigations. The primary measured quantity is the ΔH in column two. From this ΔH, the heat of formation of the iodoethane parent follows directly. By estimating the C–I bond energy, the R–X bond energy of the radical photofragment can be inferred. The values for CH_2BrCH_2I have been approximated for comparison. (We employed the basic assumption: $D_0^\circ(CH_2BrCH_2\text{–}H) = D_0^\circ(CH_3CH_2\text{–}H)$.)

The most surprising result in Table II is the ΔH for $CF_2ICF_2I \longrightarrow CF_2CF_2 + 2I$, which implies a $D_0^\circ(CF_2CF_2\text{–}I)$ of about 8 kcal/mole. Based on the heat of formation of CF_2ICF_2I in the literature,[6] the CF_2CF_2I radical would be expected to be unstable. As has been discussed in Chapter 3, a barrier to secondary dissociation could cause a high estimation of the R–X bond energy of the radical. The effect of a centrifugal barier should be unimportant, but an intrinsic barrier could cause an erroneous result. However, the fact that Cl addition to a double bond has no barrier[7] suggests that the analogous I atom addition would not have a barrier, and if one did exist, it would not be as high as 8 kcal/mole. The trend toward higher C–Br bond energies with increasing fluorine substitution in bromoethyl radicals shows that perfluorination considerably increases the stability of a haloethyl radical and thus adds additional validity to the observation of a higher-than-expected C–I bond energy in CF_2CF_2I. Therefore, the literature value must be in error.

REFERENCES

1. Krajnovich, *et al.* (reference 3, below) were the first to study CF_2BrCF_2I at 266 nm, but our data had better signal-to-noise, so we could determine the $P(E_T)$ distribution and $\Delta H^{\circ}_{f,0}(CF_2BrCF_2I)$ more accurately.

2. S. Riley and K.R. Wilson, Discuss. Faraday Soc. **53**, 132 (1972).

3. D. Krajnovich, L.J. Butler, and Y.T. Lee, J. Chem. Phys. **81**, 3031 (1984).

4. Absorption spectra were taken in our laboratory—unpublished.

5. L.J. Butler, Ph.D. thesis, University of California, Berkeley, 1985.

6. E.-C. Wu, J.M. Pickard, and A.S. Rodgers, J. Phys. Chem. **79**, 1078 (1975).

7. H.B. Schlegel and C. Sosa, J. Phys. Chem. **88**, 1141 (1984).

TABLE I. Summary of principal results for all iodoethanes studied by photo fragmentation translational spectroscopy. Under "iodine product state," I refers to $I(^2P_{3/2})$ and I* refers to $I(^2P_{1/2})$.

					$P(E_T)$				E_T/E_{avl}				
Molecule	λ(nm)	iodine product state	relative prob. of diss. chan.	E_{avl}	E_T(min)	E_T(max)	$< E_T >$	FWHM	E_T(min)	E_T(max)	rigid rad. pred.	$< E_T >$	β
CH_3CH_2I[a]	266	I	0.25	53.2	13	51	34.3	13	0.24	0.96	0.65	0.64	$0 < \beta \leq 2$
		I*	0.75	31.5	7	32	22.6	11	0.22	1	0.65	0.72	$0 < \beta \leq 2$
CF_3CF_2I[b]	248	I*	1.00	41.3	12.3	30.7	20.9	6.8	0.30	0.74	0.86	0.51	1.87
CH_2ClCH_2I	248	I	0.40	58.0	21.0	36.0	27.5	9	0.36	0.62	0.62	0.47	1.8
		I*	0.60	36.3	13.0	26.0	22.0	5.5	0.36	0.72	0.62	0.61	1.8
	266	I	0.25	50.5	14.3	31.0	24.0	8.3	0.28	0.61	0.62	0.48	1.8
		I*	0.75	28.8	8.3	21.5	17.4	5.0	0.29	0.75	0.62	0.60	1.8
	308	I	1.00	35.8	4.0	27.0	19.3	7.7	0.11	0.75	0.62	0.54	1.75
CH_2BrCH_2I	248	I	0.04	59	26.0	51.0	38.4	12	0.44	0.86	0.57	0.65	1.6
		I*	0.96	37.3	6.0	32.0	18.3	7.6	0.16	0.86	0.57	0.49	1.6
	266	I	0.11	51.5	18.0	29.0	22.6	4.5	0.35	0.56	0.57	0.44	1.8
		I*	0.89	29.8	4.0	22.0	14.5	5.0	0.13	0.74	0.57	0.49	1.8
	308	I	1.00	36.8	4.0	26.0	16.4	7.5	0.11	0.71	0.57	0.45	1.5
CF_2BrCH_2I	248	I	0.25	59.2	16.7	34.7	24.4	7.4	0.28	0.59	0.62	0.41	1.6
		I*	0.75	37.5	5.7	22.7	15.5	6.7	0.15	0.61	0.62	0.41	1.25
	266	I	0.10	51.7	18.0	30.0	23.5	6.0	0.35	0.58	0.62	0.45	1.6
		I*	0.90	30.0	5.0	22.0	13.7	5.0	0.17	0.73	0.62	0.46	1.6
	308	I	0.67	37.0	10.0	27.0	18.8	6.0	0.27	0.73	0.62	0.51	1.2
		I*	0.33	15.3	2.0	16.0[c]	10.0	4.5	0.13	1	0.62	0.65	1.2
CF_2BrCF_2I	248	I*	1.00	41.3	10.0	31.0	19.5	11.1	0.24	0.75	0.84	0.47	1.84
	266	I*	1.00	33.8	7.0	30.5	17.9	10.5	0.21	0.90	0.84	0.53	1.8
	308	I	0.23	40.8	16.0	34.0	24.6	10.6	0.39	0.83	0.84	0.60	$1 < \beta \leq 2$
		I*	0.77	19.1	4.0	21.0[c]	13.9	4.7	0.21	1	0.84	0.73	$1 < \beta \leq 2$
CF_2ICF_2I	308	I	0.40	40.8	10.0	36.0	21.6	12.5	0.25	0.88	0.86	0.53	1.8
		I*	0.60	19.1	4.0	20.0[c]	13.1	5.2	0.21	1	0.86	0.69	1.8

[a]Reference 2

[b]Reference 3

[c]Initial parent internal energy can cause the maximum energy in translation E_T(max) to be higher than E_{avl}, which is calculated simply by subtracting the estimated C–I bond energy from the photon energy.

TABLE II. Compilation of thermochemical data for iodoethanes obtained by photofragmetation studies. The experimentally determined quantities are the reaction enthalpies ΔH in column two.

Parent (RXI)	$\Delta H(0\ \mathrm{K})$ $\mathrm{RXI} \longrightarrow \mathrm{R} + \mathrm{X} + \mathrm{I}$	$\Delta H^\circ_{f,0}(\mathrm{RXI})$	Estimated $D^\circ_0(\mathrm{RX–I})$	Estimated $D^\circ_0(\mathrm{R–X})$
CH_2ClCH_2I	76.5±1	−7.8±1	57.0±1	19.5±1
CH_2BrCH_2I[a]	~61.8	~0.7	56.0±1	~5.8
CF_2BrCH_2I	67.5±2	−92.6±2	55.8±1	11.7±2
CF_2BrCF_2I	73.3±1	−176.1±1	52.0±1	21.3±1
CF_2ICF_2I	60.1±1.5	−165.4±1.5	52.0±1	8.1±1.5
	51.8±1[b]	−157.1±0.5[c]		~0

[a]Thermochemical quantities for this molecule were estimated by assuming $D^\circ_0(CH_2BrCH_2–I) = D^\circ_0(CH_3CH_2–H)$.

[b]Calculated from $\Delta H^\circ_f(0)$ obtained from literature (see footnote *c*).

[c]Calculated from $\Delta H^\circ_f(298)$ in Ref. 6 by correcting for thermal energy.

FIGURE CAPTIONS

Figure 1. C.M. recoil translational energy distributions for C–I bond fission in the photodissociation of CH_2BrCH_2I at 248, 266, and 308 nm. The *solid* curve shows the total $P(E_T)$ derived from fitting the time-of-flight data for the iodine fragment. The *dashed* curves depict the estimated deconvolution of the total $P(E_T)$ into the distributions for each of the two possible dissociation channels. The relative probability of each channel is shown under the product iodine state.

Figure 2. C.M. recoil translational energy distributions for C–I bond fission in the photodissociation of CF_2BrCF_2I at 266 and 308 nm.

Figure 3. C.M. recoil translational energy distributions for C–I bond fission in the photodissociation of CF_2ICF_2I at 308 nm.

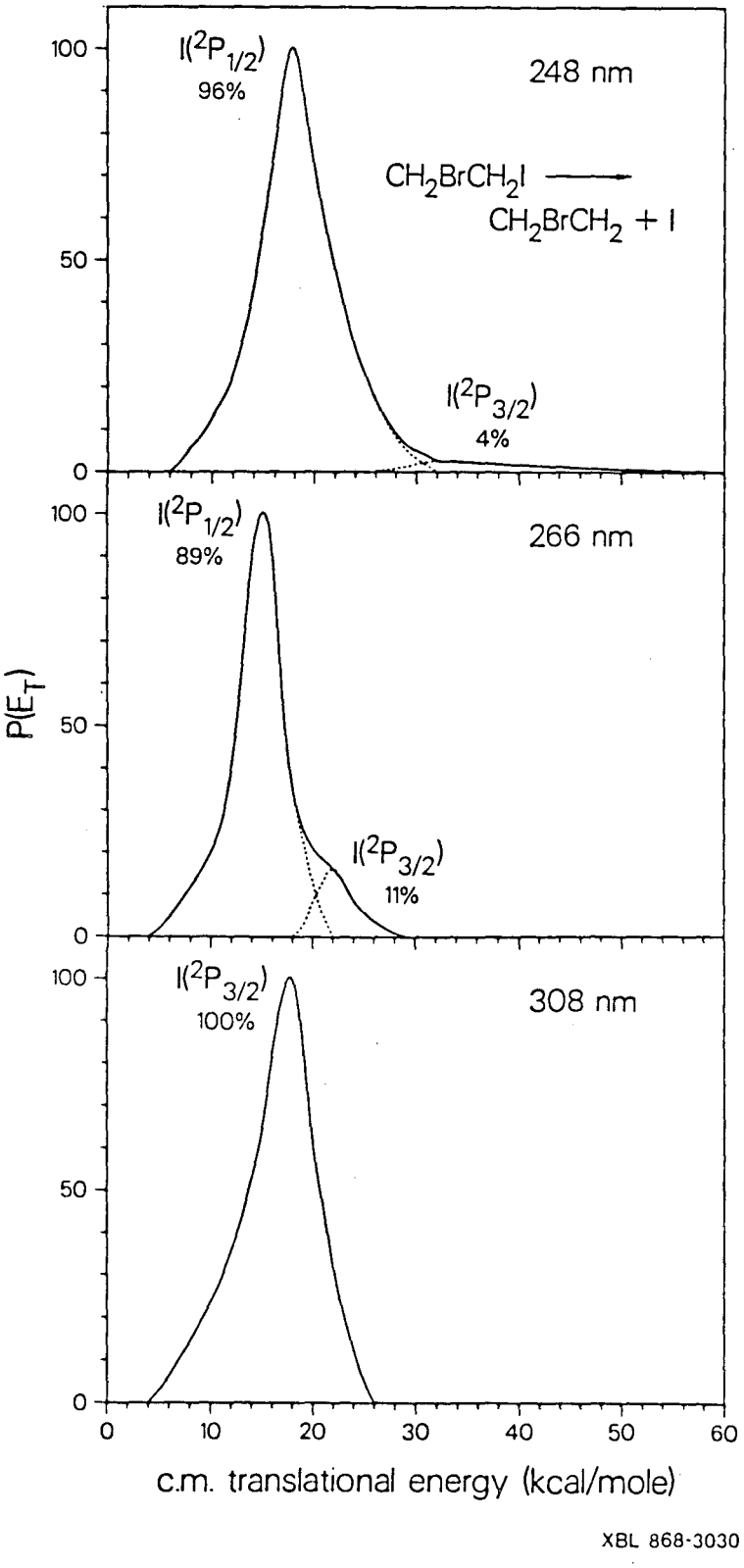
I(2P1/2)
96%
248 nm
CH2BrCH2I
CH2BrCH2 + I
I(2P3/2)
4%
I(2P1/2)
89%
266 nm
I(2P3/2)
11%
I(2P3/2)
100%
308 nm
P(ET)
100
50
0
0
10
20
30
40
50
60
c.m. translational energy (kcal/mole)
XBL 868-3030

Figure 1

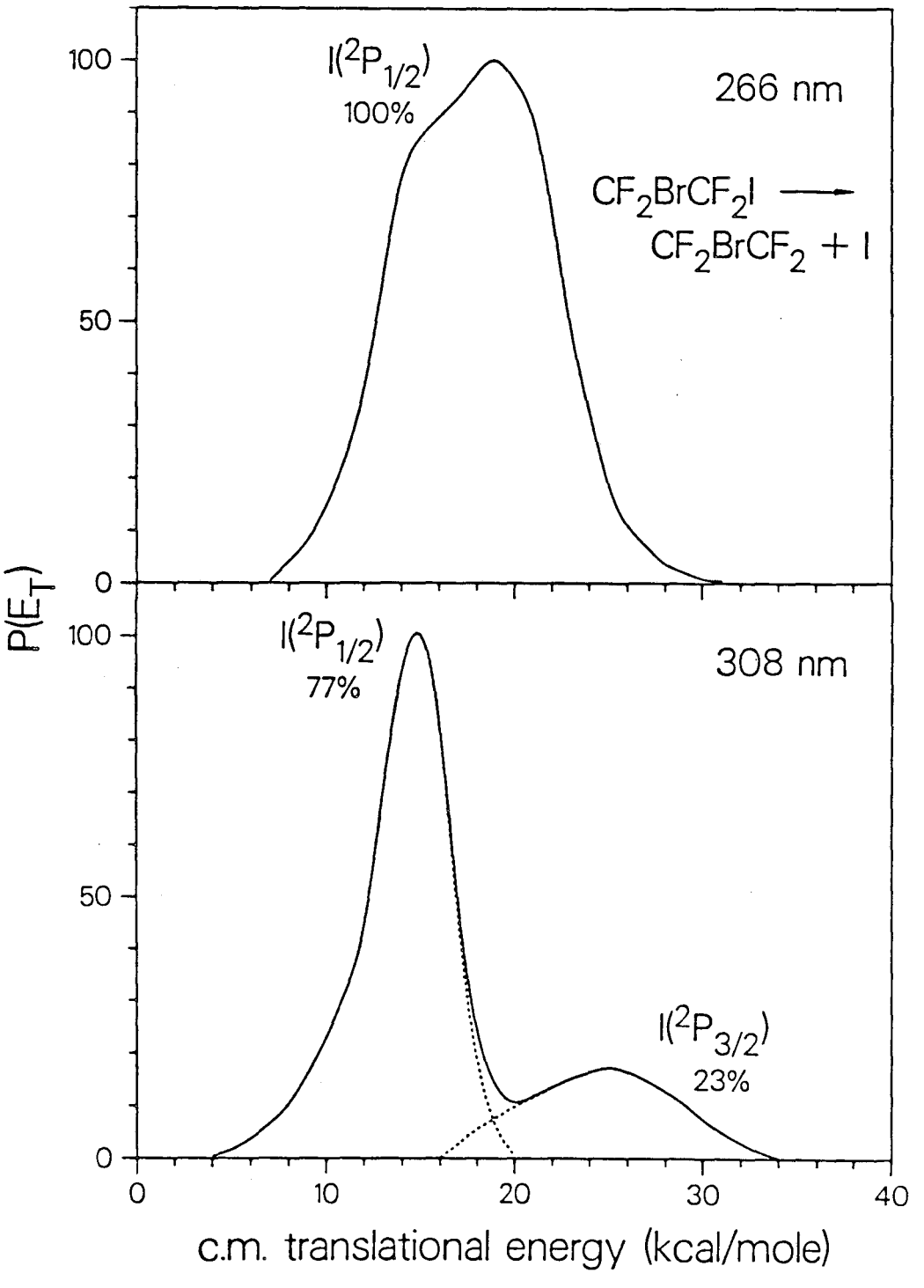
100
50
0
$I(^2P_{1/2})$
100%
266 nm
$CF_2BrCF_2I \longrightarrow$
$CF_2BrCF_2 + I$
$P(E_T)$
100
50
0
$I(^2P_{1/2})$
77%
308 nm
$I(^2P_{3/2})$
23%
0
10
20
30
40
c.m. translational energy (kcal/mole)
XBL 868-3029

Figure 2

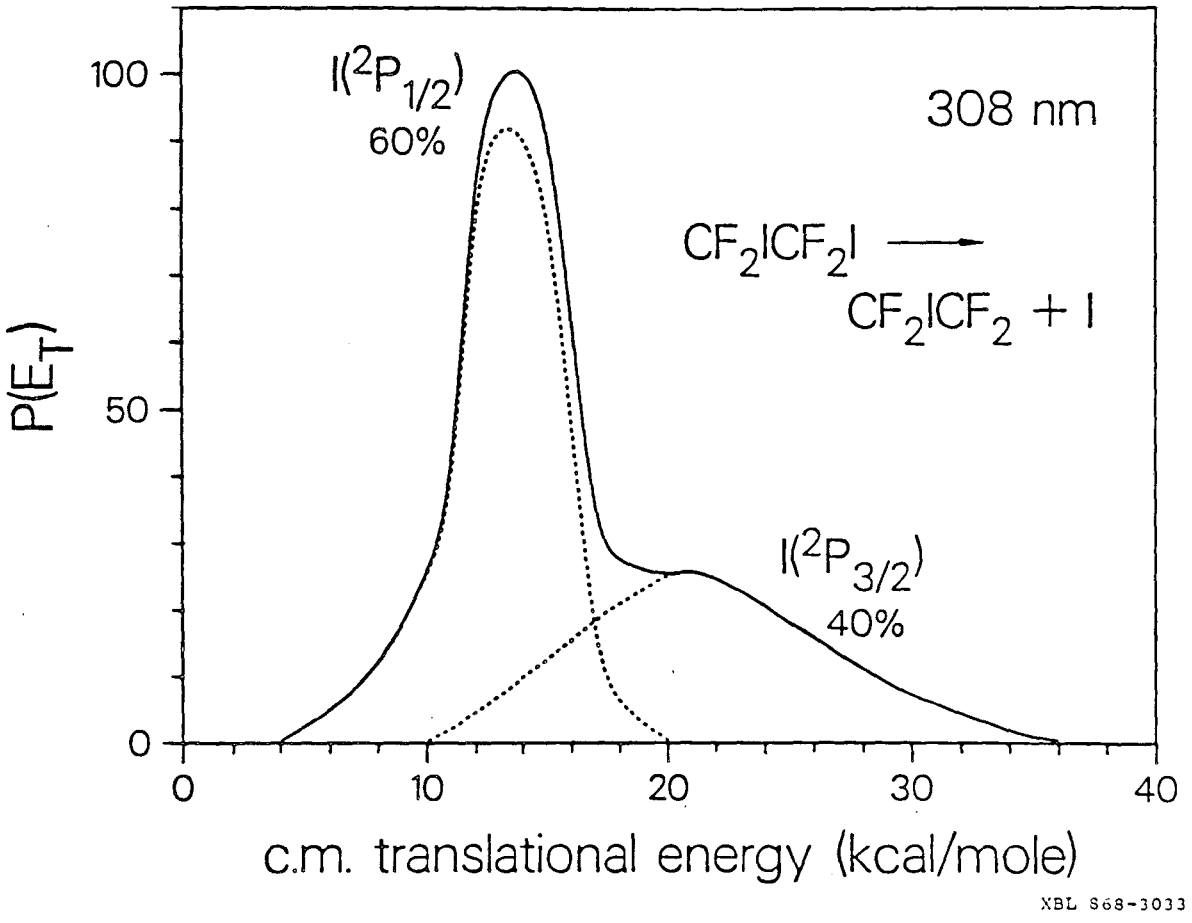
100
50
0
P(E_T)
I(²P_1/2)
60%
308 nm
CF2ICF2I ⟶
CF2ICF2 + I
I(²P_3/2)
40%
0
10
20
30
40
c.m. translational energy (kcal/mole)
XBL 868-3033

Figure 3

This report was done with support from the Department of Energy. Any conclusions or opinions expressed in this report represent solely those of the author(s) and not necessarily those of The Regents of the University of California, the Lawrence Berkeley Laboratory or the Department of Energy.

Reference to a company or product name does not imply approval or recommendation of the product by the University of California or the U.S. Department of Energy to the exclusion of others that may be suitable.

LAWRENCE BERKELEY LABORATORY
TECHNICAL INFORMATION DEPARTMENT
UNIVERSITY OF CALIFORNIA
BERKELEY, CALIFORNIA 94720